JPRS-CST-91-010
17 MAY 1991

Foreign Broadcast Information Service 50 ANNIVERSARY 1941 - 1991

JPRS Report

Science & Technology

China

NOTICE

NEW FBIS REPORT ON SOVIET REPUBLIC AFFAIRS

In May FBIS will begin publication of a new report entitled ***FBIS Report/Soviet Union: Republic Affairs.*** The report will contain open-source material from the Soviet Union on a wide range of republic political, economic, military and social issues. Material on the Soviet republics that was previously published in the JPRS reports ***Soviet Union: Political Affairs*** and ***Soviet Union: Economic Affairs*** will now appear in the new ***FBIS Report/Soviet Union: Republic Affairs***. The ***Daily Report: Soviet Union*** will continue to publish current material on the Soviet republics, but less time-sensitive items that formerly appeared in that publication will now be found in ***FBIS Report/Soviet Union: Republic Affairs.***

TO SUBSCRIBE:

U.S. Government

U.S. Government subscribers to JPRS reports ***Soviet Union: Political Affairs; Soviet Union: Economic Affairs;*** and ***Daily Report: Soviet Union*** will automatically receive the new ***FBIS Report/Soviet Union: Republic Affairs*** report.

U.S. Government subscribers who do not currently subscribe to the reports mentioned above may obtain subscriptions to ***FBIS Report/Soviet Union: Republic Affairs*** at no charge through their sponsoring organizations. For additional information or assistance, call FBIS, (202) 338-6735, or write to P O Box 2604, Washington, DC. 20013. Department of Defense consumers are required to submit requests through appropriate command validation channels to DIA, RTS-2C, Washington, DC, 20301 (Telephone: (202) 373-3771, Autovon: 243-3771).

Public Sector

The public may subscribe to ***FBIS Report/Soviet Union: Republic Affairs*** through the National Technical Information Service (NTIS), 5285 Port Royal Road, Springfield, Virginia 22161 (Telephone: (703) 487-4630). Subscription rates will be provided by NTIS upon request. Subscriptions are available outside the United States from NTIS or appointed foreign dealers.

Science & Technology
China

JPRS-CST-91-010 17 May 1991

CONTENTS

MICROELECTRONICS

SUPERCONDUCTIVITY

TELECOMMUNICATIONS R&D

PHYSICS

Variable-Thrust, Multiple-Restart Liquid Rocket Engine Developed

91P60147 Beijing KEJI RIBAO [SCIENCE AND TECHNOLOGY DAILY] in Chinese 29 Mar 91 p 2

[Article by Li Wei [2621 1792]: "Variable-Thrust Liquid Rocket Engine Developed"]

[Text] Changsha, 27 Mar—The multiple-restart, bipropellant, twin-regulated variable-thrust liquid rocket engine developed over a 5-year-plus period by a University of Science and Technology for National Defense research team headed by Prof. Chen Qizhi [7115 0796 2535] passed the formal technical appraisal organized by the National Defense Commission of Science, Technology & Industry in Changsha today. This engine will have wide applications in control of space launch vehicles and other spacecraft, and can be used to create new dynamic apparatus for effecting attitude control, change of orbit [i.e. orbit-raising and maneuvering], space docking, interception, planetary observation, soft landing of manned spacecraft, and other functions. Using existing equipment, Prof. Chen's team independently developed data-acquisition and real-time processing software, saving tens of thousands of yuan. The experts at the appraisal unanimously agreed that the new rocket engine's principal technical performance indicators meet 1980's international standards.

New Technical Details on Long March 4 Launch Vehicle

91FE0454 Beijing SHIJIE DAODAN YU HANGTIAN [MISSILES & SPACECRAFT] in Chinese No 1, Jan 91 pp 11-14

[Article by Long March 4 launch vehicle chief designer Xu Xinhua [1776 0207 5478] of the Shanghai Electromechanical Equipment Institute: "Long March 4 Launch Vehicle"]

[Text]

Abstract: The Long March 4 launch vehicle (LV) is a new type of the Chinese Long March rocket. It has been successfully used to launch two Fengyun-1 (FY-1) meteorological satellites into a sun-synchronous orbit 901 km high. This paper introduces the basic parameters, carrying capacity, and subsystem composition of the Long March 4 LV along with an analysis of the results of its first flight trials and scope of applications.

Key terms: launch vehicle, Long March 4, China.

China used its Long March 2 LV to launch 12 recoverable scientific experiment satellites, with gratifying success in all cases. The Long March 3 LV was also successfully used to launch six geosynchronous communications satellites. On 7 Sep 88 and 3 Sep 90, China also successfully used Long March 4 LVs to launch two meteorological satellites. The Long March 4 LV is an inexpensive three-stage rocket that uses a conventional propellant. It is capable of launching a satellite from any satellite launch site in China and is particularly well-suited to launching satellites into sun-synchronous orbits and polar orbits from the Taiyuan Satellite Launch Center.

The first and second stages of the Long March 4 LV were developed from the first and second stages of the Long March 3 LV. To increase carrying capacity, the ground thrust of the first-stage engine was increased from 2,750 kiloNewtons (kN) to 2,971 kN. The propellant storage tank of the first stage was made 4 meters longer, and the propellant was increased by 40 tons. Its third stage was newly developed. A thin-wall common-bottom fuel tank and lightweight engine short-capsule force-transfer structure was adopted and two engines capable of bidirectional swiveling [i.e. gimbaled engines] were installed. The exterior of the Long March 4 LV and its basic parameters are given in Figure 1 and Table 1.

Table 1. Basic Parameters of Long March 4 Rocket

Name	Units	First stage	Second stage		Third stage
			Main engine	Floating engine	
Length	Meters	24.897	8.286		8.718 (including length of fairing)
Diameter	Meters	3.35	3.35		2.9
Takeoff mass	Kilograms	249,000	56,000		16,700
Structural mass	Kilograms	9,998	2,887		1,751
Engine thrust	kN	2,971.16	722.078	46.233	101.028
Engine specific impulse	Meters/second	2,550	2,822	2,762	2,971
Satellite fairing diameter	Meters	Type A 2.9	Length 4.908		
		Type B 3.35	Length 8.483		
Operating time	Seconds	150.8	126.8	136.8	412

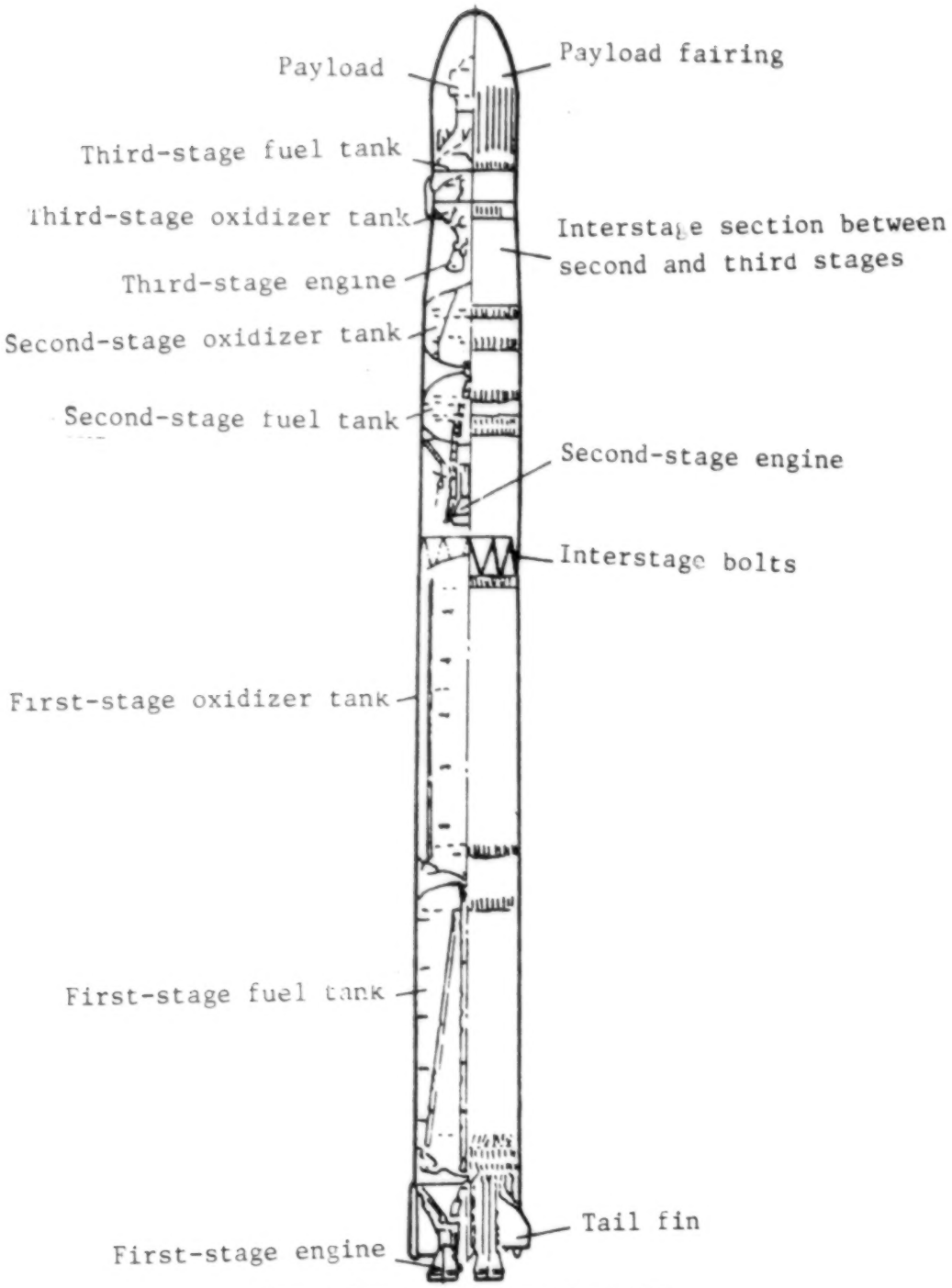

Figure 1. Exterior of the Long March 4 LV

The Long March 4 LV has a wide range of uses. Under current conditions, its carrying capacity into low-Earth orbit (LEO) (perigee altitude 200 kilometers, apogee altitude 400 kilometers) is 4,000 kilograms. Its carrying capacity for a 901-kilometer-high sun-synchronous orbit is 1,500 kilograms. Its first and second substages can be combined to make a two-stage rocket. This two-stage rocket has a payload carrying capacity of 3,100 kilograms when launching into a 200-kilometer-high 70° inclination LEO. Figure 2 and Table 2 show the carrying capacity of the Long March 4 LV for various orbits. If a solid booster with a thrust of 559 kN is strapped on to the first stage of the Long March 4 LV, its carrying capacity into LEO can increase to 6,300 kilograms.

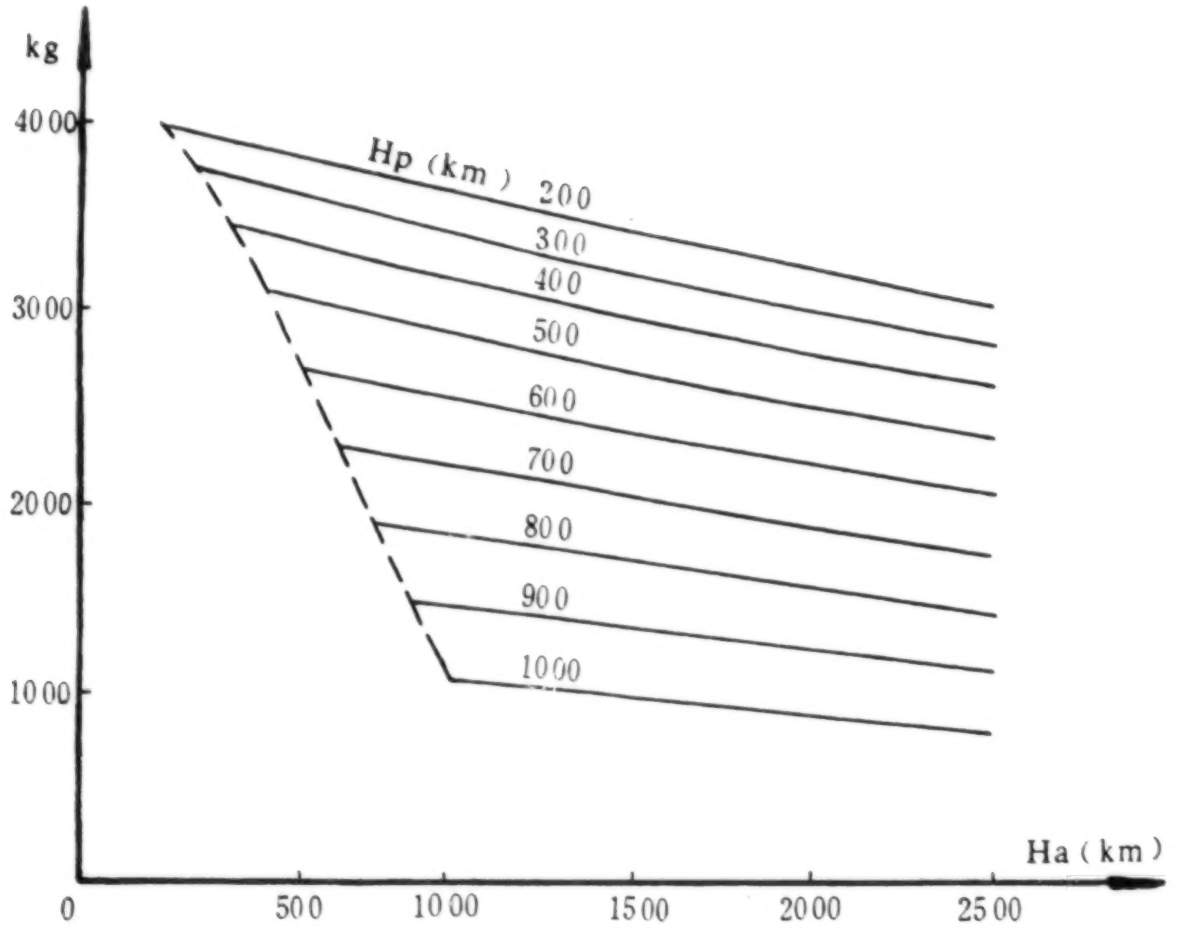

Figure 2. Carrying Capacity of the Long March 4 LV

Table 2. Carrying Capacity of Long March 4 LV for Various Orbits

Apogee (kilometers)	Payload (kilograms)			
	Perigee (kilometers)			
	200		400	
	Inclination (degrees)			
	40	70	40	70
200	4,874	4,348		
300	4,844	4,313		
400	4,799	4,243	4,264	3,788
500	4,739	4,198	4,219	3,733
600	4,684	4,153	4,159	3,673
700	4,629	4,098	4,099	3,623
800	4,569	4,043	4,039	3,573
900	4,519	3,993	3,989	3,523
1,000	4,464	3,933	3,929	3,473

I. System composition

1. First stage

The structure of the first stage of the rocket is composed of an interstage section, oxidizer tank, intertank section, fuel tank, final transition section, tail, and tail fins.

The first-stage engine is composed of four independently operating single engines capable of tangential movement that are connected in parallel by a rack. They have a total thrust of 2,971 kN (on the ground) and a specific impulse of 2,550 meters/second. The total mass of the engine is no greater than 2,850 kilograms. The maximum permissible swing angle is +- 8 degrees. The thrust chamber area ratio is 12.69 and the area of the thrust chamber nozzle outlet is 7,728.6 square centimeters.

The oxidizer tank has a total length of 9.32 meters and a diameter of 3.35 meters. Its total volume is 81,170 liters and its structural mass is 1,970 kilograms. The fuel tank has a total length of 8.229 meters and a diameter of 3.35 meters. Its total volume is 76,490 liters and its structural mass is 1,830 kilograms.

There are four trapezoidal fins on the tail section. The fin base chord length is 2.20 meters, the fin tip chord length is 0.8 meter, and the fin spread is 1.4 meters.

2. Second stage

The second-stage rocket is identical to the second stage of the Long March 3 LV.

3. Third stage

The structure of the third-stage rocket is composed of an instrument module, common-bottom storage tank, and engine module.

The instrument module has a cone-shaped exterior and its upper end is connected to the payload adapter.

The front tank of the common-bottom tank is a fuel tank and the rear tank is an oxidizer tank. The convex surface of the common bottom extends into the fuel tank and the tank is 1.92 meters long and 2.9 meters in diameter. The fuel tank has a volume of 6,249 liters and the oxidizer tank has a volume of 7,537 liters. The mass of the common-bottom storage tank is 543 kilograms.

The engine module is 1.15 meters in diameter and 0.41 meter tall. It is connected to the rear bottom of the common-bottom storage tank by bolts. The engine module is used to install the third-stage engine, counteraction attitude-control engine, anhydrous-hydrazine surface-tension fuel tank, third-stage servomechanism, and other equipment.

The third-stage engine is composed of two independently operating single engines connected in parallel that can swing in two directions. The maximum permissible swing angle is 4.5 degrees. The engine vacuum total thrust is 101.028 kN and the specific impulse is 2,971 meters/second. The nozzle outlet diameter is 630 mm and the single-unit mass is about 83 kilograms.

The counteraction attitude-control engine system is composed of 14 thrust chambers and one surface-tension fuel tank. It uses anhydrous hyrdazine as a propellant and serves to make attitude adjustments after engine shutdown and attitude control during taxiing.

4. Guidance and attitude-control system

This system is an inertial measurement component composed of three axial gyroscope stabilizing platforms and a rate gyroscope.

The detection and power amplifier and onboard digital computer serve as intermediate devices and the electrohydraulic servomechanism serves as an implementation component to control the swing of the engines and opening and closing of the counteraction attitude-control engine to create control torque, stabilize the rocket attitude, and adjust orbital drift.

The onboard digital computer implements real-time control computations and accurately transmits engine-shutdown commands, sequential command drive pulses,

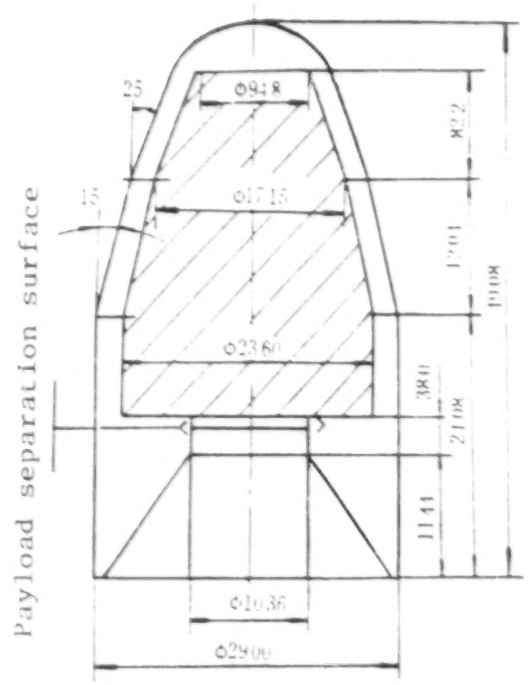

Figure 3. Exterior and Effective Space of Type-A Payload Fairing for Long March 4

transverse guidance instructions, and pitch sequence angle information for the engines of each stage. It also carries out differential and digital filtering computations for attitude control and transmits commands to the servomechanism. The master frequency of the onboard computer is 4 MHz, the word length is 16 bits, the channel instructions are 30 lines, and the basic instructions are 55 lines. It has 8-level interrupt functions.

5. Payload fairing

The Long March 4 LV has two types of payload fairings. Their structural dimensions are shown in Figure 3 and Figure 4.

The type-A fairing is composed of a spherical nose, front cone, rear cone, and cylindrical section. The fairing can be separated into two half-casing flat cones.

The type-B fairing can hold a larger volume payload. The lower portion of the fairing is an inverted cone.

6. Multi-satellite launch device

The multi-satellite launch device for the Long March 4 LV is shown in Figure 5. A second payload is added between the third-stage rocket and the payload fairing. The second payload module is composed of transition module A, transition module B, and the payload support module. The first payload is connected to the payload support module by an adapter and the second payload is connected to the front surface of the rocket instrument

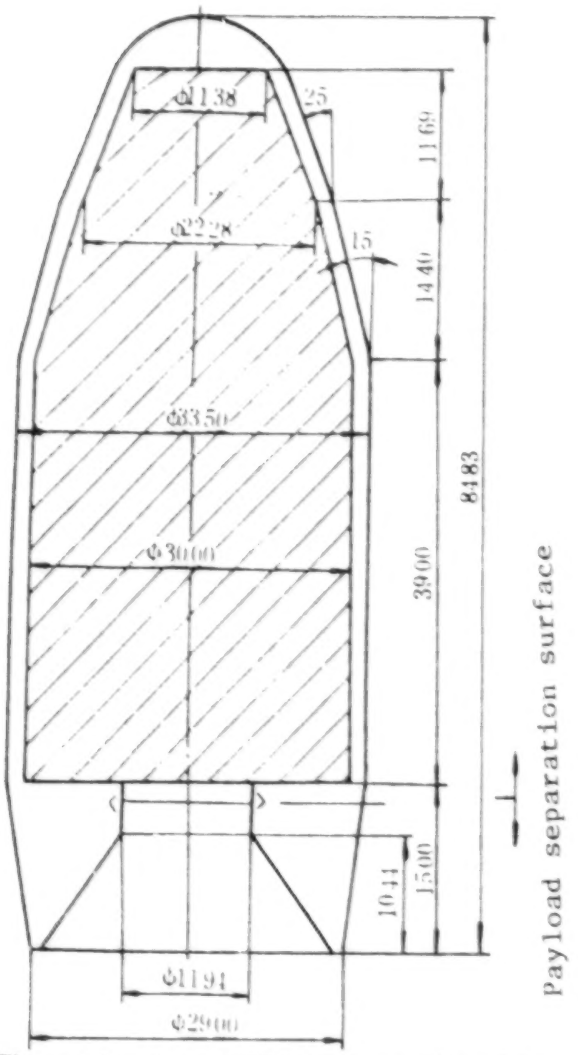

Figure 4. Exterior and Effective Space of Type-B Payload Fairing for Long March 4

module by another adapter. The dimensions of the second payload are shown in Figure 5.

After the rocket enters orbit, it first separates from the first payload and after making an attitude readjustment, it jettisons the transition module B and the payload support module. Then, the rocket again readjusts its attitude in the direction required by the payload and separates from the second payload.

II. Analysis of the Results of the First Trial Rocket Launch

The measurement and control system carried out stable tracking measurements of the rocket's flight. The telemetry system obtained telemetry parameters throughout the entire flight, including pressure, temperature, vibration, instructions, flow rates, and so on.

The LV stably followed the predetermined orbital track during its flight. The thrust and specific impulse of the engines of each stage were within the required range and they carried out startup and shutdown according to requirements. Interstage separation of each of the stages and separation of the satellite from the rocket were normal. The precision of orbital entry met design requirements. The maximum attitude angle during first-stage flight appeared at supersonic speed and the maximum dynamic pressure region. The maximum attitude angle was 0.73 degree. There was very little attitude drift at orbit entry, about 0.2 degree. Because the design adopted pressure storage vessel suppression of longitudinal coupling oscillation (POGO) measures, POGO oscillations were obviously eliminated during flight.

The orbital deviations of the first flight test were: periodic deviation -5.24 seconds, eccentricity deviation 0.003, and orbital inclination deviation 0.11 degree.

Analysis of data on the launch orbit obtained through measurements and data on the propulsion system indicated the carrying capacity of the Long March 4 LV could be as much as 1,500 kilograms (actual amount carried) for a 901-kilometer sun-synchronous orbit.

Taken at the TT&C Center, the results of orbital tracking measurements of the second FY-1 satellite launched by the Long March 4 LV showed that the orbital deviation of the second flight test was: periodic deviation 1.36 seconds, eccentricity deviation 0.00006, and orbital inclination deviation 0.058 degree.

III. Carrying Performance and Range of Applications

Because consideration was given to the need for a larger range of applications when the program for the Long March 4 LV was formulated, it is capable of launching satellites into sun-synchronous and polar orbits as well as into geosynchronous transfer orbits. Its performance is also quite good in launching satellites into LEO. The Long March 4 LV is suitable for launch from China's Taiyuan, Xichang, and Jiuquan satellite launch site facilities.

Strapping on a technically mature solid booster to the first stage of the Long March 4 LV can substantially increase its carrying capacity. This solid booster is 1.4 meters in diameter and 7 meters long. It has an average thrust of 559 kN, a specific impulse of 2,380 meters/second, and an operating time of about 66 seconds. When six of these solid boosters are strapped on to the Long March 4 LV, the payload carrying capacity into a polar orbit with a perigee of 200 kilometers and an apogee of 400 kilometers can be increased to 5,700 kilograms. The carrying capacity can be increased to 6,300 kilograms when eight boosters are strapped on.

In addition, to take full advantage of the performance of the Long March 4 LV and reduce the launch cost per kilogram of payload, work is now underway to further miniaturize the onboard instruments and equipment, utilize smaller-volume and lighter-weight inertial guidance equipment, and further improve engine performance.

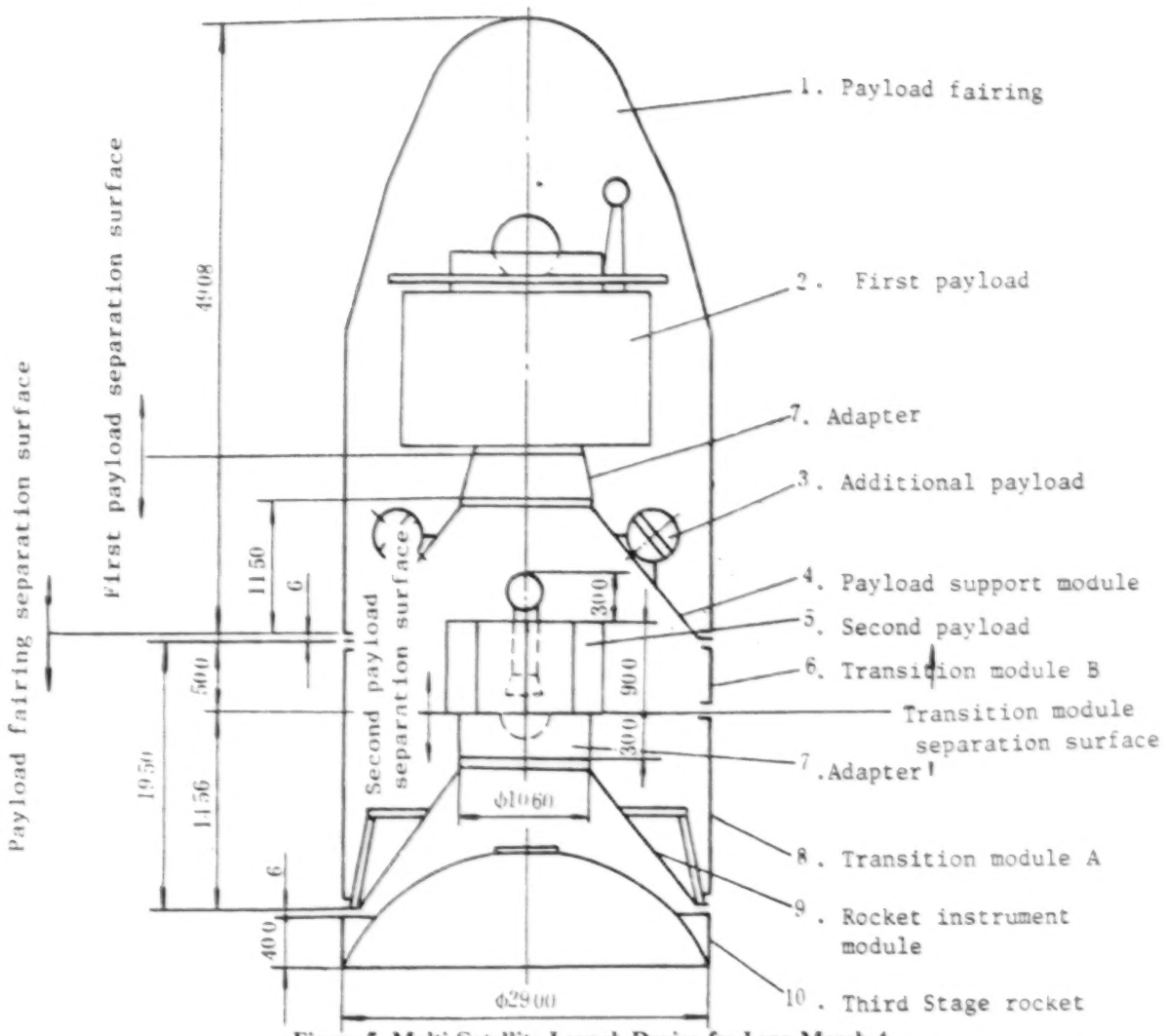

Figure 5. Multi-Satellite Launch Device for Long March 4

IV. Conclusion

After two successful launches of meteorological satellites, the Long March 4 LV has become China's basic vehicle for launching satellites into sun-synchronous orbits and polar orbits. The Long March 4 LV has a very high degree of reliability and rather large scope of applications. It is an excellent LV that can be provided to Chinese and foreign users.

Developments in Thermal Infrared Camouflaging Materials

40100035C Beijing YUHANG XUEBAO [JOURNAL OF CHINESE SOCIETY OF ASTRONAUTICS] in Chinese No 1, Jan 91 pp 62-69 (MS received 16 Mar 89)

[English abstract of article by Li Xinhua, Meng Xiaoxong, and Chen Lei of Institute 707 of the Ministry of Aerospace Industry]

[Abstract] With intensive development of thermal infrared detection techniques, thermal camouflaging materials used on the surface of objects have become an important part in the stealth technology of aircraft and spacecraft, but previous papers on the latter rarely discussed the materials. This article comprehends requirements for these materials, reviews in a relatively complete way developments in various important research fields of these materials in the past decade, and analyzes the features, level of properties, technical factors, present problems and developing trends of some important varieties of materials.

References

1. Aronson, J. R., et al., "Modeling the IR Reflectance and Emittance of Paints and Coatings," AD-A 110824 (1982).

2. Calvert, R. L., et al., "Surface Coatings for Low Emittance in the Thermal Surveillance Band," N85-12158 (1984).

3. Supcoe, R. F., "Formulation for Producing Low Infrared Coating in the 2-15 Micron Range," US-4288677 (1981).

4. Supcoe, R. F., "Blue-Gray Low Infrared Emittance Coatings," US4311623 (1982).

5. Tschulena, G., et al., "Pigmentierte Antrichstoffe mit niedrigem omissionsvermogen im Spektralbereich der Warmestrahlung," DE3118256 (1981).

6. Hugo, G., "Tarnfarbe," DE3432998 (1986).

7. Johansson, L., "Moyen de Camouflage Thermaque et Optique," FR2543286 (1984).

8. Frank, C., et al., "Transparent Heat-Reflecting Coatings Based on Highly Doped Semiconductors," THIN SOLID FILMS, 77 (1981), 107-117.

9. Karlsson, T., et al., "Window Coatings for Efficient Energy Control," INTERNATIONAL JOURNAL OF ENERGY RESEARCH, Vol 12, 23-29 (1988).

10. Beckwith, P. J., "Passive Countersurveillance—an Overview," AD-A 149086 (1983).

11. Deisenroth, Ulf, et al., "Mit einer Beschichtung versehenes Obgekt," DE3507889 (1988).

12. Lews, C. F., "Materials Keep a Low Profile," MATERIALS ENGINEERING, Jun 1988, 37-41.

13. Bach, W., et al., "Materialien zur Multispektralen Tarung im vissuellen, IR-und Mikro Millimeterwellen-Bereich," DE3606691 (1987).

14. Clement, D., et al., "Laboratory Assessment of Camouflage Materials, Effectiveness in the Thermal IR," IEE Conference Publication No. 283 (1987), 65-88.

15. Aronson, J. R., et al., "Modeling the Infrared Emittance of Paints," AD-A 121879 (1982).

Design of a BTT Missile Control System and Full Trajectory Numerical Simulations

40100035B Beijing YUHANG XUEBAO [JOURNAL OF CHINESE SOCIETY OF ASTRONAUTICS] in Chinese No 1, Jan 91 pp 16-24 [MS received 3 May 89]

[English abstract of article by Luan Zewei of the Harbin Institute of Technology]

[Abstract] The design of a BTT [bank-to-turn] missile autopilot by means of the classical control theory, and the guidance logic using the proportional guidance law without any constraint in the maximum roll angle of the missile are described. Full trajectory numerical simulations are computed and analyzed in the following different conditions of combination: without constraint in maximum roll angle or with constraint in the angle between -90 to +90 degrees, with or without a yaw channel, with or without the consideration of the dynamics of sensors in the control system. The results show that the designed guidance system, guidance logic and the autopilot are correct, reasonable and significant in practical engineering applications. They also verify that the BTT missiles have a large attacking range, good tracking performance, and can hit the targets stably when the targets are making fairly large maneuvers.

Numerical Analysis of Thrust Termination Process in Solid Rocket Motors

40100035A Beijing YUHANG XUEBAO [JOURNAL OF CHINESE SOCIETY OF ASTRONAUTICS] in Chinese No 1, Jan 91 pp 10-15 [MS received 5 Apr 89]

[English abstract of article by Xie Weimin, Zhou Jinxian, and Cao Zuo of Northwestern Polytechnical University]

[Abstract] It is pointed out that a series of pressure pulses with considerable strength will follow after opening the reversal nozzle (or auxiliary exhaust hole) in the thrust termination process of large or middle-scale solid rocket motors. Since no theoretical analysis is able to explain or predict these phenomena, this paper cites a series of cool simulation testing results, discusses the reasons for the appearance of pressure pulses, and puts forward methods to estimate pulse strength. Furthermore, an interior ballistics computer program which can be also applied to estimate the strength of pressure pulses is developed by utilizing the Characteristics Method and the Shock-Fitting Method for numerical analysis of one-dimensional unsteady flow. The predicted results are in good agreement with the experimental curves.

Study of the Structures and Properties of Al_2O_3/ZL109 Composites

40100035D Beijing YUHANG XUEBAO [JOURNAL OF CHINESE SOCIETY OF ASTRONAUTICS] in Chinese No 1, Jan 91 pp 70-75 [MS received 28 Jun 89]

[English abstract of article by Zhou Bide, Liu Zheng, Peng Delin, and An Geying of Harbin Institute of Technology]

[Abstract] The structures and the properties of alumina short fiber reinforced aluminum alloy composites are studied. The results of the study indicate that the distribution of the fiber in the composites with squeeze casting technique by using alumina short fiber as reinforcement is even, and the fiber combines with the aluminum alloy matrix well. The alumina fiber is favourable to heterogeneous nucleation of the Si phase in Al-Si alloys. Compared with the matrix, the composites have higher tensile strength under both room temperature and elevated temperature, higher hardness and a good wear resistance, and are a metal-matrix composite material with excellent properties.

Axial EM Scattering and Shape Optimization of Reflectors

40[0003]5E Beijing YUHANG XUEBAO [JOURNAL OF CHINESE SOCIETY OF ASTRONAUTICS] in Chinese No 1, Jan 91 pp 84-88 (MS received 2 Jul 89)

[English abstract of article by Deng Shuhui and Ruan Yingzheng of the University of Electronic Science and Technology of China, Chengdu]

[Text] The simple calculation formulas for nose-on scattering field and radar cross section (RCS) of reflectors are derived, where the specular field is obtained by the method of Geometrical Optics and the edge-diffracted field by the method of equivalent currents. Optimization of some rotational second-order curved convex or concave surfaces with lower RCS value are investigated. A typical example is given with spatial RCS graphs and lowest RCS values. Optimum surface parameters are obtained.

Development of Electromagnetic-Pulse Simulators

91FE0285B Beijing SHIJIE DAODAN YU HANGTIAN [MISSILES & SPACECRAFT] in Chinese No 11, Nov 90 pp 44-47

[Article by Peng Guixin [1756 6311 2450] of the Beijing Overall Institute of Electronic Engineering: "Development of Electromagnetic-Pulse Simulators"]

[Text] In the past decade, China has focussed its nuclear weapons research on pulsed power sources. Electromagnetic pulse (EMP) simulation has been responsible for the development of a class of pulsed-power systems. This paper provides a general survey of pulsed-power technology with emphasis on special applications of EMP simulation. In addition, several classic simulators are briefly described.

With rapid advances in electronics, electromagnetic interference and electromagnetic compatibility are becoming ever more important. Electromagnetic pulse (EMP) testing is mandatory for electronic devices that are intended to survive a nuclear attack. EMP simulators are basic tools to complete simulated nuclear EMP experiments.

Nuclear EMP experiments should be planned throughout the entire design and various stages of production process. Different stages have different objectives. In order to meet these objectives, different simulators are required. For example, in product evaluation, a powerful simulator is needed. In the design stage, to look for an interference coupling mechanism and weak links, a low-voltage repetitive simulator should be used to raise efficiency. Therefore, there is a need for a series of simulators.

Although there are a variety of EMP simulators for different applications, they all have the following common characteristics.

Fast rise time: The high-frequency component of the pulse is determined by the rise time. It should be approximately 10 nanoseconds. The definition is the time required for the leading edge to reach from 10 percent to 90 percent of maximum amplitude.

High field strength: 10^4 - 10^5 Volt/m.

Slow decay time: High-altitude explosion requires about 1 microsecond. In low-altitude or ground explosions, the tail is several tens of microseconds. Decay time is defined as time to drop off to 10 percent of peak value.

Relatively uniform electric field: With respect to the object under test, it should be a plane wave.

They should all provide the user with a well-shielded measurement chamber stocked with recording and control equipment; this equipment must be safe and reliable.

Let us introduce several EMP simulators available in China.

I. Bounded-Wave EMP Simulators

Their unique feature is that it is capable of confining its energy within a finite space along the transmission line. The amount of outward radiation is very small.

1. DM-140 EMP Simulator

The DM-140 is a vertically polarized small bounded-wave simulator, primarily for simulating electromagnetic pulses generated by low-altitude or ground nuclear explosion. Its operating principle is to use a high-voltage dc power supply to charge a low-inductance energy-storage capacitor. After reaching the required voltage, it is discharged through a parallel plate transmission line by a high-voltage gas-filled switch to generate a transverse EMP. Its electric field is inversely proportional to the height of the transmission line and proportional to the operating voltage. The width of the leading edge of the discharge pulse, i.e., rise time, is governed by the inductance of the capacitor and the fast switch. The trailing edge of the pulse is determined by an exponential decay process whose time constant is the product of the capacitance and the impedance of the transmission line. The so-called work space is at the middle of the parallel plate transmission line where the tested object is placed. In reality, a transmission line cannot be infinitely long. Therefore, an electromagnetic wave will reflect at the end and disrupt the field in the work space. It even may destroy the high-voltage insulation at the starting end. Therefore, it is necessary to add a load at the terminating end of the transmission line to match with the transmission line.

The dc high voltage is produced by ac rectification and then converted into 4 kHz intermediate-frequency (IF) oscillation. An IF high-voltage transformer is used to raise voltage. This is followed by a voltage-multiplying rectifier which outputs a dc high voltage of up to 200,000 volts (200 kV).

The high-speed switch is a nitrogen-filled spark gap with flat electrodes. The gap is continuously adjustable from 0 to 10 mm. Its operating pressure is continuously adjustable from 0 to 10 atm. The external case is made of Nylon 6 and it is 200 mm long and can withstand 200,000 volts.

The transmission consists of the work space and two converter segments which are connected to the high-voltage source and terminal (load), respectively. In order to ensure that the converter segment has the same wave impedance as that of the work space, it is necessary to require that the height-to-width ratio at any cross section along the transmission line remains unchanged.

The transmission line of the DM-140 is made of aluminum plates. In addition to resistance to high voltage and high power, the terminal load must have no inductance. It is usually made of copper sulfate solution.

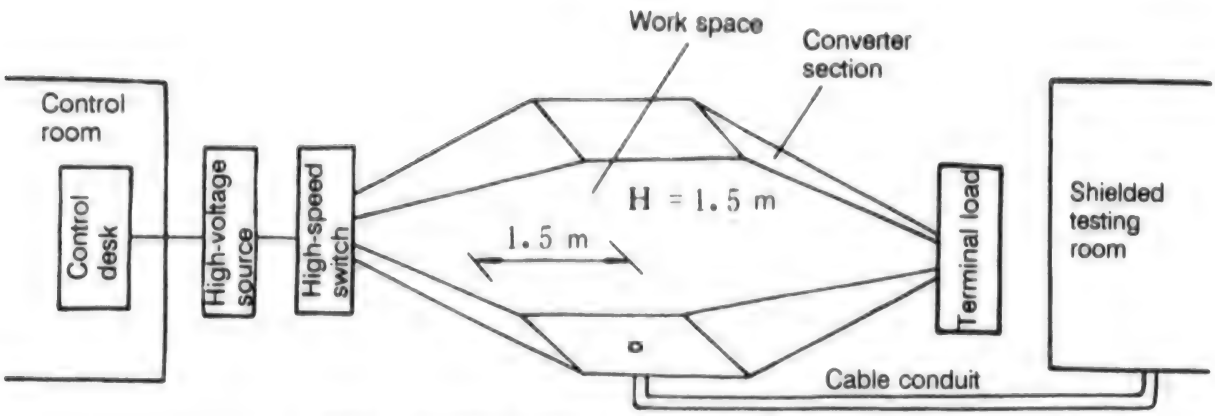

Figure 1. Schematic Diagram of the DM-140 EMP Simulator

The DM-140 simulator is equipped with a shielded measurement chamber and a control room. The measurement chamber is a hexagon made of 3-mm-thick steel plate. Electrical contact between the iron door and the walls is made through springs. At a low frequency such as 10 kHz, the shielding coefficient is approximately 80 dB, and approximately 60 dB by the door. In order to prevent series interference from the power source, it is delivered into the room through a DL-150 power-supply filter. The area of the testing room is 2 x 4 m. It is equipped with a movable three-tier instrument rack.

In order to ensure the safety of operators, the control room is made of double-layer sheet metal with excellent grounding. The control room and testing room are connected by an intercom.

Between the work space and testing room, there is a special cable conduit. It is equipped with high-frequency symmetrical (i.e., balanced) cable, 19-core high-frequency coaxial cable and 75-ohm, 50-ohm, and 100-ohm high-frequency coaxial cable for the users.

The recording instruments include a Phillips 50-MHz oscilloscope, and Tektronix 7834 storage oscilloscopes at 466 and 300 MHz.

The rise time of this simulator is approximately 10 nanoseconds, pulse width is 10 - 30 microseconds, and the electric field strength is 100,000 V/m. The work space is 1.5 x 1.5 x 1.5 m. The pulse may be repeated at an interval of less than one minute. Furthermore, its electric field strength and pulse width may be adjusted based on user demand.

2. DM-1200 EMP Simulator

This is a medium-scale bounded-wave simulator and is used to simulate EMP generated by a high-altitude nuclear explosion. Its major components include a 1,200-kV high-voltage pulse source, an electric-field illuminator composed of a transition segment and a work space, the terminal load, the underground shielded measurement chamber and suitable control and diagnostic equipment, as shown in Figure 2.

Major technical specifications for the DM-1200 are:

work space - 8.4 x 8.4 x 8.4 m.

electric field strength - 100,000 V/m.

pulse leading edge - 10 ns (10 percent to 90 percent).

pulse width - 1 microsecond (90 percent - 10 percent).

The high-voltage pulse source is a 1,200 kV Marx generator. A +/-100-kV dc high-voltage source is used to charge 11 110-kV high-voltage pulse capacitors. With a triggering pulse, six spark gaps filled with N_2 and SF_6 are discharged serially to obtain a voltage as high as 1200 kV. The dc high-voltage source is composed of an experimental 100-kV transformer, moving-coil voltage regulator, and high-voltage silicon pile.

For each stage, the capacitance is 0.033 μF and inductance is 300 nH. The unit is a cylinder, 22 cm in diameter and 50 cm in length. An S-shaped circuit is formed by connecting six spark gaps (gas-filled) together. The use of sharpened capacitor(s) and a high-speed switch is to ensure that the rise time is less than 10 ns. The switch, made of nylon, is 22 cm long and 13 cm in diameter. The flat electrode is 4 cm in diameter and is made of brass.

The charging resistor is made of $CuSO_4$ solution contained in a Plexiglass tube. The entire Marx generator is compactly hung over the cover of an oil container which is 1 m wide, 1.35 m high and 3.2 m long. The overall inductance is 7 μH and total series resistance is 4.5 ohm.

The sharpened capacitor for the DM-1200 has a coaxial structural design. It consists of cylinders and hemispheres. The inner diameter is 26 cm and outer diameter is 34 cm. The cylindrical part, 23 cm long, is oil-insulated. An open structure is used to avoid insulation

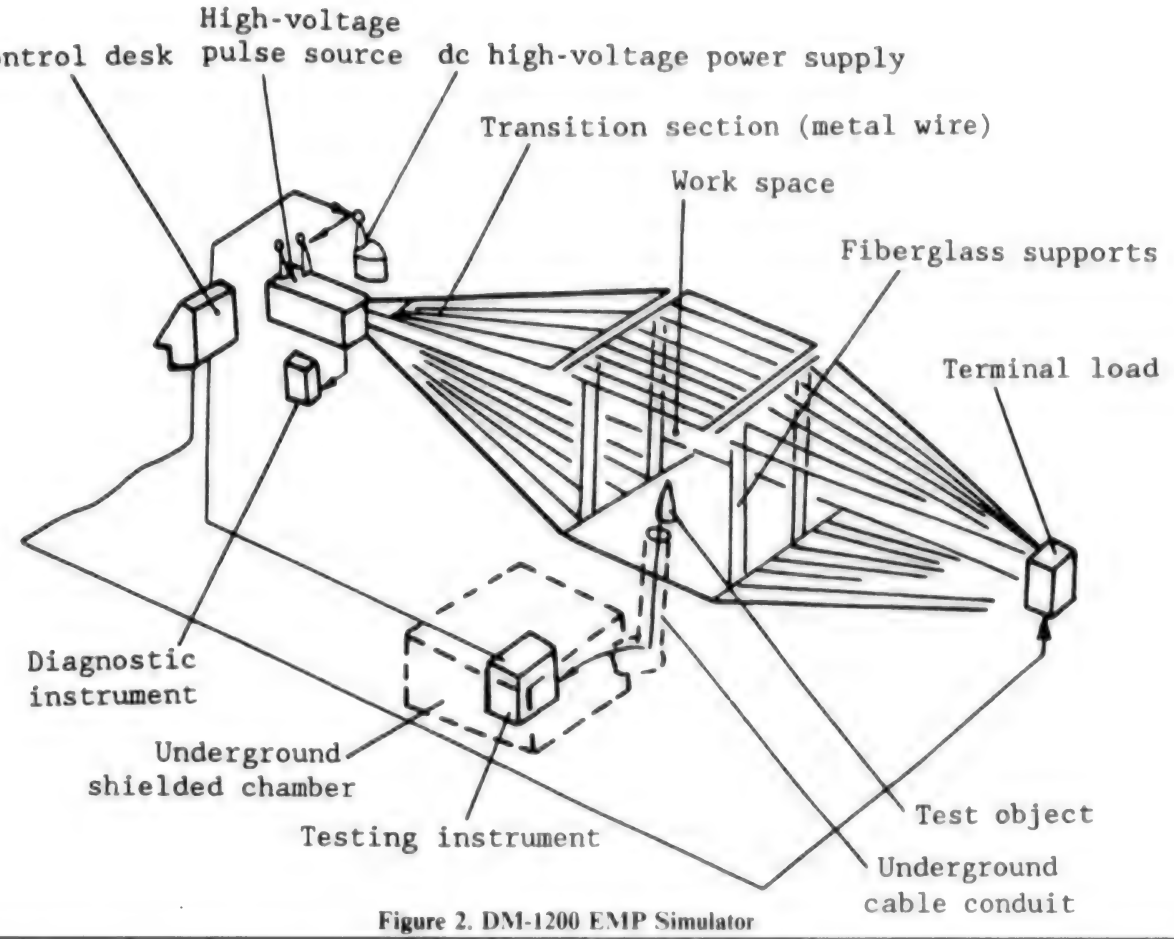

Figure 2. DM-1200 EMP Simulator

difficulty at the external case; i.e., it is suspended in the oil tank of the Marx generator by a nylon rope. The capacitance, which can be changed by adjusting the nylon lever to vary the overlap between the inner and outer cylinders, is 229 pF.

The electric field illuminator (transmission line) is 40 m long and 8.5 m high. It is supported by 43 fiberglass rods. The impedance of the transmission line, 165 ohms, is a function of the height-to-width ratio. The terminal load is composed of six $CuSO_4$ resistors in a parallel ring structure; its total resistance is 165 ohms. It is stored in a temperature-regulated box with heaters to ensure its use in winter time.

In addition to its main structure (high-voltage power supply, transmission line, terminal load), the DM-1200 also has an improved control system and a high-voltage and electric-field measurement system, and a top-class shielded measurement chamber.

The function of the control system is to control the normal operation of the entire experimental station, such as start-up, charging, operation of recorders, monitoring of the work space and basement, and ensuring safety. The control system is also equipped with a safe and reliable trigger. The experimental station has a number of 100-MHz single-sweep storage oscilloscopes. Based on the need, they are connected by electrical or optical cables to the basement measurement chamber. The measurement chamber and control room are completely shielded. The measurement chamber is beneath the work space with 20 m^2 of space. It has a 3 kW power supply and is well shielded. Between 1 kHz and 10,000 MHz [10 GHz], there is an attenuation of 100 dB. In order to prevent electromagnetic interference introduced by the power supply, a motor-generator assembly is used to generate its own power below the measurement chamber. The driving shaft is also insulated. The control room was welded together with sheet metal. Its power supply is also filtered and surge-protected. In addition, there is a dark room and work room for laboratory personnel. Two flood lights are provided in the work space for night-time experiments.

II. Radiation-Wave EMP Simulators

This type of simulator emits electromagnetic energy into free space to generate an electromagnetic field over a relatively large space around the antenna to perform EMP experiments with large, scattered and fixed targets.

1. Large Mobile Radiation-wave EMP Simulator

Large mobile radiation-wave EMP simulators are used to simulate the EMP from a high-altitude nuclear explosion. A cage-type double cone and cylinder-shaped horizontal dipole antenna is used as the radiation body. The antenna diameter is approximately 6 m. It consists of 40 modules. Its total length is 300 m and it is 20 m above ground. Its function is to convert gigavolt high-voltage electrical energy into a radiative-type electromagnetic field. It is an ideal tool to test and evaluate the EMP resistance of ground radar stations, communications and command centers, guided-missile sites and other large fixed facilities. The experimental range is 50 m x 100 m or larger. The minimum electric field strength is 1 x 10^4 V/m. The leading edge of the pulse is 10 ns and its width is greater than 700 ns.

The antenna is a hybrid type. The double cone part is a high-frequency transmitter which provides the leading edge of the pulse. The cylinder part provides the trailing edge. The entire antenna is a dipole. Due to different experimental zones and incident angles, it was designed to be a horizontal dipole. Its terminating end is grounded through a non-inductive matching load.

The pulse source of a large mobile EMP simulator can store energy in a short period of time and then release it instantaneously to obtain a high-power pulse. This is an important device in a simulator. Its performance can directly affect the technical specifications of the simulator. The pulse source is a highly difficult and costly system. It consists of two Marx generators, a pulse-sharpening circuit, and a triggering system. The two 2-MV Marx generators have symmetric voltage outputs, but opposite in polarity. They are placed in the two cones, respectively. Because the Marx generator itself has significant inductance, it is not able to deliver a fast-rising current pulse. Therefore, a sharpening capacitor Cp and a 4-MV output switch are used to sharpen the waveform produced by the Marx generator.

The working procedure for the control and testing system is as follows. The ground control desk controls gas sources to make sure that all switches in the pulse source reach their operating pressure. Hydraulic pumps are turned on to operate the power generator. The system also controls the +/-50 kV dc high-voltage source to charge the Marx generators. All equipment is put on standby. Ground-issued trigger control signals are transmitted by fiber optic cable to trigger the Marx generators to discharge the pulse source.

The testing system works as follows: When the Marx generators are charging, if they operate at rated voltage, it is necessary to measure the charging voltage to prevent it from exceeding the rated voltage of the capacitor. During discharge, the pulse voltage or current across the sharpening capacitor is monitored. An oscilloscope is used to observe the synchronization between the two pulse generators in order to adjust the trigger delay to obtain a synchronized output.

2. DMF-600 Mobile Radiation Simulator

This is a medium-size mobile radiation-wave EMP simulator. The radiation body is an antenna comprised of a caged double cone and a dipole. The overall length of the antenna is 2 x 150 m and it is 20 m above ground. Its diameter is 2.8 m and it is made of 16 pieces of #6-diameter aluminum-alloy pipe. There is a gas spark gap which is filled with a mixture of SF_6 and N_2. The length of the double cone is 2 x 3 m and the cone angle is $2\theta = 90$. The impedance of the double cone is 100 ohms. Two 300-kV dc high-voltage power supplies with positive and negative polarities are used to feed the antenna from both ends. After the spark gap breaks down, a voltage step wave formed on the antenna propagates toward both ends. Approximately 30 m away from the projection point of the antenna, the electric field approaches 10^4 V/m. Several non-inductive coil resistors are scattered on both ends of the antenna to serve as loads to gradually absorb the energy in order to prevent ringing of the antenna. The trigger is done by gas discharge. The system can operate at a repetition frequency of 10 Hz. The entire antenna is supported by fiberglass rods and the entire device is on a vehicle.

3. "V-shaped" Horizontally Polarized Mobile Radiation-wave Simulator

This is a multi-purpose simulator and horizontal polarization is one of its operating modes. Its primary function is to perform EMP penetration experiments on underground facilities and bunkers. Both the ground net and antenna are made of metal wires. The ground net, antenna and pulse source are mounted on a hydraulic lift vehicle with a lift height of 8 m. The height of the power supply is 2.9 m. The total height can reach 11 m. In order to meet the requirement that there is a 30 percent inhomogeneity over 3 x 5 m at the antenna outlet, the antenna is 2.13 m above ground. The source is a 600-kV SF_6-filled Marx generator. The dc power supply uses a 400-cycle inversion converter, instead of an electronic circuit, to avoid high-voltage impact.

This device was successfully used to perform EMP penetration experiments on an air-raid shelter with a 5-m-thick dirt cover and underground bunkers covered with a dozen meters of rocks. In order to verify its penetrating power, special care was taken to use no electric cables or metal pipes into the bunker. The measurement system is a 100-MHz fiber optic system. This eliminates the possibility that the electromagnetic field is established through metal pipes and cables. It was found that this device is capable of evaluating EMP resistance of underground defence facilities and command centers.

The technical specifications of the device are as follows:

The source is a 600-kV Marx generator with an impedance of 250 ohms. Its dc charging voltage is 100 kV. The source may also be used for other purposes, such as an injection source or vertical polarization. The electric field strength E at the outlet of the antenna is greater than or equal to 50 kV/m. The leading edge of the pulse is 10-15 ns and the pulse width is 1 microsecond. Over a 3 x 5 m test area, its inhomogeneity is less than 30 percent.

New Kind of Sonar Signal Processor Described

91P60131A Beijing SHENGXUE XUEBAO [ACTA ACUSTICA SINICA] in Chinese Vol 15 No 6, Nov 90 pp 450-462

[Article by Cai Huizhi [5591 1920 2535], Sun Zeng [1327 1073], and Sun Changyu [1327 7022 3842] of the CAS Institute of Acoustics: "New Kind of Sonar Signal Processor"; MS received 8 Jun 89]

[Summary] A method for combining several TMS32020 digital signal processing (DSP) chips along with other chips to construct a CPU suitable for use in fleet submarine tactical sonars is described. The system processes data from three independent receiver subarrays in order to determine target range and bearing. The system has a pipelined structural design and can handle different detection methods via a function code sent from the control center (CC). Results of system trials with four different operating modes are given. Employing advanced DSP chips and technology, this high-speed system is small in volume, and highly reliable and accurate.

Figure 1 is a logic diagram for the mutual-spectrum precision method.

The time-delay range for a two-signal system can be great, for example, with a sampling frequency of 25k[Hz], according to the originally designed two subarrays spaced 22 m apart with a total beam angle of +/- 60°, the maximum delay is over 300 sample points. Due to the limit (+/- 1 sample point) of the mutual-spectrum measurement range, the above analog system cannot provide the required accuracy, and an adaptive coarse-measurement circuit meeting the requirements must be added to the front end, along with a pre-delay circuit; this circuit's data are fed back to the CC, and the CC then updates the pre-delay unit. To save on hardware, the adaptive coarse-measurement and mutual-spectrum precision-measurement circuits share the same RAM.

A multifunctional signal processor can operate in any of the following five modes for simultaneous determination of the bearing and range of three targets:

(1) Mutual-spectrum precision delay method. In the frequency domain, this method segments the signals, estimates the delay for each resolving element, then processes the signals' power spectrum via application of a weighting factor to produce an accurate estimate of the delay. The authors employed a 64-point mutual-spectrum operation, whose front-end pre-processing results (digital filtering, adaptive noise-canceling coarse-measurement delay) were quite satisfying.

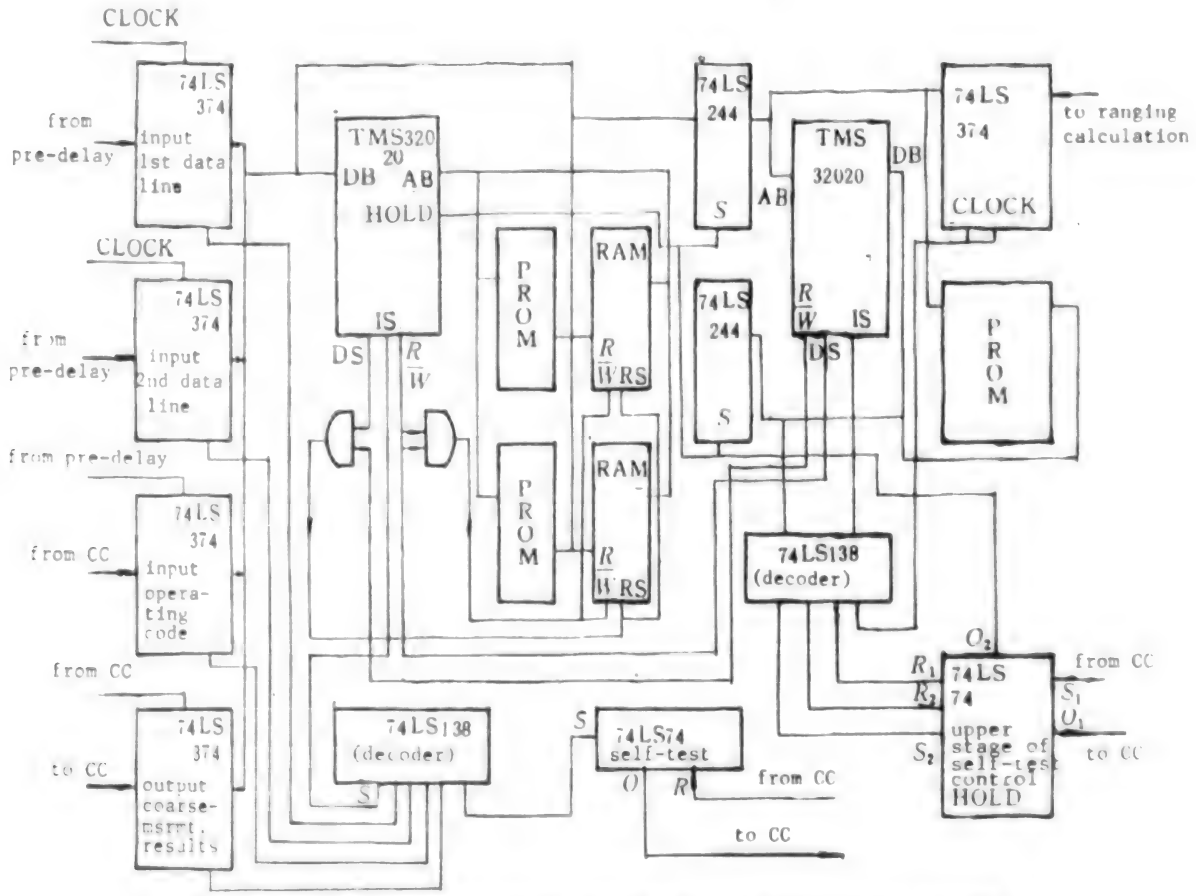

Figure 1. Logic Diagram of Mutual-Spectrum Precision-Measurement Method

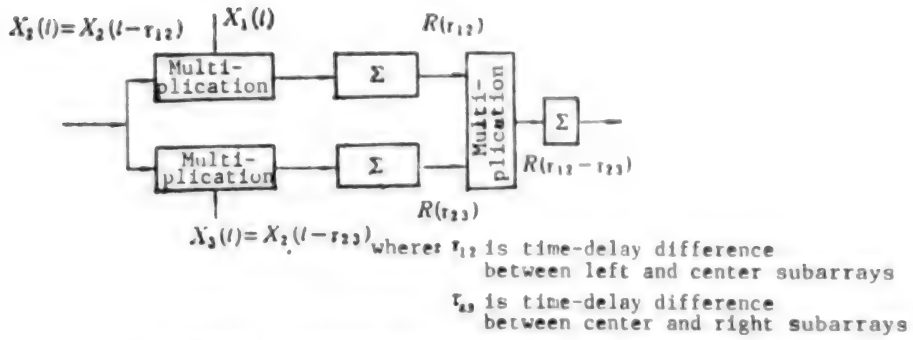

Figure 2. Schematic Diagram of Second-Order Correlation

(2) Second-order correlation method, depicted in Figure 2 below. This technique eliminates signal-transmission fluctuation phenomena that cannot be canceled by first-order correlation.

A parabolic three-point interpolation method, shown below in Figure 3, may be added. The formula for this method is:

$$t_0 = [(Y_1 - Y_3)/(4Y_2 - 2Y_1 - 2Y_3)]\ T_s$$

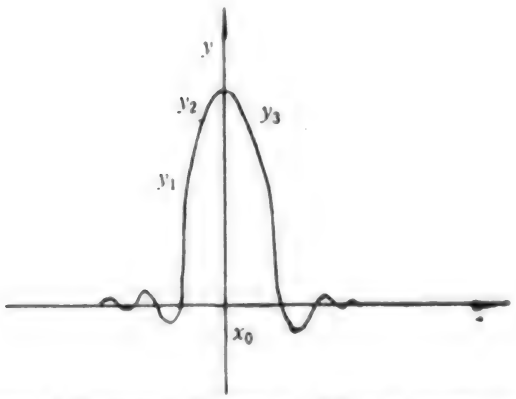

Figure 3. Schematic Diagram of 3-Point Interpolation

(3) Adaptive interpolation method, shown below in Figure 4. This technique employs tapped-delay-line (TDL) adaptive filters, LMS [least mean square] algorithms, and weighting coefficients for interpolation. Average accuracy in delay estimation is better than 40 μs, and this can be reduced to 5 μs if the three-point interpolation method is added on afterward. The LMS algorithm is:

$$W(j+1) = W(j) - u[d(j) - x(j)W(j)]X(j)$$

where W(j) is the weighting coefficient vector, d(j) is the jth sample of the delayed beam, and X(j) is the vector for the leading beam at the multitap.

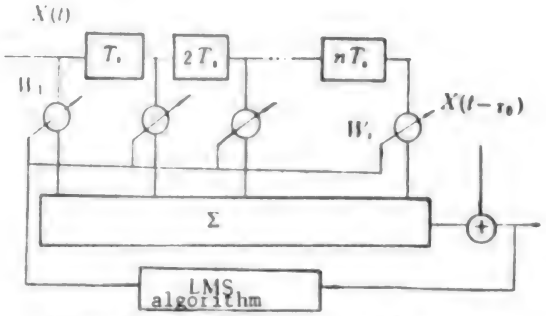

Figure 4. Adaptive Interpolation Method

(4) Split-beam method. This technique splits each of the three subarray inputs into two beams (total of six beams), and then carries out the mutual-spectrum operations on each. The formula for target range is:

$$R = d \sin\alpha/[\sin(\alpha + \beta)]$$

where α and β are the angular separations of the two subarrays.

(5) Polarity correlation method. This high-bit-rate, low-cost technique correlates the polarity among the signals.

Hardware design includes the following main modules: 1) a CC unit, using one TMS32020 chip; 2) A/D converter; 3) filter unit, using three TMS32010 chips, each chip processing three signals; 4) pre-delay unit; 5) an adaptive circuit, using six TMS32020 chips; 6) a mutual-spectrum calculating circuit, using six TMS32020 chips; 7) a unit for calculating range, bearing, and degree of confidence, using one TMS32020 chip; 8) a circuit for displaying range, bearing, degree of confidence, frequency-band code, and self-checking results; 9) a polarity-correlation front-end processor; 10) a unit for calculating range, bearing, and degree of confidence in the polarity correlation, using one TMS32020 chip; 11) a display module; and 12) a clock module. The basic hardware schematics are shown in Figures 5 and 6 below.

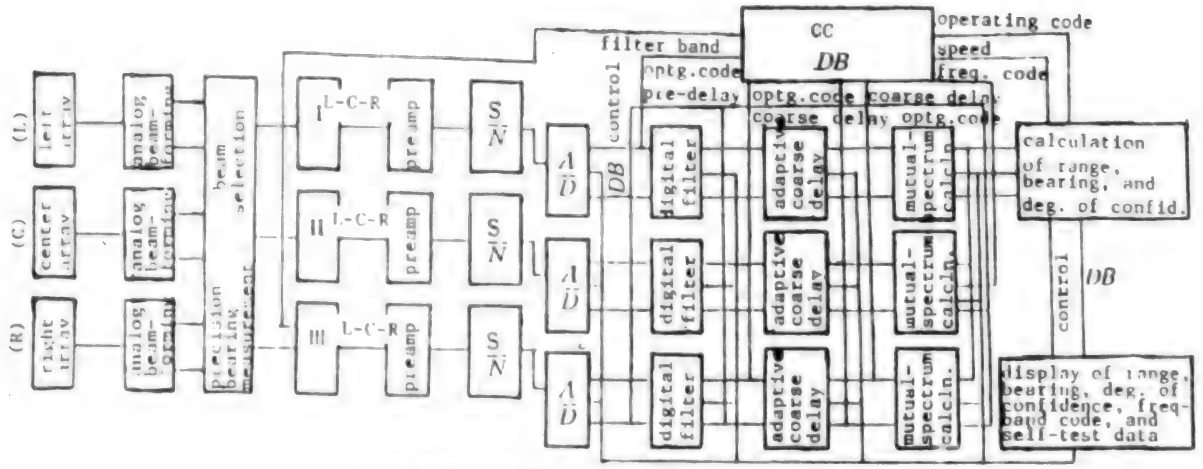

Figure 5. Overall Hardware Schematic

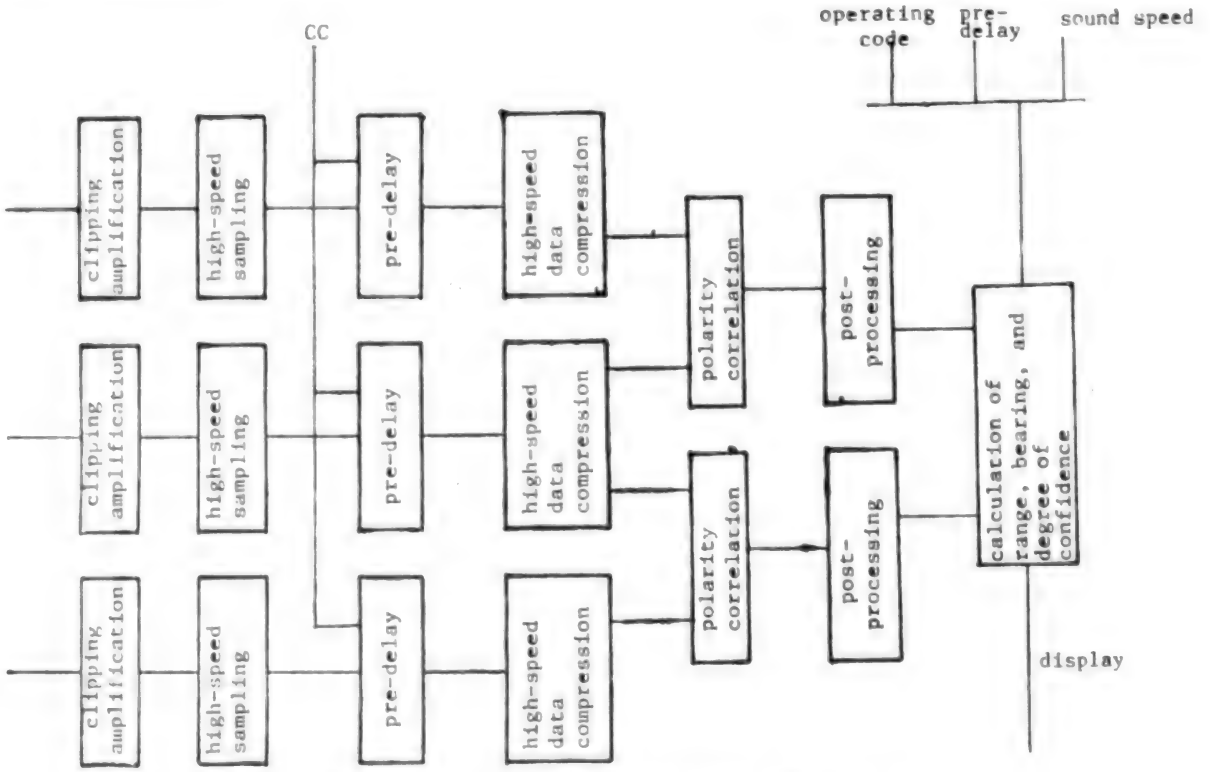

Figure 6. Schematic of Polarity-Correlation Hardware

All the TMS320-series chips in these modules are programmed according to TMS320 assembly-language routines. Flow charts are depicted in Figures 7-10 [not reproduced].

In laboratory simulation of the new sonar signal processor, the authors utilized delay signals generated by the analog delay system independently developed by state-run Plant 613; after amplification and broadband (2kHz-10kHz) filtering with automatic gain control, the signals were sent to the system's input stage. At sea-state level [or stage] 6, with an SNR of 6 dB, range of 15 km, and sound velocity of 1,460 m/s, the targets had a circular motion of 0.1°/s. Using the various operating modes, for targets from 210 to 330° omnibearing, simultaneous tracking measurements of all three targets were carried out, and range values were taken for each 2°. Measured values are shown in Tables 1-4.

Table 1: Measured Range Accuracy Data, Sea-State Level 6, D = 15km, SNR = 6dB, ΔA = 0.1°/s, V = 1460m/s
Time: December 3, 1989
Operating mode: Mode #0 (adaptive mutual-spectrum method)

bearing angle	210°	212°	214°	216°	218°	220°	222°	224°
D_1	17.5	17.2	17.2	16.8	16.5	16.3	16.0	15.7
D_2	14.3	14.5	14.9	14.9	15.0	15.3	15.5	15.7
D_3	14.2	14.4	14.8	14.9	15.1	15.3	15.6	15.8

bearing angle	226°	228°	230°	232°	234°	236°	238°	240°
D_1	15.5	15.4	15.9	14.9	15.8	15.9	25.9	15.7
D_2	15.9	15.9	15.9	16.1	16.5	16.2	16.0	16.0
D_3	15.9	15.9	16.0	16.0	16.2	16.2	16.0	16.0

bearing angle	242°	244°	246°	248°	250°	252°	254°	256°
D_1	15.7	15.5	15.4	15.4	15.4	15.1	15.0	15.0
D_2	15.9	15.8	15.6	15.4	15.4	15.5	15.5	15.4
D_3	15.9	15.7	15.5	15.4	15.4	15.4	15.4	15.4

bearing angle	258°	260°	262°	264°	266°	268°	270°	272°
D_1	14.9	14.6	14.8	14.7	14.9	15.0	15.1	15.1
D_2	15.4	15.4	15.5	15.3	15.2	15.1	15.2	15.1
D_3	15.4	15.3	15.4	15.2	15.1	15.1	15.3	15.2

bearing angle	274°	276°	278°	280°	282°	284°	286°	288°
D_1	14.8	14.7	14.9	14.6	14.6	15.2	15.4	15.6
D_2	15.0	15.0	15.0	14.9	14.8	14.7	14.6	14.6
D_3	15.1	15.1	15.0	14.9	14.7	14.7	14.7	14.7

bearing angle	290°	292°	294°	296°	298°	300°	302°	304°
D_1	15.2	15.1	15.1	15.3	15.4	15.2	15.4	15.7
D_2	14.6	14.6	14.7	14.6	14.5	14.7	14.7	14.6
D_3	14.6	14.7	14.7	14.7	14.5	14.5	14.5	14.5

bearing angle	306°	308°	310°	312°	314°	316°	318°	320°
D_1	15.7	15.7	15.9	15.7	15.9	16.0	16.3	16.3
D_2	14.7	14.6	14.5	14.5	14.7	14.5	14.5	14.6
D_3	14.6	14.6	14.5	14.5	14.6	14.5	14.5	14.7

bearing angle	322°	324°	326°	328°	330°
D_1	16.4	16.7	16.8	17.0	16.6
D_2	14.6	14.5	14.4	14.5	14.4
D_3	14.6	14.5	14.4	14.5	14.4

Table 2: Measured Range Accuracy Data, Same parameters as in Table 1 except for operating mode: mode #1 (Second-order correlation method)

bearing angle	210°	212°	214°	216°	218°	220°	222°	224°
D_1	15.9	16.0	15.6	15.3	15.0	15.0	15.1	15.0
D_2	14.7	14.6	14.3	14.7	14.3	14.2	14.3	14.2
D_3	14.1	13.8	13.6	13.3	13.3	13.5	13.7	13.7
bearing angle	226°	228°	230°	232°	234°	236°	238°	240°
D_1	14.9	14.8	14.7	14.7	14.5	14.6	14.7	14.7
D_2	14.1	14.0	14.0	14.0	13.9	14.0	14.1	14.2
D_3	13.7	13.8	13.8	13.8	13.7	13.8	13.9	14.0
bearing angle	242°	244°	246°	248°	250°	252°	254°	256°
D_1	14.8	14.9	14.9	15.1	15.3	15.5	15.7	15.8
D_2	14.3	14.4	14.4	14.6	14.7	14.9	15.1	15.2
D_3	14.2	14.3	14.5	14.6	14.8	14.9	15.2	15.3
bearing angle	258°	260°	262°	264°	266°	268°	270°	272°
D_1	14.8	14.8	15.8	15.7	15.5	15.6	15.6	15.6
D_2	15.2	15.0	15.2	15.1	14.9	15.0	15.1	15.0
D_3	15.3	15.3	15.4	15.3	15.0	15.1	15.1	14.9
bearing angle	274°	276°	278°	280°	282°	284°	286°	288°
D_1	15.5	15.4	15.4	15.4	15.3	15.5	15.4	15.3
D_2	15.0	14.8	14.9	14.7	14.7	15.0	14.9	14.8
D_3	14.9	14.7	14.8	14.9	14.9	14.9	14.8	14.7
bearing angle	290°	292°	294°	296°	298°	300°	302°	304°
D_1	15.3	15.2	15.2	15.2	15.1	15.0	14.9	15.0
D_2	14.8	14.8	14.5	14.7	14.6	14.5	14.5	14.4
D_3	14.8	14.7	14.7	14.6	14.6	14.5	14.4	14.4
bearing angle	306°	308°	310°	312°	314°	316°	318°	320°
D_1	15.1	14.9	14.7	14.5	14.4	14.6	14.3	14.0
D_2	14.5	14.8	14.6	15.0	14.7	14.8	14.8	14.8
D_3	14.3	14.7	14.4	14.4	14.2	14.3	14.2	14.2
bearing angle	322°	324°	326°	328°	330°			
D_1	13.9	13.9	13.7	13.3	13.3			
D_2	15.1	15.0	15.0	15.1	15.1			
D_3	14.0	14.0	14.2	14.1	14.1			

Table 3: Measured Range Accuracy Data, Same Parameters as in Table 1 except for operating mode: mode #2 (first-order correlation interpolation method)

bearing angle	210°	212°	214°	216°	218°	220°	222°	224°
D_1	15.8	16.1	15.9	15.6	15.9	15.5	15.3	15.0
D_2	15.0	15.7	16.2	15.8	16.0	15.7	15.7	15.8
D_3	14.6	14.5	14.4	14.5	14.6	14.8	15.5	15.2
bearing angle	226°	228°	230°	232°	234°	236°	238°	240°
D_1	14.8	14.8	14.9	14.8	14.4	14.6	14.9	14.9
D_2	16.3	15.9	15.8	15.4	15.0	15.0	14.9	14.8
D_3	15.2	15.4	15.8	16.0	15.5	15.5	15.3	15.3
bearing angle	242°	244°	246°	248°	250°	252°	254°	256°
D_1	14.9	15.1	15.2	15.4	15.5	15.6	15.7	15.8
D_2	14.7	14.7	14.8	15.0	15.0	15.1	15.1	15.2
D_3	15.5	15.3	15.3	15.7	15.9	15.7	15.8	15.6
bearing angle	258°	260°	262°	264°	266°	268°	270°	272°
D_1	15.7	15.9	15.8	15.8	15.7	15.8	15.8	15.7
D_2	15.2	15.3	15.3	15.2	15.3	15.2	15.2	15.3
D_3	16.1	16.2	16.1	16.0	15.9	15.8	15.8	15.6
bearing angle	274°	276°	278°	280°	282°	284°	286°	288°
D_1	15.7	15.7	15.5	15.6	15.5	15.5	15.5	15.4
D_2	15.3	15.3	15.2	15.1	15.0	15.0	15.0	14.9
D_3	15.5	15.5	15.4	15.3	15.2	15.4	15.3	15.2
bearing angle	290°	292°	294°	296°	298°	300°	302°	304°
D_1	15.3	15.4	15.3	15.2	15.1	15.1	15.2	15.2
D_2	14.9	14.8	14.7	14.6	14.7	14.7	14.7	14.7
D_3	15.0	15.2	15.3	15.6	15.5	15.3	15.1	15.3
bearing angle	306°	308°	310°	312°	314°	316°	318°	320°
D_1	15.0	15.0	14.9	14.6	14.1	14.0	13.7	13.8
D_2	14.5	14.6	14.6	14.5	14.9	14.8	14.8	14.7
D_3	15.1	15.2	15.0	15.0	14.9	14.8	14.8	14.7
bearing angle	322°	324°	326°	328°	330°			
D_1	13.6	13.4	13.3	13.2	13.1			
D_2	14.0	14.1	14.4	14.7	14.9			
D_3	15.1	14.9	14.9	14.7	14.6			

Table 4: Measured Range Accuracy Data, Same Parameters as in Table 1 except for operating mode: mode #4 (correlation mutual-spectrum method)

bearing angle	210°	212°	214°	216°	218°	220°	222°	224°
D_1	14.8	15.3	15.7	16.0	16.4	16.5	16.8	16.8
D_2	14.6	15.4	15.9	16.3	16.2	16.2	16.1	16.1
D_3	14.5	14.9	15.1	15.3	15.5	15.6	15.9	15.7
bearing angle	226°	228°	230°	232°	234°	236°	238°	240°
D_1	17.0	16.9	16.8	16.8	16.7	16.6	16.5	16.2
D_2	15.5	15.0	15.0	15.0	14.1	14.4	14.9	15.1
D_3	15.8	15.6	15.6	15.5	15.5	15.5	15.3	15.2
bearing angle	242°	244°	246°	248°	250°	252°	254°	256°
D_1	16.1	16.0	16.0	15.8	15.9	15.7	15.7	15.7
D_2	15.3	15.4	15.1	15.1	15.3	15.7	15.9	15.7
D_3	15.1	14.9	15.2	15.0	15.1	15.0	14.9	15.0
bearing angle	258°	260°	262°	264°	266°	268°	270°	272°
D_1	16.0	15.9	15.8	15.9	15.8	15.8	15.8	15.6
D_2	15.6	15.4	15.4	15.1	15.4	15.2	15.0	14.8
D_3	15.1	15.1	15.0	14.8	14.7	14.7	14.7	14.8
bearing angle	274°	276°	278°	280°	282°	284°	286°	288°
D_1	15.7	15.7	15.5	15.4	15.5	15.3	15.3	15.4
D_2	15.1	14.9	15.1	15.1	15.1	14.9	14.8	14.9
D_3	15.1	14.9	15.1	15.1	15.1	14.9	14.8	15.2
bearing angle	290°	292°	294°	296°	298°	300°	302°	304°
D_1	15.2	15.0	15.0	15.1	15.1	15.1	15.1	15.2
D_2	15.0	15.0	14.9	14.9	15.0	15.0	15.1	14.9
D_3	14.9	14.8	15.0	14.9	14.9	14.9	14.7	14.6
bearing angle	306°	308°	310°	312°	314°	316°	318°	320°
D_1	15.2	15.1	15.1	15.1	15.3	15.3	15.4	15.4
D_2	14.8	14.2	14.0	14.3	15.0	15.0	14.7	14.7
D_3	14.5	14.7	14.7	14.9	15.0	15.3	15.5	15.4
bearing angle	322°	324°	326°	328°	330°			
D_1	15.6	15.6	15.7	15.9	15.9			
D_2	14.8	14.8	15.0	14.8	14.7			
D_3	15.3	15.2	15.3	15.0	14.8			

The authors employed the following RMS error formula

$$a = \sqrt{\frac{\sum_{i=1}^{N} (R_{i\text{ mes}} - R_{\text{mes}})^2}{N}} \Big/ R_{\text{mes}}$$

Figure 7. Ka-Band CW Semiactive Seeker

Percentages of range error are given in Table 5

Table 5. Percentage Error in Range-Finding Accuracy

Range (°)	Percentage error in ranging with different operating modes				
	Target #	Mode 0	Mode 1	Mode 2	Mode 4
-30	1	2.25	3.2	3.9	4.9
-30	2	3.0	2.1	1.5	2.1
-30	3	3.8	2.5	4.7	3.0
-60	1	6.3	3.9	5.0	6.3
-60	2	3.7	3.3	6.1	3.4
-60	3	3.7	5.4	3.8	2.2

As can be seen from this table, the system fully satisfies the requirements for small-sector (+/- 30°) error of under 5 percent and large-sector error of under 8 percent

Domestic Millimeter-Wave Guidance Technology

91P60146 Beijing SHIJIE DAODAN YU HANGTIAN [MISSILES & SPACECRAFT] in Chinese No 1, Jan 91 pp 42-47

[Article by Liu Luqin [0491 7627 0530] of the Beijing General Research Institute of Electronic Engineering: "Millimeter-Wave Guidance Technology and Its Applications"]

[Summary] Millimeter-wave (MMW) homing guidance is one of the four main types of MMW guidance (the other three being MMW command guidance, MMW beam-riding guidance, and dual-mode homing guidance). A subset of MMW homing guidance is MMW semiactive homing guidance, a technology which requires separate receiving and transmitting stations. The radar transmitter, deployed on the ground or other level surface, irradiates the target. The homing head, or seeker, receives the signal scattered by the target, tracks the target, and outputs commands to adjust the missile's course.

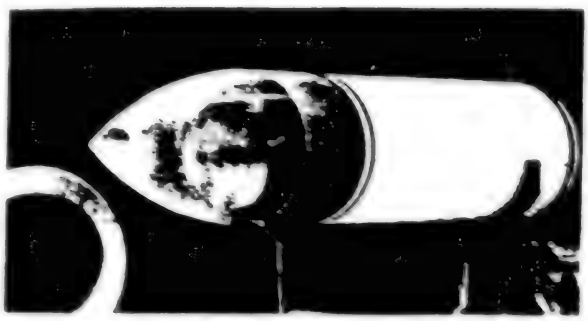

Figure 6. Ka-Band CW Semiactive Seekers

Figure 7. External Appearance of Radome for Ka-Band CW Semiactive Seeker

Figure 6, shown below, is a photograph of a Ka-band continuous-wave (CW) semiactive seeker we have designed. This seeker, which has anti-minimumaltitude-target and antitank capabilities, uses a quasi-feedback-type feed source and a parabolic reflecting plate. When connected up with a dynamic gyro, it can be used for conical scanning. The seeker's radome, in the shape of a pointed cone (see photograph, Figure 7 below), utilizes composite organic materials, which provide good mechanical performance, high transmissivity, and very low aiming error. The receiver front-end processor incorporates hybrid integrated circuits (HICs): the nose returnwave receiver and the tail direct-wave phase-lock receiver are integrated onto one microstrip substrate, as shown in a photograph of the front-end unit (Figure 8, below).

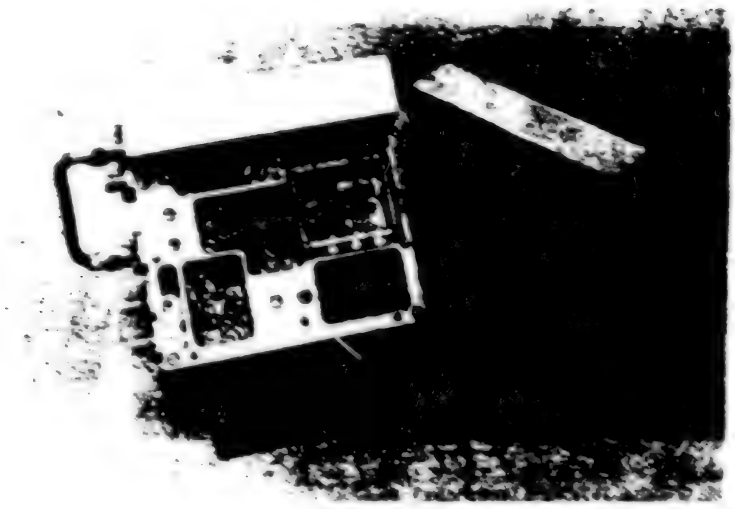

Figure 8. HIC Front-End Processor for Ka-Band Seeker (Includes Nose Receiver, Tail Receiver, Power Supply System, Thermostat System, Voltage-Controlled-Oscillator Loop, etc.)

References

[1] Nicholas C. Currie, Charles E. Brown, "Principles and Applications of Millimeter-Wave Radar."

[2] Thomas W. Glynn, "Millimeter-Wave Radar Seeker A Historical Perspective," MSM, 12/1988.

[3] Mike Williams, "Millimeter-Wave Radar Affordable Sensors for Smart Weapons," MILITARY TECHNOLOGY, 5/1989.

[4] Bill Sweetman, "MLRS to Launch New Weapons," INTERNATIONAL DEFENSE REVIEW, 11/1987.

[5] Brian Wanstall, "Recognising Target at Stand-Off Range—A Place for MMW and IR Sensors," INTERAVIA, 6/1988.

[6] Liu Luqin, "Dynamic Analysis of Precision-Guidance Weapons Development," QINGBAO YANJIU BAOGAO [INFORMATION RESEARCH REPORT], 1/1990.

[7] Mark Hewish, "Inexpensive Millimeter-Wave Seeker on the Way," DEFENSE ELECTRONICS & COMPUTING (SUPPLEMENT TO IDR, 9/1989).

China's TT&C Network

91FE0285A Beijing SHIJIE DAODAN YU HANGTIAN [MISSILES & SPACECRAFT] in Chinese No 11, Nov 90 pp 18-22

[Article by Yang Zhenming [2799 7201 2494] of the National Defense Commission of Science, Technology and Industry (NDCSTI): "China's TT&C Network"]

[Text] Abstract: China's telemetry, tracking & control (TT&C) network consists of two main systems, i.e., launch-vehicle TT&C systems and satellite TT&C network. There are three major launch centers in China, located in Jiuquan, Xichang and Taiyuan, to carry out different launch missions. Satellite TT&C and recovery and performed by the Xi'an Satellite Control Center (XSCC) and five fixed and two mobile TT&C stations and the [two] instrumentation ships called "Yuan Wang."

In April 1970, China successfully launched its first satellite, which signified the establishment of a preliminary TT&C system. China's TT&C network consists of two main systems, i.e., the launch-vehicle TT&C system and the satellite TT&C network. To date, the network has successfully completed the telemetry and control of 29 satellites and is still doing it for three of these satellites which will remain in orbit for some time.

1. Launch-Vehicle TT&C System

The three launch TT&C systems in China serve the three inland launch sites, i.e., the Jiuquan Launch Center in Gansu, the Xichang Launch Center in Sichuan, and the Taiyuan Launch Center in Shanxi, respectively. In November 1975, China successfully launched and recovered a re-entry experimental scientific satellite. That marked the completion of the launch and low-earth-orbit (LEO) satellite TT&C system at Jiuquan. This TT&C system can control launch of satellites with a larger angle of inclination. It is suitable for launching satellites for various exploratory and experimental purposes. In April 1984, an experimental geosynchronous communications satellite was successfully launched from Xichang. This marked the completion of the Xichang launch TT&C system and geosynchronous satellite TT&C system. It controls the launch of low-inclination satellites and is

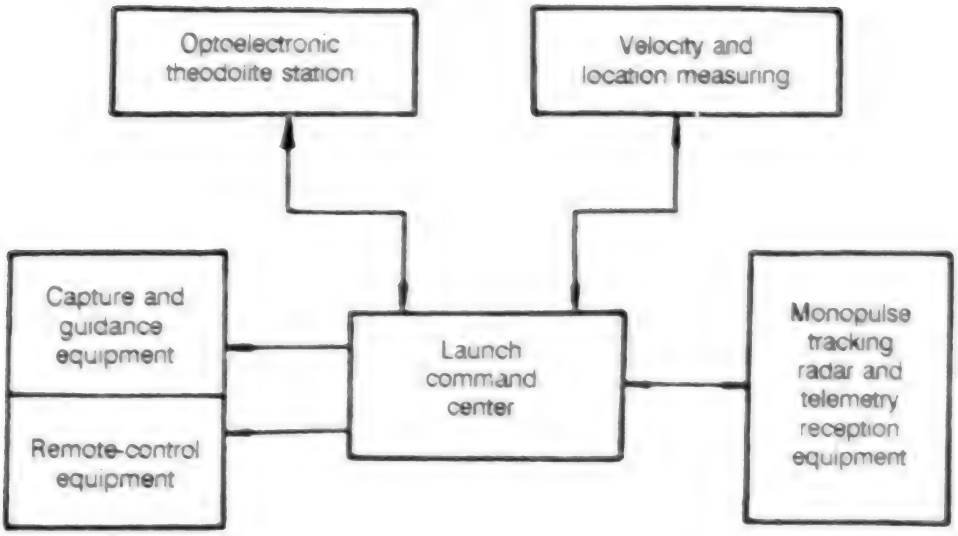

Figure 2. Launch Site Launch-Vehicle TT&C System

primarily used in the launch of geosynchronous satellites. In September 1988, a sun synchronous meteorological satellite, FY-1, was successfully launched from Taiyuan. This marked the completion of the Taiyuan TT&C system which is primarily used for the launch of solar synchronous satellites. These launch sites are shown in Figure 1 [map not reproduced]

Launch vehicles sent up from these sites fly over some cities and industrial installations. Therefore the flight TT&C system has to be able to select a proper point to detonate the rocket in the event of failure to avoid or minimize any damage to cities and industrial installations along its path. This requires high-accuracy measurement of trajectory, real-time data processing, precision safety judgment, and capability to control point of impact. The TT&C also tracks the entire flight of the launch vehicle and provide its data to the next tracking station. It receives the telemetry data sent by the launch vehicle for real-time monitoring and post-flight analysis.

The launch-vehicle flight TT&C system has a launch command center and a tracking and telemetry station. Figure 2 shows an organizational block diagram. Tracking stations located near two flight-control areas may be shared. A launch TT&C system has the following capabilities

Command Center

This receives data from tracking stations and completes real-time processing of measured data, computation and display of flight trajectory, safety determination and issuance of safety control commands. The command center exchanges data with every tracking station (ship) through a variety of means of communication. Remote-control devices are installed nearby and its operating range covers the flight path of the launch vehicle.

Theodolite Station

This is primarily used to monitor the takeoff and first-stage flight. Its typical specifications are as follows. The range of the main camera system is not less than 150 km, overall dynamic angular error (root-mean-square or RMS) is not greater than 10 seconds, and total range error (RMS) is less than 1 m.

High-Accuracy Long-Base-Line-Interferometry Velocity and Position Tracking Station (Jiuquan Launch Center) or Short-Base-Line-Interferometry (SBLI) Velocity Monitoring System with Monopulse Radar Tracking Station

This is the primary source of information for the safe control of the launch vehicle in flight with thrust on. It is slightly inferior to the MISTRAM-1 system used in the U.S. The accuracy of velocity component measurement using the SBLI is 0.1-0.5 mps.

Monopulse Radar Tracking Stations

These form a measurement chain with the transponder on the rocket to measure the external trajectory of the rocket in flight. Fixed radar facilities are usually used over land. In addition, mobile radar tracking stations and the "Yuan Wang" instrumentation ships in the satellite tracking network can be used to expand the tracking range. For fixed monopulse tracking radar, the overall angular error is below 0.2 mil, total range error is less than 10 m (including transponder), and ranging variability is under 0.2 mps. The telemetry system receives data transmitted by the rocket during the entire flight.

All telemetry and tracking facilities and equipment are concentrated when possible for ease of construction, management and command as long as the technical requirements can be met. In the Xichang flight control

area, from takeoff to rocket separation, the flight path covers over 7,000 km. There are five land-based stations and two instrumentation ships. One ship is located near the equator, where the satellite enters its orbit. The measurement range for the Jiuquan and Taiyuan flight-control area is under 3,000 km. There are three major tracking stations. If the flight path is getting longer, then there is a need to add instrumentation ships or mobile stations on islands.

II. China's Satellite TT&C Network

China's satellite TT&C network includes an LEO satellite TT&C network (orbit below 5,000 km) and a geostationary-orbit satellite launch control and position-fixing support network. It mainly consists of XSCC, five fixed-site stations, two mobile stations, mobile recovery stations and two instrumentation ships.

1. Xian Satellite Control Center (XSCC)

XSCC is capable of real-time automatic programming and can simultaneously control several (6) satellites. Inaddition, the system has the capability to perform post-mission analysis and software development.

Central Computer System

It consists of three NCI2780 and two VAX8700 computers and is connected by star couplers through Ethernet, as shown in Figure 3. NCI2780-1 and NCI2780-2 are the two computers forming the independent duplexer. They are not members of the cluster. Their C1 connections only serve as a spare for the Ethernet. The two VAX8700's, NCI-2780-3, and two HSC-50's [sic] form the computer system. These computers are connected to the duplexer through Ethernet. Hence, it is more reliable and has powerful processing capability. The system is equipped with software for multiple satellite control.

Monitoring and Display System

The system provides flight path information and major engineering parameters of the spacecraft to the commander and operators. It displays the information in the form of tables and graphs to protect the mission (see Figure 4 [photograph not reproduced]).

Tracking and Control Software

XSCC has developed a full-range tracking and control software system. Based on the mission, it can be roughly classified into two categories.

(1) LEO satellite tracking and control software (including satellite recovery).

(2) Geosynchronous satellite tracking and control software.

The full-range tracking and control software can be divided into telemetry processing, command generation and verification, orbit data processing, orbit determination and forecast, attitude data processing and attitude determination, orbit and attitude maneuverability, satellite recovery control and monitoring, system-wide simulation, and other ancillary software.

After many years of experience, the XSCC tracking and control software system can meet different requirements for satellite tracking and control in terms of capacity and performance. This is a very effective system.

2. Five LEO Satellite TT&C Stations

These are distributed in eastern, central and western China. They are located at Changchun, Minxi (western Fujian), Nanning, Weinan (southern Henan) and Kashi (Kaxgar) (see Figure 5 [map not reproduced]).

These TT&C stations perform routine tracking and control of LEO and medium-orbit satellites. The Weinan and Minxi stations are responsible for the launch and routine tracking and control of geosynchronous satellites. Nanning and Minxi stations are also responsible for tracking launch vehicles during launch of geosynchronous satellites and tracking and control of LEO satellites upon orbit entry.

3. Two Mobile Stations

These are primarily responsible for the precision control and tracking of recoverable satellites and accurate prediction of landing points. They are also used to cover areas not adequately monitored by fixed stations in rocket flight areas and under certain satellite orbits.

4. Mobile Recovery Station

The function of this station is to search and locate recoverable satellites. The station is equipped with a helicopter, capable of finding, lifting and transporting the re-entry vehicle within a short period of time.

5. Two Instrumentation Ships (see Figure 6 [photograph not reproduced])

These perform re-entry measurement of the launch vehicle at the point of impact over the ocean, track the trajectory of the third stage of the Changzheng-3 [Long March 3] rocket over water and receive measured and telemetry data, and monitor characteristic points of the trajectory, second ignition of the third stage, separation of rocket and satellite and satellite entry into orbit.

Major equipment in a TT&C station includes:

(1) The VHF/UHF TT&C system has either a dispersed (scattered) or unified carrier wave. The scattered system employs a dual-frequency velocimeter to measure the rate of distance change. Its RMS error is below 0.1 mps. With a telemetry demodulating terminal, it is possible to receive satellite signals modulated at the dual frequency band. Its bit rate is less than 10 kbps. The independent remote-control unit issues various commands and provides all kinds of data to the satellite. A unified carrier-wave system shares the same antenna for transmission

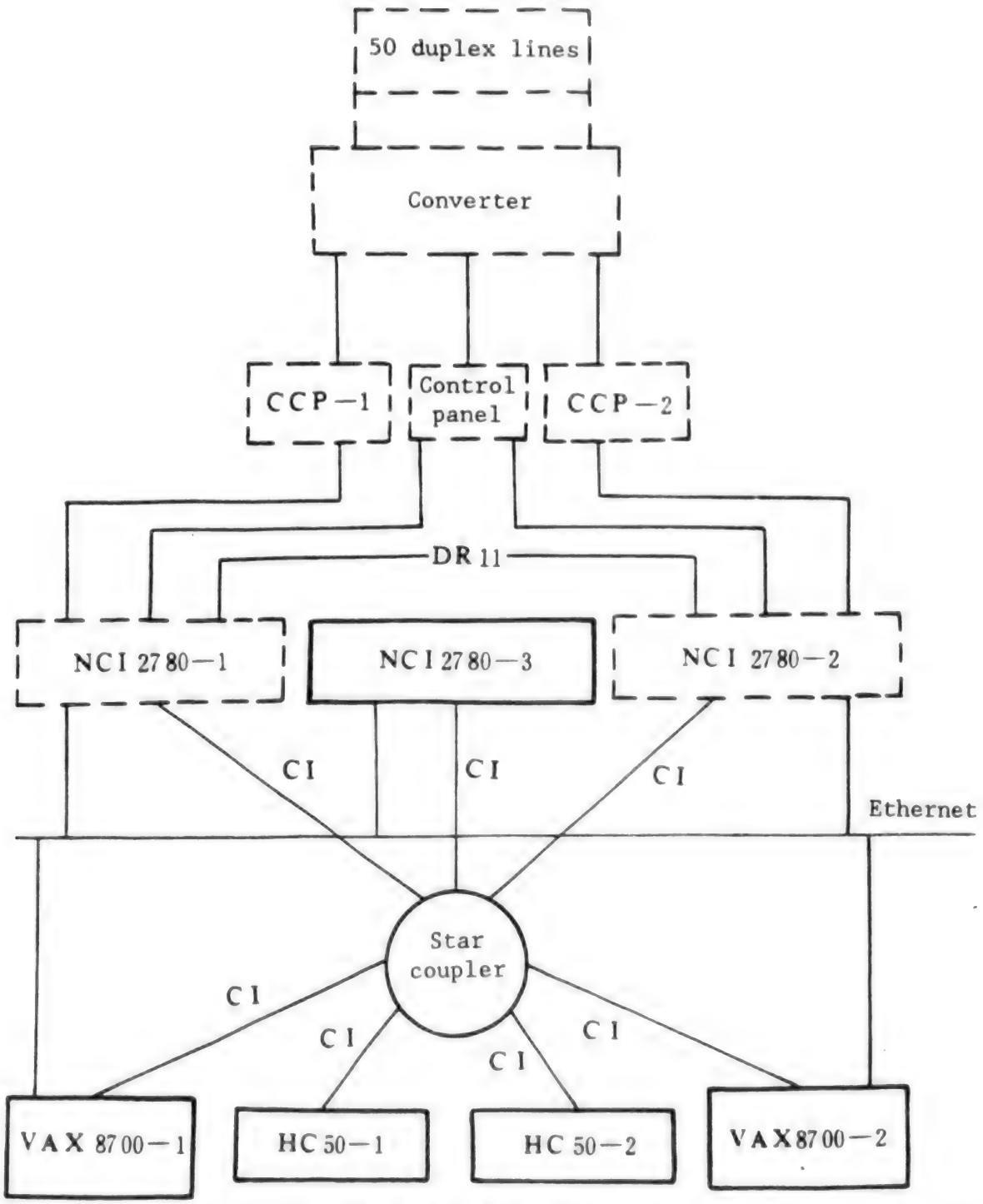

Figure 3. XSCC Central Computer System

and reception. Furthermore, its capability to measure distance and angle is enhanced.

(2) A few TT&C stations are equipped with C-band monopulse radar. Because this radar has more measuring elements, the data obtained is more reliable for orbit-determination. Hence, it is deployed at point of orbit entry and upon satellite re-entry back to earth.

(3) Station computer and display equipment for monitoring and control are used to complete pre-processing of orbit measuring data in a unified manner, to capture digital data obtained from equipment at the station, to transmit data and commands, and to exchange data with XSCC in order to reduce demand on the communication lines.

(4) Timing equipment, command, dispatch and communications equipment are installed for protection.

Geosynchronous Satellite TT&C Stations:

The geosynchronous satellite launch TT&C network includes XSCC (sharing the same facility with LEO satellite TT&C network), Minxi TT&C station, Weinan TT&C station and the two instrumentation ships deployed near the point of orbit entry. Minxi and Weinan TT&C stations and one instrumentation ship are equipped with a C-band unified carrier-wave TT&C system (see Figure 7 [photograph not reproduced]). In coordination with the transponder on the satellite, the system has the capability of orbit tracking, telemetry and remote control of high-orbit satellites below 40,000 km. Its orbit-tracking capability includes measurements of distance, rate of change in distance, orientation (bearing) and pitch angle. A combination of pseudo-coding and sidetone ranging is used in distance measurement. Telemetry includes coded telemetry and analog telemetry. Remote control includes command control and synchronous control. The unified carrier-wave system employs PM/FM modulation for the uplink and PM modulation for the downlink. The accuracy of measurement is summarized as follows. For angle measurement, the random error is 0.15 mil and system error is less than 0.2 mil. For distance measurement, both random error and system error are less than 10 m (uplink carrier-wave phase modulation). Uplink frequency modulation error is 30 m. Uplink phase modulated rate of distance change measurement error is less than 0.03 mps.

Each TT&C station has a C-band unified-carrier TT&C system and a guidance instrument operating at the same frequency. Minxi and Weinan TT&C stations are each equipped with two computers in duplex operation to perform data processing within the station and data exchange with XSCC. In addition to controlling geosynchronous satellites over long periods of time, various other assignments such as attitude and orbit tracking and control are also completed. Moreover, in order to prepare for future missions, TT&C stations must conduct drills to simulate satellite launch and re-entry. In this case, one computer is used for dynamic modelling of a satellite, while the other is used to perform the real mission.

During the launch of a geosynchronous satellite, an instrumentation ship is deployed at the equator near the point of orbit entry. The unified C-band system on the ship is used to perform TT&C and command after the satellite enters its orbit. The C-band monopulse tracking radar can measure the short-arc gliding trajectory of the launch vehicle and its UHF telemetry equipment can receive telemetry data from the carrier rocket to determine the initial orbit of the satellite. During the launch of Asiasat 1, its orbit elements were calculated using these techniques. The ship can receive some satellite telemetry data over a few orbit segments in the first orbit after passing apogee. Furthermore, it can exchange data with XSCC through a satellite communications channel. This TT&S network has successfully completed the tracking and control of five geosynchronous satellites and their routine management.

III. Communications Network

A communications network is used for dispatch and command communications, data transfer and other communications-related services. This comprehensive communications network consists of three parts.

1. Local Communications Network

It is equipped with an internal telephone network, paging equipment, and closed-circuit television. It includes all the internal communications facilities inside a center, TT&C station, or instrumentation ship.

2. Long-range Communications Network

Different means, including wired, radio and dedicated satellite lines, are used to connect all the TT&C stations under the jurisdiction of the launch command center, the TT&C stations (ships) belonging to the satellite control center, the Beijing Command Center under NDCSTI, the launch command center and the satellite control center to ensure long-range command and control, provide data transfer and other services.

3. International Communications

International satellite communications stations were constructed in Beijing, Xian and Xichang. These ground stations have direct access to the INTELSAT network to protect lines leased by the user. During the launch of Asiasat 1, the Xichang international ground station was used.

IV. Further Development of TT&C Network

As space technology advances, a portion of the equipment in China's TT&C network needs to be updated, modified and gradually perfected.

[The nation needs to:]

1. Modify and perfect the launch-support network for geosynchronous satellites to enhance TT&C capability over water. Modify the land-based unified-carrier-wave system to meet requirements for domestic and international C-band satellite tracking and control frequency system.

2. Install S-band unified-carrier-wave system for future use in the launch of [Earth] resources satellites. In addition, establish an international S-band network.

3. From a long-range viewpoint, it is necessary to establish a space-based TT&C system. It can also complete satellite data transfer.

Presently, China's TT&C system can also provide services in launching foreign satellites. It can also support foreign satellites and be linked to foreign satellite networks. As the scope of international cooperation expands, after importing some advanced technology, China's TT&C network will be further perfected.

Growth of Single Crystals of Ytrrium Orthoaluminate Doped With Erbium Ions

40100037A Beijing GUISUANYAN XUEBAO [JOURNAL OF THE CHINESE CERAMIC SOCIETY] in Chinese Vol 18 No 6, Dec 90 (manuscript received 30 Jan 90) pp 524-528

[Article by Li Gansheng, Lu Jian, et al.; Fujian Institute of Research on the Structure of Matter, CAS]

[Abstract] Developing lasers of new wavelength is one of the directions in solid-state laser development nowadays. Erbium-doped yttrium orthoaluminate crystal (Er^{3+}:$YAlO_3$) is an important solid-state laser material for the wavelength of 1.66 μm as well as that of 2.7-2.9 μm. The key problem, however, is the quality of the crystal. Stress has therefore been laid in this paper on the effects of raw material with the addition of nitric acid to eliminate hydration water, nitrogen atmosphere added to a little oxygen and the melt superheat on the quality of Er^{3+}:$YAlO_3$ crystal during the growth process.

Growth of Photorefractive Crystal KTN by Flux Pulling Method

40100037B Beijing GUISUANYAN XUEBAO [JOURNAL OF THE CHINESE CERAMIC SOCIETY] in Chinese Vol 18 No 6, Dec 90 (manuscript received 17 Jan 90) pp 529-535

[Article by Liu Yaogang, Guan Qingcai, et al.; Shandong University]

[Abstract] Growth of large-size, high-quality K(Ta, Nb)O_3 (KTN) crystals by flux pulling method is reported. The size of well-faceted and transparent cubic-phase KTN crystal grown is up to 35 x 33 x 10 mm. The components, homogeneity, electrical and thermal properties of KTN have been measured. Preliminary observations of the photorefractive phenomenon of this crystal are also carried, out. Finally, the relationship between seed orientation and growth shapes is discussed.

Military Distributed Real-Time Operating System Developed

91P60133 Beijing ZHONGGUO DIANZI BAO [CHINA ELECTRONICS NEWS] in Chinese 15 Feb 91 p 3

[Article by Zhang Hancai [1728 3211 2088]: "Distributed Real-Time Operating System XDRMS Prototype Developed"]

[Summary] The "Tactical-Command-Oriented Real-Time Distributed Operating System Applications Research" project undertaken by a Xidian University team led by Prof. Cai Xiyao [5591 1585 1031] has yielded positive results, and the system prototype, designated XDRMS, passed technical appraisal on 11 January [1991]. The development of this system—a key research project assigned to the National Defense Commission of Science, Technology & Industry in the Seventh Five-Year Plan—has overcome problems such as software and hardware resource sharing among different microcomputers, multitasking arising from different requirements of the various users, and real-time data processing. XDRMS will have numerous applications in tactical command systems, real-time data acquisition and processing systems, TT&C systems, embedded computer systems, and other military and civilian computing areas.

Experimental Research on "Dual-Target Butt Joint" Ne-Like Ge High-Gain Soft X-Ray Laser

91P60154A Beijing ZHONGGUO KEXUE, Series A, in Chinese No 2, Feb 91 pp 151-160

[Article by Wang Shiji [3769 0013 4921], Gu Yuan [7357 2266], et al. of the China Engineering Physics Institute's Shanghai Laser Laboratory, Shanghai 201800; Peng Huimin [1756 1920 3046], Sheng Jiatian [4141 1367 3944], et al. of the Beijing Research Institute of Applied Physics & Computational Mathematics, Beijing, 100088; and Lin Zunqi [2651 1415 3825], Wang Shusen [3769 2885 2773], et al. of the High-Power Laser Physics Joint Laboratory (HPLPJL), Shanghai, 201800: " 'Dual-Target Butt Joint' High-Gain Ne-Like Ge Soft X-Ray Laser Experimental Research"; MS received 20 Aug 90]

[Abstract] Utilizing a novel "dual-target butt joint" technique for the two thick, flat, neon-like germanium (Ne-like Ge) targets irradiated by the 1.2 x 10^{13} W/cm^2 (12 terawatts per square centimeter target-surface radiant laser intensity) focused output of a 1.053-μm-wavelength 1-nanosecond-pulse-width, two-beam "Shen Guang" ["Magic Light"] neodymium phosphate glass laser at HPLPJL, the authors observed five Ne-like Ge spectral lines (the 3p-3s transition lines), with respective wavelengths of 19.6, 23.2, 23.6, 24.7, and 28.6 nm. For the 23.2-nm and 23.6-nm lines, the gain-length product GL exceeded 13. The experimental apparatus is shown in Figure 5 below.

Additional parameters of the experiment are as follows:

output energy of each laser beam: approx. 600J
size of laser focal line at target surface: 2.5 cm long x 120 μm wide
positional error between two beams: not over 10 μm
included angle: not over 1 mrad
time delay between beams I and II reaching target: 90 plus or minus 5 ps
size of Ge targets: 2 mm thick (both)
6 mm wide (both)
2.2 cm long (target 1)
0.6-1.8 cm long (target 2)
planar-focal-field grazing incidence grating spectroscope:
grating nominal grid pitch: d_0 = (1/1200) mm
grating concave curvature radius: R = 5649 mm
slit width for incident light: approx. 15 μm
spacing between slit and target chamber center: approx. 65 mm
grazing incidence angle: 87°
film: Kodak 101-07
spectral wavelength: 5-30 nm
spectral resolution: approx. 0.01 nm
Loran circular grazing incidence grating spectroscope:
grating grid pitch: d = (1/1200) mm
grating concave curvature radius: R = 988 mm
slit width for incident light: 5-30 μm
spacing between slit and target chamber center: 60 mm
grazing incidence angle: 88°
film: Kodak 101-01
spectral wavelength: 3-30 nm
spectral resolution: approx. 0.005 nm

Ten other diagrams show various graphs of the data and photos of the spectral lines observed. Table 1 below depicts experimental results, while Table 2 compares the results with those of another Chinese lab, a U.S. lab (Naval Research Laboratory), and a British lab (Rutherford Appleton Laboratory).

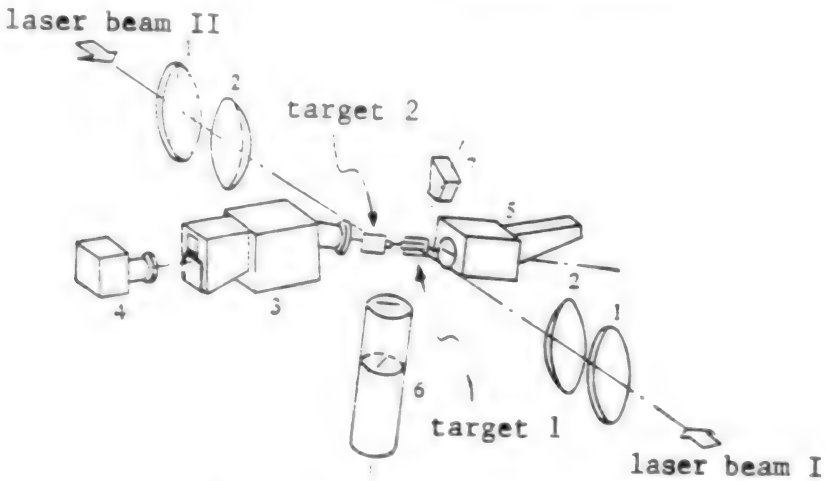

Figure 5: Schematic Diagram of "Dual-Target Butt Joint" Experimental Apparatus

Key: 1. Cylindrical lens array 2. aspherical main lens 3. planar-focal-field grazing incidence grating spectroscope 4. scanning soft-X-ray camera 5. Loran circular grazing incidence grating spectroscope 6. dual-slit X-ray camera 7. KAP flat-crystal X-ray spectrograph

Table 1: Time-Integrated Gain of Ne-Like Ge 3p-3s Transition Spectral Lines

Wavelength λ(nm)	Experimental Results						Simulated results*
	radiant laser intensity 1.2 X 10^{13} W/cm^2			gain factor G(cm^{-1})	radiant laser intensity 0.8 x 10^{13} W/cm^2		
	max. target length L (cm)	gain factor G(cm^{-1})	maximum GL value	max. target length L (cm)	gain factor G(cm^{-1})	maximum GL value	
19.6	4.0	2.26	9.0	4.4	2.06	9.1	2.81-6.06
23.2	4.0	3.35	13.4	4.4	2.25	9.9	3.20-5.64
23.6	4.0	3.39	13.6	4.4	2.28	10.0	3.04-5.04
24.7	3.4	2.27	7.7	—	—	—	1.54-1.98
28.6	3.4	3.21	10.9	—	—	—	3.28-5.68

*In the computer simulation, radiant laser intepsity was (1.2-1.8) x 10^{13} W/cm^2, electron temperature T_e in the plasma gain region was about (7-8) x 10^6K, ion temperature T_i was about 5.6 x 10^6 K, electron density n_e was about (1-2) x 10^{20} cm^{-3}, Ne-like ion abundance N_i (Ne) was about 0.25 N_i, F-like ion abundance N_i (F) was about 0.30 N_i, ion density N_i was about n_e/23

Table 2: 23.6-nm-Wavelength Ne-Like Ge X-Ray-Laser Spectral Line Gain-Length Product (GL) and Its Ratio to Radiant Laser Power (GL/P)

Laboratory*	radiant laser intensity (10^{13}W/cm^2)	effective focal line		gain factor G(cm^{-1})	GL value	GL/P (TW^{-1})
		length (cm)	width (m)			
SLL	1.2	4.0	120	3.4	13.6	23.5
NRL[11]	0.6	1.8	200	4.1	7.4	34.2
INPC[12]	1.0	1.8	180	4.0	7.2	22.2
RAL[2]	2.5	3.2	150	3.8	12.2	19.1

*SLL: Shanghai Laser Laboratory; NRL: U.S. Naval Research Laboratory; INPC: Southwest Nuclear Physics & Chemistry Institute; RAL: U.K.'s Rutherford Appleton Laboratory

References

1. MacGowan, B.J. et al., PROC. SPIE, 688 (1986), 36.

2. O'Neill, D.M. et al., OPT. COMMUN., 75 (1990), 406.

3. Jaegle, P. et al., "Proceedings of the OSA Topical Meeting on Short-Wavelength Coherent Radiation: Generation and Applications, Sep. 26-29, 1988"; North Falmouth, Cape Cod, MA, 1990, Vol 2, 21.

4. Matthews, D. et al., J. OPT. SOC. AM., B, 4 (1987), 575.

5. Hagelstein, P.L., PLASMA PHYS., 25 (1983), 1345.

6. Peng Huimin et al., JISUAN WULI [COMPUTATIONAL PHYSICS], 1 (1990), 91.

7. Chew Wannian et al., CLEO '90, CWF 42 (1990).

8. Eidmann, L. et al., LASER AND PARTICLE BEAMS, 4 (1986), 521.

9. Henke, B.L. et al., ATOMIC DATA AND NUCLEAR DATA TABLES, 27 (1982), 1.

10. Linford, G.J. et al., APPL. OPTICS, 13 (1974), 379.

11. Lee, T.N. et al., PHYS. REV. LETT., 59 (1987), 1185.

12. Peng Huimin et al., IQEC '90, QTh 26, 1990.

1.0-1.7-Micron-Wavelength InGaAs/InGaAsP/InP SAGM APD Developed

91P60151A Shanghai HONGWAI YU HAOMIBO XUEBAO [JOURNAL OF INFRARED AND MILLIMETER WAVES] in Chinese Vol 10 No 1, Feb 91 pp 67-72

[Abstract of article by Li Feng [2621 6912], Wang Shutang [3769 2885 1016], et al. of the Physics Division, Institute of Semiconductors, CAS, Beijing, 100083: "InGaAs/InGaAsP/InP Long-Wavelength Avalanche Photodiodes Studied"; MS received 10 Jul 90, revised 11 Oct 90 (see earlier report in JPRS-CST-91-006, 5 Mar 91 pp 26-27)]

[Abstract] Low-dark-current mesa-type long-wavelength InGaAs/InGaAsP/InP avalanche photodiodes (APDs) with separate absorption, grading, and multiplication (SAGM) regions have been fabricated via liquid-phase

epitaxial growth of InGaAs and InGaAsP layers on an InP substrate. The main characteristic parameters of the device are as follows:

spectral (i.e., wavelength) range λ: 1.0-1.65μm
breakdown voltage V_B: 80V (60V min., 120V max.)
dark current I_D (at $V_R = 0.9V_B$): 20nA (50nA max.)
responsivity R (at λ = 1.3μm): 0.7 μA/μW (0.6 min., 0.8 max.)
pulse response time t (at λ = 1.3 μm, M = 10): 100ps (300 ps max.)
excess noise factor F (at M = 10): 5
maximum multiplication factor M_{max}: 30 (20 min., 50 max.)
sensing-surface diameter D: 75μm

A cross section of the device is shown in Figure 1 below. Six other figures (not reproduced) depict the electric-field distribution in the depletion region, the relation between charge densities of different layers, InP thickness as a function of growth time, lattice-mismatch parameters for varying InAs content, the influence of environmental humidity on V_B, and dependence of photocurrent and dark current on reverse bias. Two tables list the design parameters and the aforementioned main characteristic parameters.

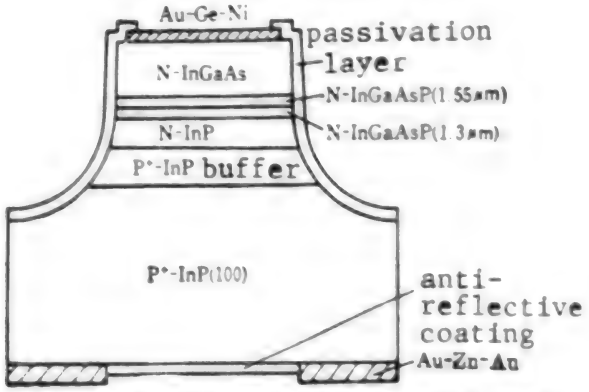

Figure 1. Cross Section of InGaAs/InGaAsP/InP SAGM APD

References

1. Hurwitz, C.E., Hsieh, J.J., APPL. PHYS. LETT., 1978; 32 (8): 487.

2. Osaka, F., Mikawa, T., IEEE J. QUANTUM ELECTRON, 1986; GE22 (3): 471.

3. Matsushima, Y., Sakai, K., IEEE ELECTRON DEVICE LETT., 1981; EDL2 (7): 179.

4. Nakajima, K., Yamazaki, S., J. CRYSTAL GROWTH, 1982; 59 (3): 572.

5. Nakajima, K., Kusunoki, T., FUJITSU SCI. TECH. J., 1980; 16 (4): 59.

New Method of Track Processing HF Skywave OTH-B Radar

91P60138A Beijing DIANZI XUEBAO [ACTA ELECTRONICA SINICA] in Chinese Vol 19 No 1, Jan 91 pp 1-6

[Article by Jiao Peinan [3542 1014 0589] of the China Research Institute of Radio-Wave Propagation, Xinxiang: "New Method of Track Processing in HF Skywave OTH-B Radar"; MS received Jun 89, revised Feb 90]

[Abstract] The concept of the pattern-recognition tracking/coordinate-transfer data processor for a high-frequency (short-wave) skywave backscatter over-the-horizon radar (OTH-B radar) is described. Based on algorithms previously published by the author [7,8,9], a comprehensive new method for determining the ground distance D of the target and its track from a conversion of the radar time delay P (i.e., a new P-D transfer method)—in conjunction with the other input variables such as Doppler frequency f_d, operating frequency f, and time t—is presented. The data can be obtained from a monostatic (i.e. single-station) radar system; there is no need to know the ionospheric data of the middle point.

In testing of the new technique, an experimental OTH-B system with a detection energy of 97dB-joules was employed. The emitter array consists of an eight-element vertically polarized log-periodic (VPLP) antenna fan array, while the receiver array consists of a 300-m-aperture 32-element VPLP antenna linear broadside array. The linear-frequency-modulated pulsed Doppler radar has an average power of 90kW, a pulse width (τ) of 3.5 milliseconds, a repetition frequency of 150Hz, and a coherent storage time of 5 seconds. This radar was tested at 40 different times in various seasons over a 3-year period with a variety of targets—the 40 sorties tracked included flights of aircraft ranging in size from a B747 down to a Jian-6 fighter. Comparing the track results calculated by the system with the actual ground-track data provided by three ground tracking stations (Jiuquan, Minqin, and Wuzhong), an average error of only 4 percent was found. Two examples (shown in Figure 4 below) are given: the track of a B707 (flight #PK752) on 19 December 1982 at three different frequencies—20.5, 18.5, and 14.5MHz; and the track of a B707 (flight #CA948) on 22 December 1982 at two different frequencies—22.0 and 14.5MHz. As shown in the figure, target range ran from 900 to 1550 kilometers. The other three figures (not reproduced) depict the effect of the ionosphere on the P-f relationship, a block diagram of a feedback-type pattern-recognition tracking device, and the relationship of the experimental data with the data provided by the ground tracking stations.

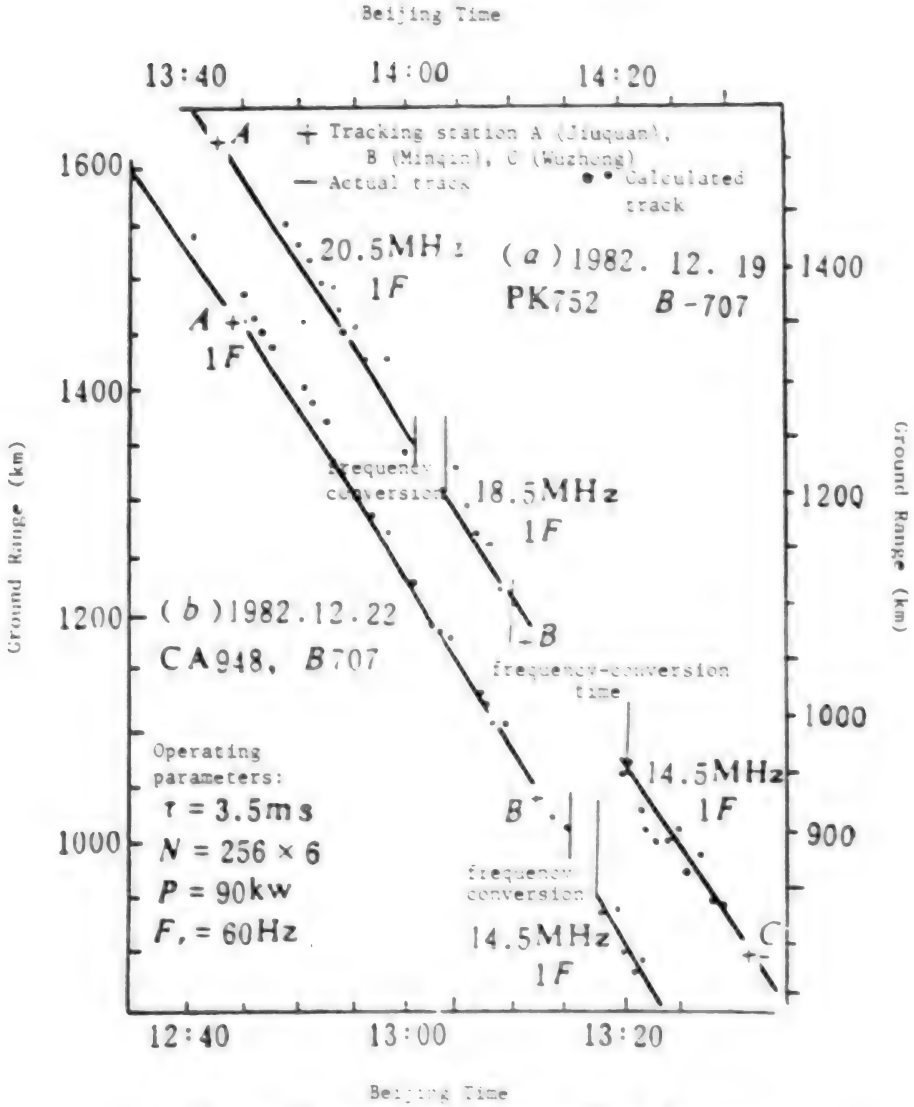

Figure 4. Two examples of Results of Track Processing

References

[1] J.M. Headrick and M.I. Skolnik, PIEEE, Vol 62, No 6, 1974, pp 664-671

[2] P.N. Dewitt, AD-A013648.

[3] Li Chonggeng, XIANDAI LEIDA [MODERN RADAR], Vol 6, No 4/5, 1984, p 276.

[4] IU. A. Chernov, "Vozvratno-naklonnoye Zondirovanie Ionosfery" ["Reverse-Slope Sounding of the Ionosphere"], 1971.

[5] T.A. Croft, RADIO SCI, No 3, 1968, pp 69-74

[6] Huang Xiwen, Li Yongjun, DIANBO KEXUE XUEBAO [JOURNAL OF ELECTRIC WAVE SCIENCE], Vol 1, No 2, 1986, pp 36-42.

[7] Jiao Peinan, Zhu Qiguang, WUHAN DAXUE XUEBAO [JOURNAL OF WUHAN UNIVERSITY], Vol 4, 1985, pp 63-70.

[8] Jiao Peinan, Du Junhu, KONGJIAN KEXUE XUEBAO [CHINESE JOURNAL OF SPACE SCIENCE], Vol 7, No 1, 1987, pp 59-64.

[9] Du Junhu, Jiao Peinan, KONGJIAN KEXUE XUEBAO [CHINESE JOURNAL OF SPACE SCIENCE], Vol 7, No 3, 1987, pp 229-233.

Computer Simulation of Digital Compensation for Radar Transmitted Signals

91P20138B Beijing DIANZI XUEBAO [ACTA ELECTRONICA SINICA] in Chinese Vol 19 No 1, Jan 91 pp 15-19

[Article by Xie Yun [6200 5089] and Mao Yuhai [5403 0060 3189] of the Department of Electronic Engineering, Qinghua University "Computer Simulation of Digital Compensation for Radar Transmitted Signals", MS received Apr 89, revised Dec 89]

[Abstract] Digital compensation to eliminate instabilities in the frequency, phase, and amplitude of transmitted radar signals is an effective method studied worldwide since the early eighties for improving the performance—especially in terms of the signal-to-noise improvement factor I—of power-oscillating-type radar moving target indicators (MTI) or moving target detectors (MTD) [2,3]. The basic digital-compensation system, shown in block-diagram form in Figure 1 below, consists of a digital dynamic transversal filter. After filtering of the A/D sampled radar echo, the signal's impulse response after A/D sampling then becomes the next transmitted radar pulse, or its inverse on the time axis (convolution or correlation, respectively, of the transmitted wave with the radar echo). In this study, computer simulation of the digital compensation is carried out; a QU-68000 microcomputer is used, and the program is written in the FORTRAN-77 high-level program language

Simulation results are: for suppression of pulse-to-pulse frequency jitter (1st-order phase jitter) in the transmitted signal, the digital-compensation convolution processing technique raised I by 12-13dB over the value obtained from the correlation technique and by 16dB over the uncompensated signal. Additional results are given in Tables 1 and 2 below

Table 1. Digital Compensation for Suppression of Common Phase Jitter

limit of I for transmitter signal pulse-to-pulse phase jitter		limit of I for transmitter signal after digital compensation	
1st-order phase	2nd-order-and-higher phase	convolution processing	correlation processing
30dB	30dB	42.6dB	33.7dB
42dB	30dB	43.5dB	42.3dB
30dB	45dB	46.6dB	33.8dB

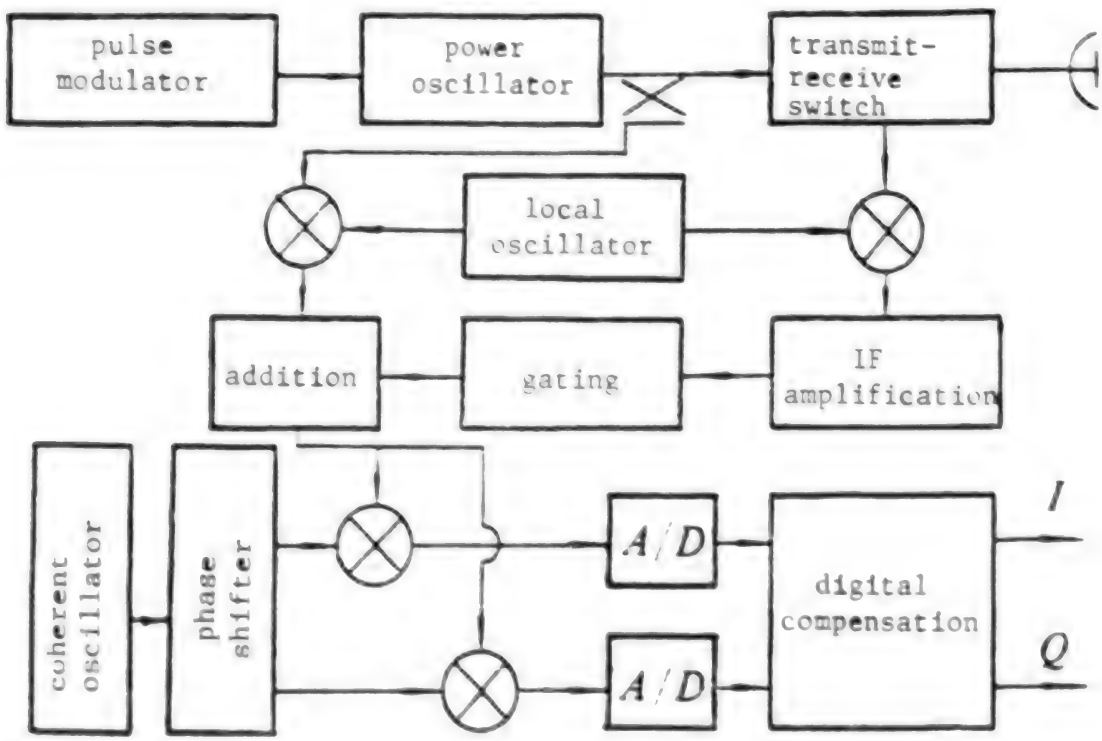

Figure 1. System Schematic

Table 2. Comparison of Convolution, Correlation, and Non-linear Processing

limit of I for transmitter signal		limit of I for transmitter signal after digital compensation		
1st-order phase	2nd-order-and-higher phase	convolution processing	correlation processing	non-linear processing
30dB	30dB	42.6dB	33.7dB	35.1dB
42dB	30dB	43.8dB	42.3dB	40.0dB
30dB	45dB	46.6dB	33.8dB	37.1dB

Four additional figures show various graphs of the data. The results of the simulation indicate that convolution processing can provide a maximum I of 18dB for instabilities in the transmitted signal. More detailed results are given in reference [6]. Actual domestic testing of the system demonstrates that 10-12-point convolution processing can raise the limit of I for instabilities in the radar transmitted signal by about 10dB.

References

[1] M.I. Skolnik, "Radar Handbook" [trans. into Chinese], National Defense Industries Publishing House, 1974.

[2] Liu Shusheng, "Some Problems in Radar Anti-Jamming," XITONG GONGCHENG YU DIANZI JISHU [SYSTEMS ENGINEERING AND ELECTRONIC TECHNOLOGY], No 6, 1986, pp 21-29.

[3] Ji Guoliang, "Transformation Paths and Prospects for China's Outmoded Magnetron Radars," SELECTED PAPERS ON RADAR ANTI-JAMMING, Electronic Countermeasures Editorial Department, April 1986, pp 34-41.

[4] R.L. Trapp, "Improved Coherent-on-Receive Radar Processing with Dynamic Transversal Filter," RADAR-82 International Conference, October 1982, pp 505-508.

[5] Zheng Qingyi, "Digital Correction of Radar Transmitter System Instabilities," Master's Thesis, Qinghua University, 1984.

[6] Xie Yun, "Use of a Monolithic Signal Processor for Digital Compensation of Transmitted Radar Signal Instabilities," Master's Thesis, Qinghua University, 1986.

[7] Shan Xiuming et al., "Ideal Receiver Coherence Method for an Improved Transmitter with Instabilities," XINHAO CHULI [SIGNAL PROCESSING], Vol 4, No 4, December 1988, pp 214-219.

Spaceborne SAR Imagery Processing

91P60138C Beijing DIANZI XUEBAO [ACTA ELECTRONICA SINICA] in Chinese Vol 19 No 1 Jan 91 pp 20-24

[Article by Li Chunsheng [2621 2504 0581], Li Jingwen [2621 2529 2429], and Zhou Yinqing [0719 5593 3237] of Beijing Aerospace University: "Spaceborne SAR Imaging Processing"; MS received 26 Apr 89, revised Dec 89]

[Abstract] A method for implementing spaceborne synthetic aperture radar (SAR) image processing is proposed. A time-domain/frequency-domain hybrid correlation technique is applied for azimuth compression, and a clutterlocked self-focusing multiview processing technique is used on the subimages to estimate Doppler center frequency and deviations in Doppler frequency rate of change induced by antenna pointing error or SAR dynamic instabilities and to perform image restoration. The results of computer simulation show that this method is effective. Three figures depict a block diagram for a basic SAR system and two 3-D plots (unscaled) showing spikes (towers) in f_D (Doppler center frequency) and f_R (rate of change of Doppler frequency).

References

[1] J.C. Curlander, C. Wu, A. Pang, "Automated Processing of Spaceborne SAR Data," JPL, California Institute of Technology.

[2] Chialin, K.Y. Liu, Michael Jin, "Modeling and a Correlation Algorithm for Spaceborne SAR Signals," IEEE TRANS., Vol AES-18, No 5, September 1982.

[3] F.K. Li, D.N. Held, J. Curlander, [C.] Wu, "Doppler Parameter Estimation for Spaceborne Synthetic Aperture Radars," IEEE TRANS. ON GEOSCIENCE AND REMOTE SENSING, Vol GE-28, No 1, January 1985.

[4] Michael Y. Jin, "Optimal Doppler Centroid Estimation for SAR Data from a Quasi-Homogeneous Source," IEEE TRANS. ON GEOSCIENCE AND REMOTE SENSING, Vol GE-24, No 6, November 1986.

Simultaneous Motion Compensation, Radar Imaging

91P60138D Beijing DIANZI XUEBAO [ACTA ELECTRONICA SINICA] in Chinese Vol 19 No 1 Jan 91 pp 122-125

[Article by Wu Xiaoqing [6762 1420 7230] and Zhu Zhaoda [2612 0340 6671] of the Department of Electrical Engineering, Nanjing Aeronautical Institute: "Simultaneous Motion Compensation and Radar Imaging"; MS received Aug 89, revised Mar 90]

[Abstract] Motion compensation—a key problem in inverse synthetic aperture radar (ISAR)—and radar imaging are treated as problems of localization of multiple scatterers[4]. The maximum-likelihood technique is used to simultaneously estimate target motion parameters and target radar image. The DFT (discrete Fourier transform) is introduced, and computational efficiency is greatly enhanced by applying its FFT (fast Fourier transform) shortcut under certain assumptions. When the range between radar and target is a quadratic time

function, it can be represented by a simplified algorithm—derived on the basis of the trackfitting method[2,3] and presented here—to simultaneously achieve motion compensation and imaging.

Figure 1 (not reproduced) depicts the geometrical relationship between target and radar. Computer simulation was carried out with the target shown in Figure 2 below as the scatterer. In Figure 3, also shown below, the normal-line range R_0 from target to linear flight track is 30km, and the angular separation φ between the radar-to-target axis of sight and the aforementioned normal is 20°. Target velocity is 200 m/s. Radar wavelength is 3cm, prf is 800Hz, and the pile-up pulse number is 2048. Target corner is 0.92° and range resolution is 0.5m. In the simulation, the authors employed the spatial-domain

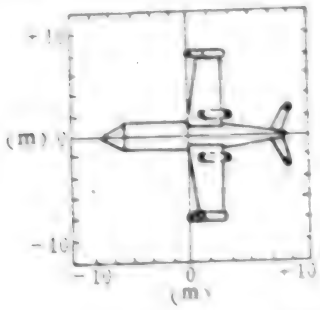

Fig. 2: Aircraft Scatter Model

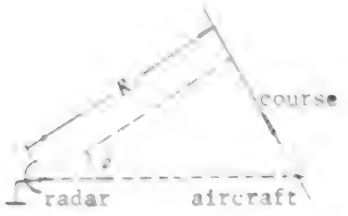

Fig. 3: Aircraft Linear Flight Track

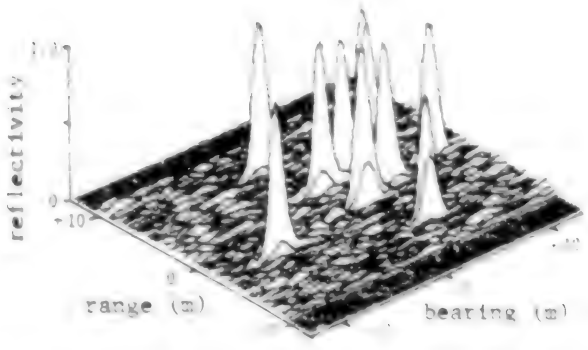

Fig. 4: Image of Aircraft in Linear Flight Realized Via Simultaneous Motion Compensation and Imaging Method

cross-correlation technique to effect range alignment. Figure 4, also shown below, depicts the results of applying the new technique to generate an image of the aircraft in straight-line flight with an SNR of 3dB.

References

[1] M.J. Prickett and C.C. Chen, "Principles of Inverse Synthetic Aperture Radar Imaging," IEEE 1980 EASCON Record, pp 340-345.

[2] C.C. Chen and H.C. Andrews, "Target-Motion-Induced Radar Imaging," IEEE TRANS, Vol AES-16, pp 2-14, 1980.

[3] K.K. Eerland, "Application of Inverse Synthetic Aperture Radar on Aircraft," PROC OF THE INTERNATIONAL CONFERENCE ON RADAR, Paris, pp 618-623, 1984.

[4] L. Peter, Jr. and E.C. Weimer, "Tracking Radars for Complex Targets," PROC IEEE, Vol 51, pp 2149-2162, December 1963.

[5] G. Dike, et al., "Inverse SAR and Its Application to Aircraft Classification," IEEE 1980 INTERNATIONAL RADAR CONFERENCE Record, pp 161-167.

10kW-Level CO_2 Laser Unveiled

91P60135b Beijing ZHONGGUO KEYUE BAO [CHINESE SCIENCE NEWS] in Chinese 22 Feb 91 p 2

[Article by Huang Xin [7806 6580]: "10,000-Watt-Level CO_2 Laser Unveiled in Shanghai"]

[Summary] Shanghai—A CAS Shanghai Institute of Optics & Fine Mechanics (SIOFM) research team led by Research Fellow Wang Runwen [3769 3387 2429] recently successfully completed a 5-year project to develop a tube-plate-type [guan ban shi] 10-kilowatt-level CO_2 laser, signifying that the nation's research on high-power CO_2 lasers is at the international state-of-the-art. This apparatus, used in surface heat treatment of metals, molten covering [rong fu], deep-penetration welding, thick-steel-plate cutting, and similar laser-machining processes, has heretofore been developed only by a small number of nations, including the U.S., USSR, and Japan. The SIOFM-developed laser has a non-plated-film domestically made zinc-selenide output window, a stable-cavity iris mode-selection device, a 6KW low-order-mode output, good beam directionality, and a divergence angle (full angle) of 2.2 milliradians.

State-of-the-Art YAG Laser

91P60140A Beijing RENMIN RIBAO in Chinese 5 Mar 91 p 5

[Article by Zhu Yuquan [2612 3768 3123]: "Two Important Achievements in Laser Instrument Research Obtained"]

[Summary] Two laser instruments, a YAG-laser-pumped dye laser and an argon-ion-laser-pumped ultrashort pulsed dye laser, have been developed by the Precision Instruments Department of Tianjin University and the Institute of Modern Optics at Nankai University respectively. The quasi-continuous YAG-laser-pumped dye laser is the first to use an acousto-optical Q-switched internal-cavity multiple-frequency YAG laser as a pumping source to remove obstacles encountered in using semi-continuous-pumped dye lasers. The repetition rate, tuning range, and output power of the YAG-laser-pumped dye laser have all reached world advanced levels. This instrument is an important tool for conducting research in laser spectra, laser detection, isotope separation and nuclear science. The argon-ion-laser-pumped dye laser is capable of producing even narrower light pulses. Compared with products made abroad, it is superior in terms of length of operating life, narrowness of pulse width, and continuously adjustable range of output pulse wavelength. It will be useful for studying ultrafast phenomena in physics, chemistry and biology because of its capability to slow down the ultrafast process. The instrument can record speeds as fast as a trillionth of a second (a picosecond), encountered in the photosynthesis process, and is also a powerful tool for conducting high-tech research in optical communications, optical computing, molecular tailoring and new-material synthesis.

29 Optoelectronics Projects Accredited

91P60134A Beijing ZHONGGUO DIANZI BAO [CHINA ELECTRONICS NEWS] in Chinese 17 Feb 91 p 1

[Article by Ren Guangquan [0117 0342 3123]: "Optoelectronics Technology in Seventh 5-Year Plan Again Reaches New Stage"]

[Summary] It has been learned from MMEI's Institute 44 that 29 key State Seventh 5-Year Plan projects and "863" Program ("information acquisition and processing" area) optoelectronics-related items developed by the institute have recently passed expert technical appraisal. Of these, 20 items are in the lead domestically, and 16 have technical indicators that match the eighties international state-of-the-art. The breakthrough development of the type GT1352 1.3-micron-wavelength single-mode all-metallized-coupling packaged laser diode assembly and six other projects belong to the Seventh 5-Year Plan, while the development of the type GT5560F all-metallized-coupling packaged InGaAs avalanche photodiode (APD) and other projects are part of the "863" Program. The laser diode package, InGaAs APD and other optoelectronic devices among the 29 projects will find applications in fiber-optic communications equipment, fiber-optic sensors, graphics/text FAX equipment, laser products, and defense engineering equipment.

New Dye Laser Used in Eye Treatment

91P60140B Beijing ZHONGGUO KEXUE BAO [CHINESE SCIENCE NEWS] in Chinese 5 Feb 91 p 2

[Article by Cai Dashu [5591 1129 1859]: "New Medical High-Tech Product Developed by Shanghai Fudan University and Shantou Weida Corporation"]

[Summary] A new DOL-IV-type dye laser instrument for eye treatment has been developed by the Shantou Weida Medical Instruments Group and Shanghai Fudan University. The instrument has been clinically tested in several hospitals including Guangdong Provincial People's Hospital, and remarkable results have been obtained. The instrument produces pulses which excite a thyratron to put high pressure on the dye laser device containing a ring-like electrode and a coaxial xenon lamp pump. The steady laser beam generated by this laser device is the source used for eye treatment. The new instrument can be used for treating several eye diseases such as angle-closure glaucoma.

Overview of Domestic Radar Industry in Seventh 5-Year Plan

91P60138E Beijing ZHONGGUO DIANZI BAO [CHINA ELECTRONICS NEWS] in Chinese 17 Feb 91 p 1

[Article by Liu Dong [0491 2639]: "Mixed Results for Radar Industry"]

[Summary] The nation's radar industry in the Seventh 5-Year Plan can be summarized as follows: numerous achievements, numerous problems. China's military radar has improved in terms of reliability and degree of automation. Domestically made airborne radars, shipborne radars, land anti-aircraft radars, tracking and control radars, and anti-jam radar employ advanced Doppler pulse technology, frequency agile technology, digitized technology, and phased array technology; they have improved to the late-seventies/early-eighties international level. Some Chinese-made military radars have been sold abroad. Another bright spot is the nation's first Air-Force-grade theater multifunctional command and control system, independently developed by MMEI's Research Insitute 28; this system consists of [60] pieces of equipment, including over [100] networked minicomputers and microcomputers, has ruggedized software written with 540,000 lines of code, a multi-tasking overall design, a monitor vocoder, superior anti-aircraft weapons, a man-machine interface, and Chinese-character-processing and Chinese-speech-input functions. It is at the forefront domestically and meets mid-eighties international standards.

Civilian radar has also advanced to the eighties international level. One of the more prominent examples of direct economic benefits produced by civilian radar is associated with the model CTL-88 digital weather radar manufactured by the Changhai Machinery Plant in Guilin. In 1990, this radar accurately predicted [illegible]

rainfalls on over 10 separate occasions, thereby alerting managers at saltworks to cover 50,000 tons of product salt with plastic sheeting. Problems have also surfaced, principally due to shortages of investment funds for R&D at the nation's 40-odd radar R&D/manufacturing plants.

China already has a sufficient number of such units—including facilities under MMEI, the Ministry of Aerospace Industry, the former Ministry of Ordnance, and the China State Shipbuilding Corp.—but better government planning and inter-plant cooperation is needed for further progress. Greater efforts are also needed in the area of domestic market share: while the nation's military radars are all made domestically, many of the civilian radars are imported, despite the fact that Chinese-made radars that meet the needs of civilian users are available. Government authorities should adopt the relevant policies for ensuring that domestically made radars are purchased first.

GaAs/AlGaAs DH Lasers Fabricated on Space-Grown Si-GaAs Monocrystalline Substrate

91FE0254A Beijing BANDAOTI XUEBAO [CHINESE JOURNAL OF SEMICONDUCTORS] in Chinese Vol 11 No 10, Oct 90 pp 795-798 [MS received 9 Nov 89]

[Article by Shi Zhiwen [4258 1807 2429], Luo Liping [5012 7787 5493], and Lin Lanying [2651 5695 5391] of the CAS Institute of Semiconductors, Beijing, supported by the Chinese National Natural Science Foundation: "GaAs/AlGaAs DH Lasers Fabricated on Space-Grown Si-GaAs Monocrystalline Substrate"; see earlier brief report in JPRS-CST-90-006, 23 Feb 90, pp 11-12]

[Text]

Abstract: For the first time, GaAs/AlGaAs proton-bombardment DH (double heterojunction) lasers with CW [continuous-wave] operation at room temperature were successfully fabricated on single-crystal Si-GaAs grown in space on a Chinese satellite. The DH layers were grown by LPE (liquid phase epitaxy). The minimum threshold current is 20 mA, the lasing wavelength is 857 nm, and the output power is as high as 30 mW.

I. Introduction

As space technology advances, study of space materials is also moving forward. Monocrystalline Te-GaAs was first successfully grown on a Chinese satellite in 1987. A number of studies have been conducted to analyze this single crystal.[1,2,3,5] It was used as the substrate of a GaAs/AlGaAs SH [single heterojunction] LED.[4] In 1988, monocrystalline Si-GaAs was successfully grown in space. This paper describes a GaAs/AlGaAs DH laser with CW operation at room temperature; this laser was developed in July 1989 using that single crystal as its substrate.

II. Laser Fabrication

Number 6 wafer of the space-grown Si-GaAs single crystal was used as the substrate. It is located at the center of the single crystal with $n = 1.28 \times 10^{18}$ cm^{-3}. It is a small round piece, 6.5 mm in diameter. The DH epitaxial layers were grown by LPE at 800°C. At the same time, a small round piece of space-grown Si-GaAs substrate, approximately 7.5 mm in diameter with $n = 5 \times 10^{18}$ cm^{-3}, was also grown epitaxially. These epitaxial wafers were made into proton-bombardment laser stripes using the same technique. Figure 1 shows the schematic diagram of the GaAs/AlGaAs DH laser and growth parameters for various layers.

III. Optoelectronic Characteristics of the Laser

Lasers fabricated on space-grown and earth-grown substrates were found to be capable of CW operation at room temperature. The minimum threshold current density for the broad-contact space-grown-substrate laser is 850 A/cm^2. Figure 2 shows the L-I [light output power vs. current] curve of a H$^+$-bombardment stripe laser on a space-grown substrate under CW operation at room temperature. The threshold current is 50 mA and the light output power is 30 mW. The minimum threshold current is 20 mA. The L-I curve of some lasers has a kink and is not linear. Figure 3 shows the laser spectrum under CW operation at 30°C. The wavelength is 857.7 nm and the spectral half width is 0.3 nm.

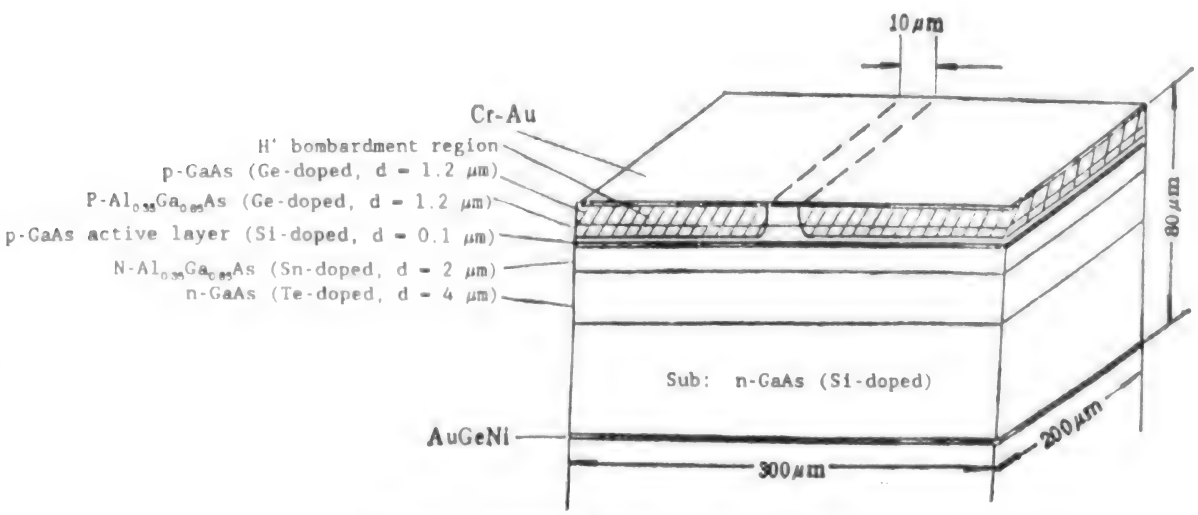

Figure 1. Structure of GaAs/AlGaAs DH laser

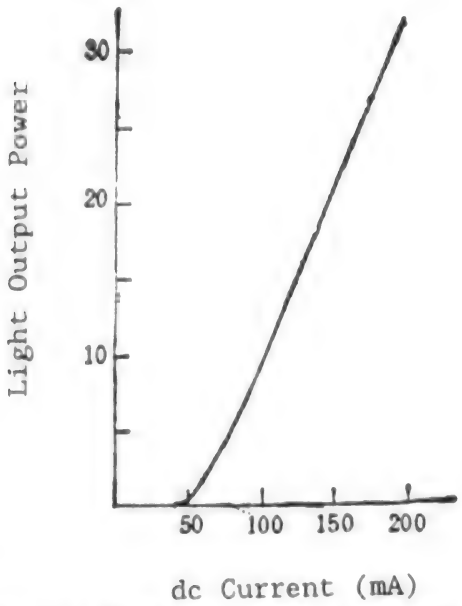

Figure 2. L-I Curve of GaAs/AlGaAs DH Laser Fabricated on Space-Growth Substrate

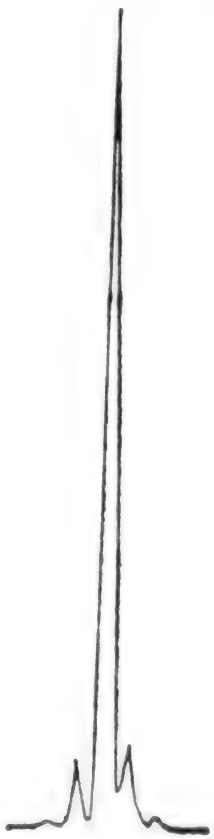

Figure 3. Spectrum of GaAs/AlGaAs DH Laser on Space-grown Substrate in CW Operation

IV. Preliminary Life Test

The procedure for this preliminary life test is to operate all CW devices at 2 mW for 8 hours at 60°C. It is also known as a pre-screening step.

After this preliminary life test, approximately half of the CW lasers fabricated on space-grown substrates showed signs of early deterioration. The remaining devices could still function in CW operation. However, compared to pre-test L-I curves, the behavior has changed. In general, the threshold current rose significantly. Figure 4 shows the L-I curves of two typical lasers before and after screening. (a) shows L-I curves before screening and (b) after screening. The L-I curve for the laser on the left has kinks at 1.5 mW and 10 mW before screening. After screening, the kinks disappeared. The L-I curve became more linear and the threshold current rose slightly. Between 1.5 and 10 mW, the L-I curves essentially overlap each other before and after aging. There is little deterioration for this laser. The right side of Figure 4 is another laser. After pre-screening, its threshold current rose; and η_d fell: it deteriorated by more than 5 percent. Based on pre-screen data, the lifetime of these lasers at room temperature is estimated to be ranging between several hundred to several thousand hours. Because the life test has not been completed, actual lifetime of these lasers is not available. Figure 5 shows the distribution of threshold current of CW lasers after pre-screening. Approximately 12 percent are under 40 mA. The highest proportion, approximately 22 percent, are between 50 and 60 mA.

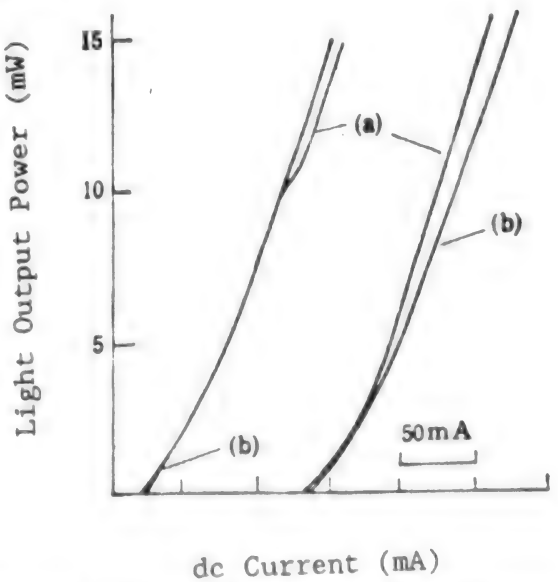

Figure 4. L-I Curves of Two GaAs/AlGaAs DH Lasers Before and After Pre-screening

Key: (a) L-I curves before pre-screening; (b) L-I curves after pre-screening

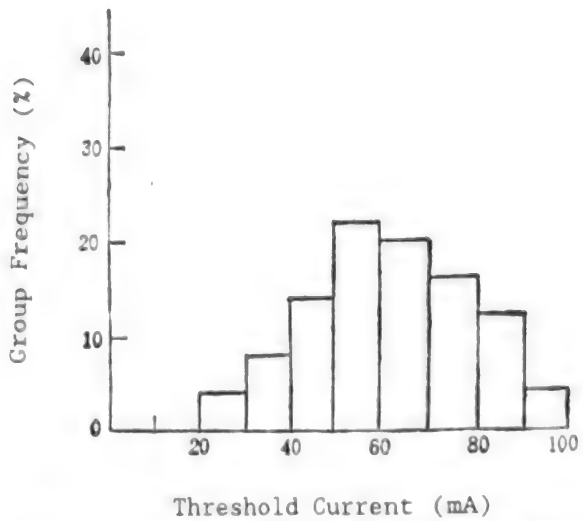

Figure 5. Frequency Distribution of Threshold Current of Lasers Made on Space-grown Substrate

V. Discussion

Space-grown GaAs is scarce and research in this area has just begun. On a single piece of space-grown substrate, room-temperature CW lasers were successfully fabricated. Based on preliminary life test data, their lifetimes range from several hundred to a few thousand hours. Although this is not very long, it is nonetheless very encouraging. The following is a discussion on the causes that lead to their rapid deterioration and relatively short lifetime.

The major cause of deterioration for a GaAs/AlGaAs DH laser is the formation of dark-line or dark-point defects in the active region. The formation of such defects is closely related to dislocation. A part of the defects in the epitaxial layer is due to the epitaxy process and the rest is an extension from the substrate. Surface defects on the substrate, to some extent, have an important effect on defects in the epitaxial layers. Therefore, defect density in the epitaxial layers is dependent upon that on the substrate surface; this affects the yield and quality of the device.[8]

Crystal growth in space is subject to many limitations and constraints. Due to energy and load limitations, it is not possible to lower the temperature over an extended period of time during growth. Other studies on this space-grown crystal[5,6,7] show that it is not homogeneous and its defect density is also relatively high. The dislocation density of the space-grown single-crystal substrate is 1.7×10^5 cm^{-2}. It is estimated that the dislocation density of the DH epitaxial layer is of the same order of magnitude as that of the substrate, which is high. This causes rapid deterioration of the lasers and short lifetimes. Conditions to grow crystals in space must be improved in order to demonstrate the superiority of single crystals grown under microgravity.

References

[1] Zhou Bojun [0719 0130 7486], Zhong Xingru [6988 5281 0320], Cao Funian [2580 4395 1628], Lin Lanying, Da Daoan [6671 6670 1344], Wu Kailin [0702 7030 2651], Huang Liangfu [7806 5328 3940], Zheng Songhui [6774 2646 6540], and Xie Xie [6200 3610], BANDAOTI XUEBAO [CHINESE JOURNAL OF SEMICONDUCTORS], 9, 548, 1988 [see JPRS-CST-89-001-L, 13 Jan 89 pp 82-88].

[2] Wang Zhanguo [3769 0594 0948], Shi Zhiwen, Xu Shouding [1776 1108 1353], Fu Jianming [0265 1696 2494], and Lin Lanying, BANDAOTI XUEBAO [CHINESE JOURNAL OF SEMICONDUCTORS], 9, 553, 1988 [see JPRS-CST-89-001-L, 13 Jan 89 pp 88-95].

[3] Jiang Sinan [5592 0934 0589], Fan Tiwen [5400 4895 2429], Li Chengji [2621 2052 1015], and Lin Lanying, BANDAOTI XUEBAO [CHINESE JOURNAL OF SEMICONDUCTORS], 10, 76, 1989 [see JPRS-CST-89-014, 18 Jul 89 pp 80-88].

[4] Shi Zhiwen and Lin Lanying, First Symposium on Microgravity and Space Experiments in China, 11-14 Nov 87, 66, 1987.

[5] Jiang Sinan, et al., "Structural Defects of Space-Grown Monocrystalline Si-GaAs," to be published.

[6] Z. G. Wang, C. J. Li, F. N. Cao, Z. W. Shi, B. J. Zhou, X. R. Zhang, S. K. Wan, S. D. Xu, and L. Y. Lin, J. APPY. PHYS., Feb. 1, 1990.

[7] Zhong Xingru, et al., "Segregation of Si in GaAs Under Microgravity," to be published.

[8] Gao Weibin [7559 4850 6333], Shi Zhiwen, Ren Qingyu [0117 1987 0151], and Ju Jingli [7263 7234 7787], BANDAOTI XUEBAO [CHINESE JOURNAL OF SEMICONDUCTORS], 2, 267, 1981.

Design of 2 GHz GaAs Frequency Divider VHSIC

91FE0254B Beijing BANDAOTI XUEBAO [CHINESE JOURNAL OF SEMICONDUCTORS] in Chinese Vol 11 No 10, Oct 90 pp 799-803 [MS received 8 Nov 89]

[Article by Shi Changxin [0670 7022 1823], Wang Qingkang [3769 1987 1660], Li Xiaoming [2621 2556 2494], and Li Zhiqi [2621 1807 1142] of the Institute of Microelectronics Technology, Shanghai Jiaotong University, and Xia Guanqun [1115 0385 5028], Yang Yuefei [2799 1878 7236], and Yan Ping [0917 5493] of the Shanghai Institute of Metallurgy, CAS: "Design of 2 GHz GaAs Frequency Divider"; see earlier brief reports in JPRS-CST-89-026, 11 Dec 89, p 25, and JPRS-CST-90-005, 8 Feb 90, p 14]

[Text]

Abstract: This paper presents the design of a 2-GHz GaAs frequency divider independently developed in China. The design was proven feasible based on results from experimental circuits.

I. Introduction

The GaAs VHSIC [very-high-speed integrated circuit] has important applications in high-speed computers, electronic warfare systems and high-precision instrumentation. Since the successful realization of the first GaAs logic IC in 1974,[1] it has been rapidly developed for over a decade. To date, there are reports on a 6 k gate array[2] and on the successful development of a 6.0-10.5-GHz dynamic frequency divider using the advanced WSi [tungsten silicide] auto-alignment technique.[3] The technology is still in its infancy in China. This paper presents the design of a 2-GHz frequency divider developed domestically. Compared with an experimental circuit, satisfactory results were obtained. Therefore, the feasibility of the design is demonstrated.

II. Selection of Logic and Unit Circuit Format

There are several mature frequency-divider logic circuits.[4,5] The present design employs a single-clock logic circuit with a master-slave flip-flop, because it can operate continuous over a wide frequency range from dc to the maximum clock frequency. It also works with waveforms at any duty ratio. A single clock is for ease of use in the circuit

Figure 1(a) shows a [combinational] circuit composed of AND and NOR logic gates [physically realized by a combination of NAND and AND gates—JPRS]. The unit logic-gate circuit uses a buffered FET logic (BFL) format because of its high logic swing, better interference resistance, fast speed, and ease of fabrication due to use of the depletion-type GaAs MESFET as the source. Although the BFL format requires more devices and consumes more power, it is still very appropriate in a medium-size circuit. The circuit diagram for the gate circuit is shown in Figure 1(b).

III. Device Design and Fabrication-Process Design

Device and fabrication-process design can proceed based on the above logic and circuit and the following operating conditions: power supply V_{DD} = 4 V and V_{SS} = -3 V, logic swing V_m = 2.5 V, high-voltage and low-voltage dc noise tolerance $V_N \geq 0.5$ V, and maximum clock frequency $f_m \geq 2$ GHz.

The pinch-off voltage of the device is determined first. The technique used is ion implantation. The effective active-layer thickness is a = 0.2 micron and the mean carrier concentration is $N = 1 \times 10^{17}$ cm^{-3}. Then, the pinch-off voltage is U_p = -2.7 V, where $\varepsilon_0 = 8.86 \times 10^{-14}$ F cm^{-1}, $\varepsilon_s = 13.1$, $\mu = 4000$ cm^2 V^{-1} s^{-1} and $q = 1.6 \times 10^{-19}$ C.

DC Characteristics

Results of dc transport characteristics based on the Shockley model, including source and drain parasitic resistance, reported in references [5] and [7] are shown in

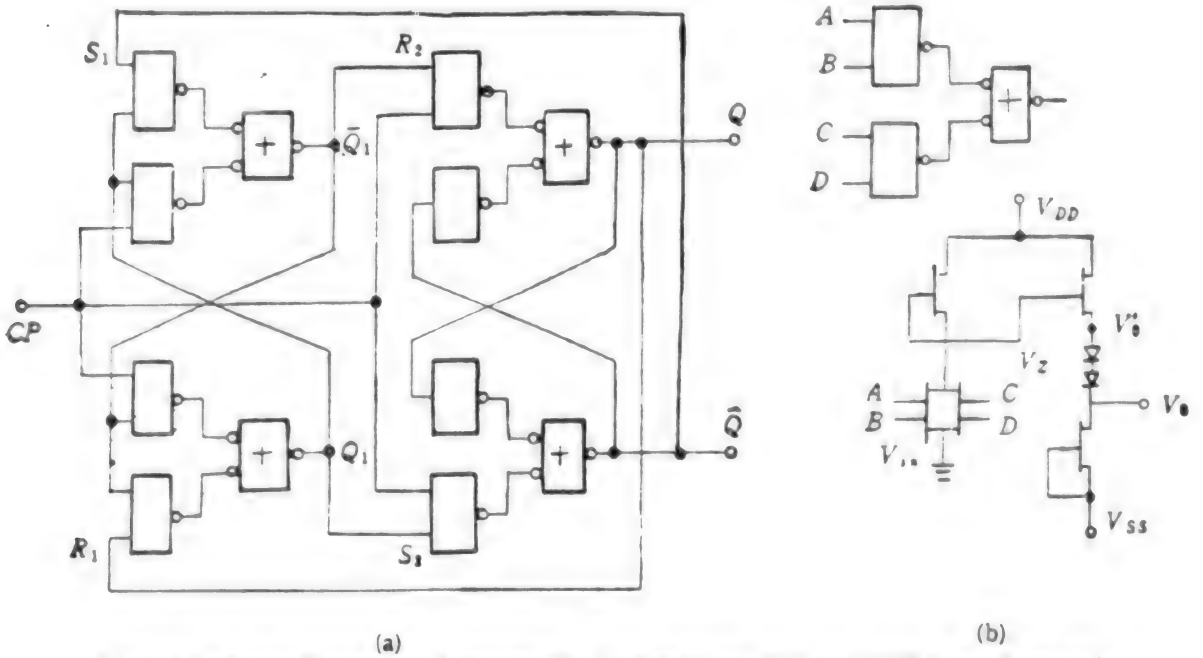

(a) (b)

Figure 1. (a) Logic Diagram for Frequency Divider Made from AND and NOR Logic Gates and (b) Unit Gate Circuit Diagram

Figure 2. They represent the transport characteristics of the logic amplifier stage and level shift buffer stage, respectively. In the figure, β is the transconductance ratio (i.e., ratio of gate width to length ratio) of the load device and the input driver. From the figure, we know that when β is 0.6 for the logic amplifier and when β is 1 for the buffer stage, a unit logic gate with dc noise tolerance $V_N \geqq 0.5$ V and good buffer-following characteristics can be obtained.

Transient Characteristics

Figure 3 depicts the waveform of the frequency divider shown in Figure 1; in Figure 3, (a) is the ideal waveform (without gate delay) and (b) is the actual waveform with a unit logic-gate delay time τ. In order to allow the frequency divider to operate normally, 2 τ must be less than one half of the clock cycle (T), i.e.:

$$2\tau \leqq T/2 \text{ or } \tau \leqq T/4 \quad (1)$$

Equation (1) shows a requirement on the unit logic gate imposed by the frequency divider, which also serves as a basis for design. The relation between gate delay and operating parameters of the device is as follows:[8]

$$\tau = 4/3\ C_L/kV_m \quad (2)$$

where $k = \mu\varepsilon_0\varepsilon_s/2a \times W/L$, W and L are the width and length of the gate, and C_L is the equivalent load capacitance. For the 2-GHz frequency divider, $\tau \leqq 120$ ps and $C_L = 0.15$ pF. From equations (1) and (2), it is possible to estimate the width-to-length ratio of the load device.

$$(W/L)_{load} \approx 5.8$$

Because β = 0.6, the width-to-length ratio of the effective input driver is

$$(W/L)_{eff\ driver} \approx 9.7$$

In an actual AND/NOR logic circuit, there are four terminals at the input end, two sets in parallel with two in series each. Therefore, the width-to-length ratio is doubled. However, the fabrication process uses a double-gate structure. Therefore, the width-to-length ratio is 1.6 times its effective value, i.e.:

$$(W/L)_{driver} = 15.5$$

Finally, we have

$$(W/L)_{load} = 9,\ (W/L)_{driver} = 18,\ \text{and}\ (W/L)_{buffer} = 15$$

From the pattern designed based on the above conditions we can calculate its parasitic parameters. By taking fabrication conditions into account, it can be calculated as follows: The sheet resistivity due to ion implantation into the active layer is

$$R^{square} = 1/Nq\mu a = 555 \text{ ohms per square}$$

Let the specific resistance of ohmic contact be $R_c = 1 \times 10^{-5}$ ohm-cm^2. The gate length is 1 micron, the gate-source and gate-drain distances are 2 microns each and the ohmic contact hole is 10 x 10 micron^2. Then, the drain and source parasitic resistance (including source-gate and drain-gate volume resistance and ohmic resistance at the lead) is

$$R_{d\ load} = R_{s\ load} = (R_{square} \times 2/10) + R_c/10 \times 10 \times 10^{-8} = 121 \text{ ohms}$$

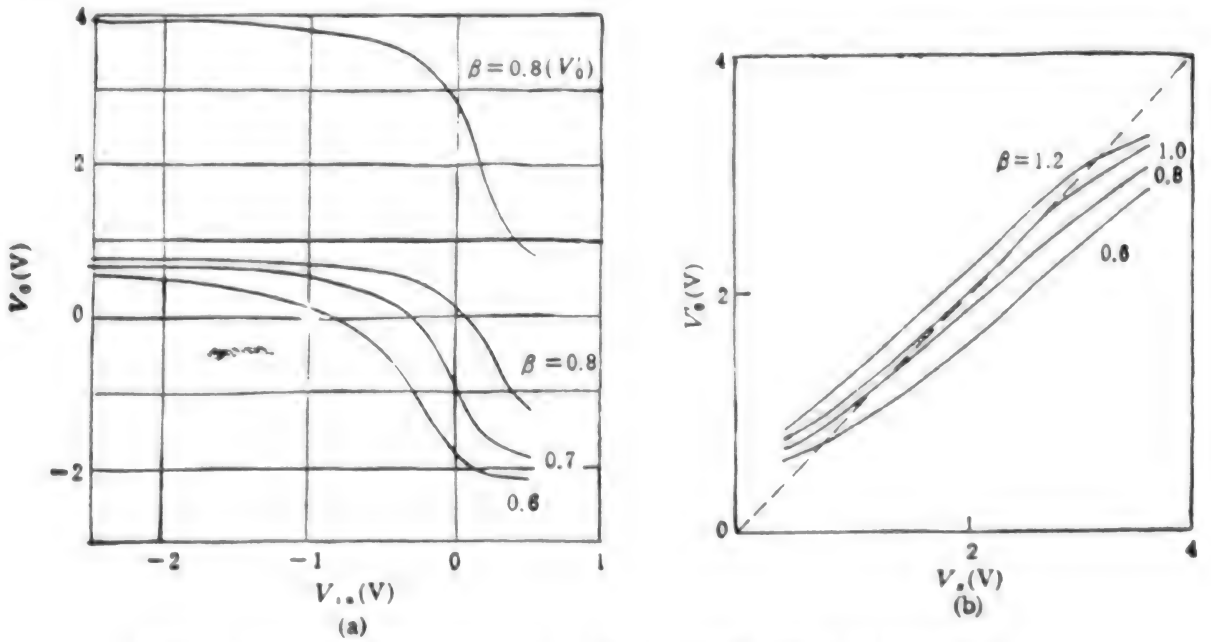

Figure 2. Transport Characteristics of: (a) Logic Amplifier Stage With BFL Logic Gates; (b) Voltage-Level Shift Buffer Stage

For the input driver (10 x 16 micron^2 contact hole), its parasitic resistance is

$R_{d\ driver} = R_{s\ driver} = (R_{square} \times 2/16) + R_c/10 \times 16 \times 10^{-8}$ = 79 ohms

The capacitance per unit gate area (zero bias) is

$$C_g = \frac{1}{2\sqrt{2}}\left(\frac{\varepsilon_0 \varepsilon_s q N}{V_{Bi}}\right)^{1/2} = 0.0008 \text{ pF/micron}^2$$

where V_{Bi} is the built-in gate potential which is 0.7 V. The input capacitance of each input driver is

$C_{g\ driver} = C_{go} \times (1 \times 18) = 0.0144$ pF

where the load capacitance $C_L = 3 \times C_{g\ driver} = 0.0432$ pF and the lead capacitance is 0.005 pF. Based on the model given in reference [7], it is possible to obtain the output waveform of each logic gate in response to a 2-GHz input signal, as shown in Figure 4. V_0 is the single-gate output waveform. The waveform on top is before the shift. This shows that it can operate at that frequency. Figure 5(a)

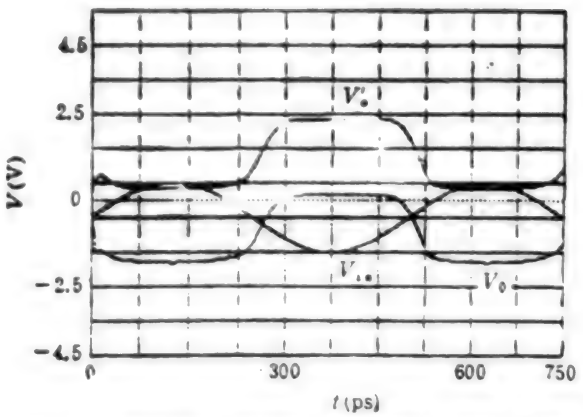

Figure 4. Computer Simulated Input and Output Waveforms of GaAs Logic Gate at 2 GHz Based on a Model in Reference [7].

[photograph not reproduced] shows the test result of a prototype circuit built by Shanghai Institute of Metallurgy. The frequency spectrum shows that it has excellent 1.5-GHz frequency-divided output characteristics with a 3-GHz clock frequency. This is because the actual gate is slightly under 1 micron. A photograph of the device chip is shown in (b) [not reproduced].

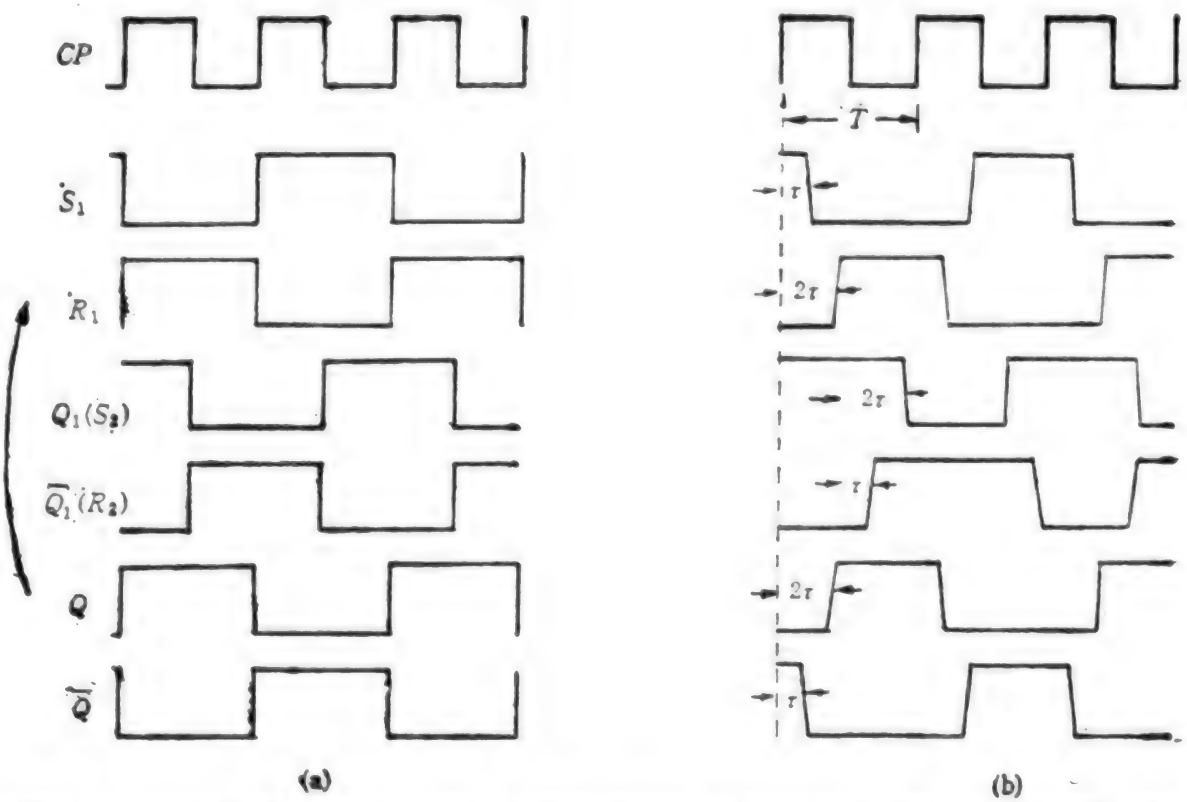

Figure 3. Waveform of the Frequency Divider. (a) Ideal Condition, (b) Actual Waveform With Gate-Delay Time .

IV. Conclusions

Compared with the experimental circuit, the design of the GaAs frequency divider presented in this paper yielded very satisfactory results. This demonstrates that it is an effective method for designing high-speed GaAs logic circuits.

References

[1] R. V. Tuyl and C. Liechti, IEEE J. SOLID-STATE CIRCUITS, SC-9, 269, 1974.

[2] A. Peczalski, et al., IEEE J. SOLID-STATE CIRCUITS, SC-23, 581, 1988.

[3] M. Shigaki, et al., IEEE TRANS. ON MTT, MTT-36, 772, 1988.

[4] R. V. Tuyl, et al., IEEE J. SOLID-STATE CIRCUITS, SC-12, 485, 1977.

[5] G. Nuzillat, et al., IEEE J. SOLID-STATE CIRCUITS, SC-17, 569, 1982.

[6] Shi Changxin and Yu Xing [0151 5281], BANDAOTI XUEBAO [CHINESE JOURNAL OF SEMICONDUCTORS] 8, 443, 1987.

[7] Wang Qingkang and Shi Changxin, SHANGHAI BANDAOTI [SHANGHAI SEMICONDUCTORS], No. 2, 30, 1989.

[8] R. C. Eden, et al., IEEE J. SOLID-STATE CIRCUITS, SC-14, 221, 1979.

Further Reports of Domestic R&D of Integrated Circuits

29 Research Projects Pass Acceptance Check

91P60134a Beijing ZHONGGUO DIANZI BAO [CHINA ELECTRONICS NEWS] in Chinese 13 Feb 91 p 1

[Article by Xie Yannan [6043 3601 0809]: "Integrated Circuit Basic Technology Research Results Are Gratifying"]

[Summary] Involving the combined efforts of over 2000 scientists and engineers over a five-year period, 29 special-topic research projects in LSI basic technology and applications passed acceptance check on 24 January [1991] in Beijing. The principal achievements of these leading-edge microelectronics projects have reached the mid-eighties international level. Included are research on the structures, physical characteristics, and fabrication processes for GaAs VHSICs, HEMTs, 3-D ICs, and similar devices; on materials and thin-film preparation methods suitable for fabrication of VLSI chips; and on the theory and practical aspects of new-generation devices. The GaAs samples devices—some of which have already been incorporated into equipment now being tested by the military and by civilian satellite communications authorities—were jointly developed and fabricated by the CAS Institute of Physics, the CAS Institute of Semiconductors, and MMEI's Research Institutes 13 and 55.

GaAs Monolithic Optical Receiver, InGaAs Monolithic Receiver

91P60134b Beijing ZHONGGUO DIANZI BAO [CHINA ELECTRONICS NEWS] in Chinese 22 Feb 91 p 1

[Article by Xiao Yuanzhen [5135 0337 4176]: "CAS Develops Optoelectronic Integrated Circuits"]

[Summary] Two mid-eighties-level optoelectronic integrated circuits (OEICs) recently developed by the CAS Shanghai Institute of Metallury—a GaAs monolithic optical receiver and an InGaAs monolithic receiver—have passed the relevant expert technical appraisal. The two OEICs, which have applications in very-high-speed high-capacity optical communications and in optical information processing, can receive extremely weak optical signals in the 0.8-0.9 and 1.0-1.6-micron bands, respectively; they also amplify the incoming signal current.

Two Key Research Projects Pass Appraisal

91P60134c Beijing KEJI RIBAO [SCIENCE AND TECHNOLOGY DAILY] in Chinese 26 Feb 91 p 2

[Article by Zhou Axin [0719 7093 2946]: "Young Researchers at CAS Microelectronics Center Complete Two Key Projects"]

[Summary] Young research fellows at the CAS Microelectronics Center have recently completed two key State Seventh Five-Year Plan research projects, entitled "Small-Size Device Performance and Physical Limits" and "interface Characteristics of Thin-Film Gate Structures for VLSI Circuits." At the formal appraisal jointly arranged the other day by MMEI and CAS, the experts unanimously agreed that the results in these two projects are at the state-of-the-art. Using less than one-tenth the funds that would have been spent on imports of such equipment, the researchers independently developed a "self-aligning GaAs FET" and a "sub-micron-size short-channel device"; these devices will be of great benefit in the development of microwave communications and the fabrication of VLSI circuits for use in the defense and aerospace industries.

Effect of Annealing Damages on Luminescences of Er, Yb-Implanted GaAs and InP

40100040A Beijing BANDAOTI XUEBAO [CHINESE JOURNAL OF SEMICONDUCTORS] in Chinese Vol 12 No 2, Feb 91 pp 80-86

[English abstract of article by Cao Wanghe and Chang Liansu (Changchun Institute of Physics, CAS) (MS received 18 Oct 89)]

[Text] The photoluminescence of Er^+ or Yb^+-implanted GaAs and InP after annealing is reported. The surface distribution of Er ions in GaAs: Er annealed samples is analysed by secondary ion mass spectroscopy (SIMS), and the rocking curves of the related luminescent samples are measured by X-ray double crystal diffraction for GaAs: Er, InP:Er and InP:Yb. The effects of the annealing damages on the luminescence of GaAs: Er and InP:Yb are investigated, and the luminescent center model of Er^{3+} complex is discussed.

Annealing Properties of $TiSi_x$/GaAs Schottky Contacts

40100040B Beijing BANDAOTI XUEBAO [CHINESE JOURNAL OF SEMICONDUCTORS] in Chinese Vol 12 No 2, Feb 91 pp 114-119

[English abstract of article by Qian He and Luo Jinsheng (Division of Microelectronics Technology, Xi'an Jiaotong University) (MS received 12 Mar 90)]

[Text] Thermal stability, chemical stability and electrical characteristics of $TiSi_x$/GaAs Schottky contacts formed by e-gun [electron-beam] multilayer evaporation have been investigated. It is found that after rapid thermal annealing (975°C, 12 s), the $TiSi_x$/GaAs contact is of good thermal stability, chemical stability and of excellent electrical properties. After conventional furnace annealing (800°C, 20 min), there is some accumulation of Ti and some chemical reaction at the interface. If rapid thermal annealing is used, $TiSi_x$ will be a good gate material for self-aligned GaAs MESFETs.

Optical Bistability in a GaAs/GaAlAs Multi-Quantum Well (MQW) Self-Electrooptic Effect Device (SEED)

40100040C Beijing BANDAOTI XUEBAO [CHINESE JOURNAL OF SEMICONDUCTORS] in Chinese Vol 12 No 2, Feb 91 pp 120-124

[English abstract of article by Wu Ronghan, Duan Hailong, et al. (Institute of Semiconductors, CAS, Beijing) (MS received 3 Jul 90)]

[Text] Based on a GaAs/GaAlAs MQW pin structure grown by a home-made MBE system, we have successfully fabricated SEED. The optical bistability and related properties of the device under symmetric operation (S-SEED) and asymmetric operation are reported.

Photo-EPR Study of $Cr^{4+}(3d^2)$ State in GaAs:Cr

40100040D Beijing BANDAOTI XUEBAO [CHINESE JOURNAL OF SEMICONDUCTORS] in Chinese Vol 12 No 2, Feb 91 pp 125-128

[English abstract of article by Mao Jinchang, Fu Jishi, et al., (Department of Physics, Beijing University) and Wang Yonghong and Ma Bichun (Beijing General Research Institute of Non-Ferrous Metals)]

[Text] The photo-EPR Study of Cr^{4+} in Semi-insulating GaAs:Cr is reported. The experimental results show that there is a maximum of the Cr^{4+} EPR signal amplitude as a function of temperature in the temperature range 20-30K. It is discovered for the first time that after turning off the white light the Cr^{4+} EPR signal increased before coming to decay. Neutron irradiation can restrain the Cr^{4+} EPR signal, but almost has no influence on the Cr^{3+} signal.

Preparation of High-J_c $YBa_2Cu_3O_{7-\delta}$ Superconducting Thin Films by Ion-Beam-Sputtering Deposition

40100039A Beijing DIWEN WULI XUEBAO [CHINESE JOURNAL OF LOW TEMPERATURE PHYSICS] in Chinese Vol 13 No 1, Jan 91 (manuscript received 12 Apr 90) pp 30-34

[Article by Chen Guoliang, Ren Congxin, et al.; Ion Beam Laboratory, Shanghai Institute of Metallurgy, CAS, Shanghai, 200050]

[Abstract] Preparation of high-Tc and high-Jc $YBa_2Cu_3O_{7-\delta}$ superconducting thin films by ion-beam-sputtering deposition is reported. The main factors affecting the composition of the films and the orientation of the crystal grains have been examined. Experimental results show that the Y, Ba and Cu composition of as-deposited films can be conveniently and accurately adjusted by a combined sputtering target which consists of a large sintered target of $YBa_2Cu_3O_{7-\delta}$ and a small one with Ba and Cu enriched ($YBa_{2.5}Cu_{3.3}O_x$. The technology for fabricating highly oriented superconducting thin films is described, and the $YBa_2Cu_3O_{7-\delta}$ superconducting films with zero resistance at 88-90.5K and critical current density Jc (at 77K) of 1.5×10^5A/cm are obtained.

Estimate of Critical Current Density on High-Temperature Superconductor Composite of Metal Matrix

40100039B Beijing DIWEN WULI XUEBAO [CHINESE JOURNAL OF LOW TEMPERATURE PHYSICS] in Chinese Vol 13 No 1, Jan 91 (manuscript received 23 Mar 90) pp 41-44

[Article by Ding Shiying and Zeng Chaoyang; Department of Physics, Nanjing University, Nanjing, 210008]

[Abstract] The critical current density Jc for high-temperature superconductor composite block embedded in metal matrix is estimated. The calculation shows that Jc is proportional to the metal conductivity, the geometric anisotropy of the high-temperature superconductor and the space of the block. With the criterion being 1 μv/cm and the resistivity being 10^{-7} ohm-cm, Jc is higher than 10^4A/cm^2 at 77 K and zero applied field. The additional advantages of the composite are discussed as well.

Preparation of 125K TlBaCaCuO Superconductor and Its Tc Degradation

40100039C Beijing DIWEN WULI XUEBAO [CHINESE JOURNAL OF LOW TEMPERATURE PHYSICS] in Chinese Vol 13 No 1, Jan 91 (manuscript received 16 Feb 90) pp 45-48

[Article by Yu Zheng, Ding Shiying, et al.; Department of Physics, Nanjing University, Nanjing, 210008]

[Abstract] TlBaCaCuO superconductor with Tc = 125K has been prepared by a step sintering method. The samples mainly consist of $Tl_2Ba_2Ca_2Cu_3O_x$ and $Tl_2Ba_2CaCu_2O_x$ phases. This can be seen from the XRD, EDAX, HRAX, HREM and ED examinations. The degradation test on T_c and other parameters has been lasting for one year, and Tc shows a profound decrease. The cause of this degradation is discussed.

A 12T NbTi-Nb_3Sn Hybrid Superconducting Magnet System

40100039D Beijing DIWEN WULI XUEBAO [CHINESE JOURNAL OF LOW TEMPERATURE PHYSICS] in Chinese Vol 13 No 1, Jan 91 (manuscript received 27 Mar 90) pp 59-66

[Article by Chen Zongzhi, Pan Qianli and Wu Xiulan; Shanghai Institute of Non-Ferrous Metals, Shanghai, 201600]

[Abstract] The design, fabrication and experimental results of the NbTi-Nb_3Sn hybrid superconducting magnet system with a clear bore of 30.3 mm are described. The maximum operational central magnetic field of the magnet is 12 T at 4.2 K. The homogeneity of the central field and the operational current stability are more than 2.7×10^{-3} (1 cm DSV) and 4×10^{-4}/h respectively. The time for exciting the magnet up to 12 T is 40 min. The magnet weighs 25.4 kg.

Preparation of Densified Bi-Sr-Ca-Cu-O Superconductor

40100038 Beijing GUISUANYAN XUEBAO [JOURNAL OF THE CHINESE CERAMIC SOCIETY] in Chinese Vol 18 No 6, Dec 90 (manuscript received 25 Jun 90) pp 561-564

[Article by Zhao Meiyu, Li Cheng'en, et al.; Shanghai Institute of Ceramics, CAS]

[Abstract] The effect of composition, molding method and sintering process on the density of Bi-Sr-Ca-Cu-O superconducting bulk materials is studied. The experimental results show that 107K Bi-Sr-Ca-Cu-O superconducting ceramics of density as high as 6.10 g/cm^3 can be made by using high-Pb content composition, small amounts of Sb^{5+} or W^{6+} and a sintering-hot pressing-annealing process.

High-Temperature Oxide Superconductor Double-Hole RF-SQUID

40100036 Beijing DIWEN WULI XUEBAO [CHINESE JOURNAL OF LOW TEMPERATURE PHYSICS] in Chinese Vol 12 No 4, Jul 90 pp 289-295 [MS received 25 Feb 89]

[English abstract of article by Qiu Jingwu, Zhang Xianfeng, Tang Zhiming, and Qian Yongjia of the Department of Physics, Fudan University]

[Text] A double-hole RF-SQUID made from sintered bulk YBCO has been developed. At both 77K and 4.2K, the devices display the typical flux modulation characteristics of the external field and operate in the lock mode. At 77K, equivalent flux noise of the device is 2×10^{-3} $\varphi_0/Hz^{1/2}$ [φ_0 (the magnetic flux quantum) is about 2.07×10^{-7} gauss-m^2] near the dc end and the noise level is decreased to lower than $5 \times 10^{-4}\varphi_0/Hz^{1/2}$ in the range from 20 to 200 Hz. The characteristics of the device show similarities to those for a liquid-helium conventional RF-SQUID. There is no detectable change in behavior of the device after being stored in air or in liquid nitrogen for more than one year and having undergone dozens of thermal cyclings between 77K and room temperature. The design and the fabrication of the device, determination of critical current and its potential use are discussed.

Long-Pulse Laser Deposition Used to Prepare YBCO Thin Film With 85K Transition Temperature

91P60136 Beijing ZHONGGUO DIANZI BAO [CHINA ELECTRONICS NEWS] in Chinese 24 Feb 91 p 3

[Article by Gao Longqiao [7559 7893 2890]: "Long-Pulse Laser Deposition Technique Used for In-Situ Growth of Superconducting Thin Film"]

[Summary] Researchers in the Superconductivity Group at MMEI's Research Institute 12 for the first time have employed the long-pulse laser deposition technique on a zirconium-oxide monocrystalline substrate for in-situ growth of a high-quality YBaCuO superconducting thin film with a zero-resistance transition temperature of 85K. Using a 750°C heater and a lens system to focus the laser beam onto the rotating target, the researchers needed only 15-20 minutes to deposit the 0.6-0.8-micron-thick film, which has good brightness and crystalline characteristics.

First Domestically Made DS5 Optical Terminal Unveiled

91P60157 Beijing JISUANJI SHIJIE [CHINA COMPUTERWORLD] in Chinese No 10, 13 Mar 91 p 43

[Untitled news brief by Yi Bei [0001 6296]]

[Text] The nation's first [domestically made] 565 Mb/s [the DS5 transmission rate] optical terminal has been unveiled at Wuhan. This fifth-generation fiber-optic communications product, developed by the [Ministry of Posts & Telecommunications'] Wuhan Institute of Posts & Telecommunications Science, can simultaneously transmit 7680 voice circuits over optical fiber; this is four times the capacity of the DS4 [140 Mb/s, 1920 voice circuits] optical terminals now commercially available worldwide. The new terminal's features include high speed and transmission capacity, low power consumption, and low bit error.

Reports on Fiber Optic Communications Technology, Projects

DS5 BER Analyzer, Other Equipment Accredited

91P60153A Beijing DIANXIN JISHU [TELECOMMUNICATIONS TECHNOLOGY] in Chinese No 3, Mar 91 pp 47-48

[Article by Wang Li [3769 4539] of MPT's Science & Technology Department: "DS5 Bit-Error Analyzer, Three Other Scientific-Research Achievements Pass Ministry-Level Appraisal"; see earlier report in JPRS-CST-91-004, 5 Feb 91 pp 30-31]

[Summary] Up to now, China has been forced to import test equipment for DS4-and-higher [140Mb/s and higher rates] fiber-optic communications systems. In order to foster development of the nation's indigenous fiber-optic communications industry, MPT [in 1986] assigned to its [Beijing] Instruments & Meters Research Institute the development of appropriate test instruments. This State Seventh Five-Year Plan project has now been completed, with the official accreditation of four types of instruments on 26 December 1990 by an MPT-sponsored panel of technical experts. The four instruments are a DS5 bit-error-rate (BER) analyzer which operates at a maximum rate of 622 Mb/s, a DS4 phase-jitter tester, a digital transmission system analyzer for DS1-DS4 [DS1 = 2 Mb/s, DS2 = 8Mb/s, DS3 = 34 Mb/s] systems, and a signal monitor [not mentioned in earlier report].

The DS5 BER analyzer directly generates four pseudo-random-number sequences at a relatively low speed and then again at a higher speed; this technique overcomes drawbacks in heavier-volume high-speed devices that operate only at the higher speeds. It is estimated that in the Eighth Five-Year Plan there will be a heavy demand for this domestically made instrument, whose cost is only one-third that of the comparable imported item.

In the DS4 phase-jitter analyzer, jitter modulation and jitter measurements are realized via a dual phase-comparator scheme. The values for testing accuracy and intrinsic jitter are better than CCITT-recommended standards. The jitter transmission element employs precision amplitude-control technology, improving stability. This test instrument will be a major boom to the domestic development of high-capacity fiber-optic communications systems.

The digital transmission system analyzer is designed for comprehensive testing of transmission system performance, including measurement of BER, number of bit errors, intrinsic jitter, input jitter margin, and jitter transfer characteristic, and can also analyze bit error and phase jitter. The instrument utilizes microcomputer control technology, with software providing the functional control; it comes with a GP-1B interface, permitting link-up with computers to create an automated testing system.

The XJ-01 signal monitor is used for monitoring digital circuit signals, multi-frequency signals, all kinds of alarm signals, and voice circuits, and has functions such as statistical call-completion rate and print-out. When used for process control, this instrument provides monitoring with uninterrupted service, and is easy to maintain.

Shanghai-Nanjing Line, Feeder Line Approved

91P60153B Beijing DIANXIN JISHU [TELECOMMUNICATIONS TECHNOLOGY] in Chinese No 3, Mar 91 p 48

[News brief by Jin Yuqi [6855 6877 3825]: "Short Waves from the Provinces"; see earlier report in JPRS-CST-91-004, 5 Feb 91 p 30]

[Text] An MPT Eighth Five-Year Plan priority project—The Shanghai-Nanjing fiber-optic cable project, including its fiber-optic-cable feeder line running from Suzhou through Changshu to Zhangjiagang—passed the design hearing conducted on 12 November 1990 in Changzhou, Jiangsu Province, and is thus formally approved. This project, which is a continuation of the Nanjing-Wuhan fiber-optic-cable project, consists of a 402-km-long trunkline and its 90.6-km-long feeder line. Ground-breaking for the project will take place in 1991. Completion of this project will ease the overcrowded state of the long-distance communications circuits between Shanghai and Nanjing as well as inter-city lines in all the provinces, and further promote economic development in East China and the Changjiang [i.e. Yangtze River] Delta area.

Yong'an-Xiamen Line in Fujian Under Construction

91P60153C Beijing DIANXIN JISHU [TELECOMMUNICATIONS TECHNOLOGY] in Chinese No 3, Mar 91 p 48

[News brief by Chen Min [7115 7044]: "Short Waves from the Provinces"]

[Text] The Fujian Yong'an-Xiamen long-distance fiber-optic-cable project is now fully under construction. This project, a major element in Fujian Province's communications development, will pass through 10 countries and cities, is 431 km in length, and has a longer repeater range. The terrain along the line is difficult, necessitating several cable-laying modes. While the line's technical complexity is high, its completion will lay a solid foundation for long-distance communications within the entire province and between the province and other nations.

Shanghai Satellite Ground Station Installs IDR Equipment, Provides International Services

91P60152B Beijing DIANXIN JISHU [TELECOMMUNICATIONS TECHNOLOGY] in Chinese No 2, Feb 91 p 48

[News brief by Shen Xin [3947 0207]: "Short Waves From the Provinces"]

[Text] The Shanghai Satellite Ground Station has installed new IDR [intermediate data rate] equipment. Since it incorporates new technologies such as speech compression and digital [speech] interpolation [DSI], it can raise the circuit utilization factor by 400 percent; with added terminal digital multiplexing equipment, a total of 1,800 circuits can be opened up. As of now, 419 international satellite circuits have been opened up toward the U.S. and Hong Kong, and other international circuits for Australia and elsewhere are about to be opened up.

Additional DMW Line Added Into Jiangsu Rural Telephone Network

91P60152A Beijing DIANXIN JISHU [TELECOMMUNICATIONS TECHNOLOGY] in Chinese No 2, Feb 91 p 48

[News brief by Jin Yuqi [6855 6877 3825]: "Short Waves From the Provinces"]

[Text] Another 2GHz 34Mb/s 480-channel digital microwave (DMW) communications line for Jiangsu Province's rural telephone network was completed in November 1990 at Meili Town in Changshu County, signifying that Jiangsu's rural telephone communications are making great strides toward the digital era. This project uses domestically made equipment throughout: the microwave transceivers are the model WSF2-01, manufactured by MPT's Xian Microwave Equipment Plant [see JPRS-CST-91-007, 25 Mar 91 p 26], and the PCM [pulse code modulation] terminals are model MDT2-01, manufactured by MPT's Shanghai Communications Equipment Plant. The two-station range is 14 km, and the initial installation consists of four PCM primary-rate 120-channel-capacity circuits, which will provide a basis for automation of the rural telephone network.

Prospective Development of High-Flux Engineering Test Reactor

91FE0405 Chengdu HE DONGLI GONGCHENG [NUCLEAR POWER ENGINEERING] in Chinese Vol 11 No 6 10 Dec 90 pp 6-10

[Article by Wu Yinghua [0702 5391 5478], Bu Yongxi [0592 3057 3556], and Hong Yonghan [3163 3057 3352] of the Southwest China Reactor Engineering Research and Design Academy, Chengdu; "Prospects for the High-Flux Engineering Test Reactor"; manuscript received 17 Jul 90]

[Text]

Abstract: This article describes development prospects for the high-flux engineering test reactor (HFETR). The focus in development and utilization of the HFETR is on irradiation experiments with nuclear power plant and power reactor fuel elements and assemblies and basic research on topics in the fields of high technology and nuclear power. The depth and breadth of reactor comprehensive utilization has been opened up in the areas of isotope development and production, source matching and applications, and irradiation processing. The HFETR has been included in state S&T development plans, and perfection of the device will allow it to serve as a national laboratory open to China and foreign countries.

Key terms: HFETR, irradiation experiments, isotope processing, national laboratory, development prospects.

I. Introduction

To develop China's atomic energy industry, meet the need for experimental research on nuclear power fuel element and materials irradiation, promote a shift to domestic production for nuclear power and application of nuclear technology in all realms of the national economy, serve as a key state engineering and construction project, and rely totally on China's own technical and industrial strengths, we basically completed the high-flux engineering test reactor at the end of 1980 along with the associated research and auxiliary facilities, and it has now been operating safely for 10 years. Since it began operation, the reactor has completed irradiation experiment research tasks for several types of nuclear materials and fuel samples. We developed and produced ^{60}Co, ^{192}Ir, ^{170}Tm, ^{99m}Tc, ^{113m}In, and other high specific activity radioactive isotopes with medical, industrial, and agricultural applications. This filled in a blank space within China and reduced substitute imports. Gratifying progress has been made in the area of reactor comprehensive utilization.

The HFETR is the largest research and experimental reactor at relatively advanced levels in Asia at the present time in reactor power scale, neutron flux levels, irradiation experiment capabilities, and other areas. Only a few countries in the world like the United States, the Soviet Union, and a few nations with advanced nuclear technology in Western Europe have such a large reactor of this type. Because the corresponding test loops were not constructed when the reactor was built and for financial expenditure and other reasons, the capabilities and uses of the HFETR have not yet been rationally fostered and fully utilized. This should receive the concern and attention of the relevant departments of the state and people in all areas to enable the HFETR to play the even greater role it should play in China's nuclear industry and scientific development over the next 10 to 20 years.

II. A Focus on Ensuring Nuclear Fuels and Materials Irradiation Experimental Research

The HFETR has a high neutron flux, short irradiation experiment cycle, large irradiation space, flexible configuration, strong reactivity, and other characteristics. The design power of the reactor is 125MW. The maximum thermal neutron flux of the reactor core is 6.2 X 10^{14}n cm^{-2} s^{-1} and the maximum fast neutron flux (E_n >0.625 eV) is 1.7 X 10^{15}n cm^{-2} s^{-1}, which are 5 to 10 times higher than regular test reactors in China. The core design allows configuration with five large irradiation ports (φ 150) and four small irradiation ports (φ 63). Single flow process irradiation experiment devices can be installed in three of the φ 150 ports. Four large irradiation ports (two φ 230 and two φ 122) also can be configured in the reflection layer. There are also several holes in the beryllium blocks and aluminum blocks and holes in the elements that can be used. The irradiation thermal neutron flux is 2 X 10^{14} to 5 X 10^{14}n cm^{-2} s^{-1} and the fast neutron flux (E_n >0.625 eV) is 1 X 10^{14} to 1.6 X 10^{15}n cm^{-2} s^{-1}, of which the E_n >1 MeV fast neutron flux is 1 X 10^{14} to 5 X 10^{14}n cm^{-2} s^{-1}. If a water cavity is configured in the center of the core, the thermal neutron flux can be greater than 1 X 10^{15}n cm^{-2} s^{-1}. The irradiation reaction inspection facility built into the HFETR is the largest in scale and most basically matched in China. It includes 13 hot rooms and 20 semi-hot rooms for dissection and breakdown, non-destructive inspection, mechanical and physical properties testing, metallic phase and materials chemistry, isotopes, and so on. It also has research laboratories for nuclear physics, radiation chemistry, coolant chemistry, isotopes, irradiation technology, irradiation protection, environmental monitoring, radiation counting second-stage station, and so on. The HFETR is the most powerful neutron irradiation experimental research tool in China. By the end of this century and the beginning of the next century, the HFETR should be playing a leading role in irradiation experimental research centered on nuclear fuels and materials.

A 500 kW high-temperature high-pressure water loop has now been built and large scale irradiation inspection of small fuel assemblies (4 X 4 - 4) for nuclear power plants will be carried out soon. It is expected that when the first phase of the inspections is completed, the maximum average fuel consumption of the single rods in the assemblies could reach 40 GW d tU^{-1}. When the

second phase of the inspections is completed, the maximum average fuel consumption of the single rods in the assemblies could be as high as 51 GW.d/t(U), which are equivalent to the average unloaded fuel consumption of 35 GW.d/t(U) and 42 GW.d/t(U) at Daya Bay Nuclear Power Plant. At that time, the fuel consumption of the high-performance fuel rods will approach 60 GW.d/t(U). Completion of this large comprehensive inspection will provide complete data on high fuel consumption properties and make important contributions to the safety and economy of nuclear power plant operation in China and the shift to domestic production of fuel assemblies.

The HFETR has prepared specific conditions for experimental research on high- temperature gas-cooled and sodium-cooled fast reactors. A large pressurized- steam generator equipment foundation is installed between the four irradiation loops at the - 6.5 m high mark in the main plant building. In the area of the reactor structure, the proper conditions were also left for installing a fully-enclosed sodium irradiation device. Looking at the long-term plans for nuclear power development, we should arrange for loop irradiation experiment tasks for new reactor types as soon as possible.

The HFETR uses highly enriched uranium as a fuel. It has a large effective breeding coefficient and a relatively large irradiation sample capacity. The core is a water-deficient dense grid with a harder energy spectrum than heavy- water reactors and swimming pool light-water reactors. Moreover, the loading configuration can be used to make local readjustments in the energy spectrum. For example, local increases in beryllium blocks will soften the neutron spectrum, while using Cd or B_4C casings to absorb neutrons can increase the fast neutron to thermal neutron ratio. This, in addition to the high neutron flux and short irradiation cycle, provides enormous advantages for materials irradiation. Post-irradiation properties data can be obtained within a short time period, which greatly accelerates the pace of new materials development and type determination.

During the Eighth 5-Year Plan, topical research in the realm of nuclear power determined by the State Science and Technology Commission in its high-tech development plan will get underway fully. All sorts of irradiation experiments and properties measurement research will be done on new materials (including element cladding, reactor structure, reflection layers, screens, and other materials) for high-temperature gas-cooled reactors, fast reactors, and fission-fusion reactors and on fuel samples to lay a foundation for development of nuclear technology in China in the 21st Century. Pressurized- water reactors, the primary reactor type in China at present, should match up further with scientific research, design, and production, continue to carry out irradiation properties research on a new generation of structural materials and special reactor materials, fully achieve a shift to domestic production of reactor materials, and improve the economic and technical indices and safety indices of nuclear power plants and power reactors. Intensive development of basic and applied research in nuclear materials science also will directly promote development and perfection of China's metallurgical, machinery, chemical, and other basic industries and make a contribution to the establishment of China's own complete nuclear power equipment manufacturing capability.

Moreover, research will be done at the HFETR on the use of U_3Si_2-Zr dispersed plate elements, burnable poisons, and so on in reactors and other irradiation research.

III. Open Up the Depth and Breadth of Comprehensive Utilization of Reactors

Research and experimental reactors in China and foreign countries have done a great deal of work in the areas of reactor applied research and service in recent years and achieved rather good social benefits and definite economic benefits. On the basis of previous development, we should continue to exploit potential in the HFETR. While attempting to reduce operating costs, we should fully utilize the characteristics and advantages of the HFETR, meaning that we should complete and place into operation the 5MW low-power reactor as a supplement for rational utilization. Reinforce surveys of market conditions and user needs, information feedback, analysis, and policymaking, orient toward society and the national economy, and use the reactor as a basis and isotope products as a tap to open up and develop the depth and breadth of comprehensive utilization and form an integrated scientific research, production, and management body. Select projects correctly, establish an integrated system for materials, irradiation, processing, and product production, achieve scale administration, and create more economic benefits and better social benefits.

A. Radioactive isotope development, production, and application services

As the number of heats and time of reactor operation increase at the HFETR, there can be substantial increases in isotope output and specific activity. Radioactive isotopes and their associated instruments are seeing ever-wider use in medicine, scientific research, and many industrial departments. High activity medical diagnosis isotopes produced by the HFETR like ^{60}Co highly-radioactive medical treatment source, ^{60}Co, ^{192}Ir, and other post-installation cavity medical treatment sources, and Mo-Tc and Sn-In isotope generators can satisfy national demand and we can carry out development and applied research on ^{192}Ir wire-shaped insertable treatment sources, ^{153}Gd bone density measurement sources, ^{125}I X-ray machine sources, ^{32}P, ^{35}S, ^{90}Sr-^{90}Y isotope generators, and other pure B radioactive drugs, ^{125}I and various radioactive immunization boxes, ^{131}I labeled monoclonal antibody boxes, ^{115}Cd-^{115m}In, ^{191}Os-^{191m}Ir, ^{109}Cd-^{109m}Ag, and other medical isotope generators.

^{57}Co, ^{170}Tm, ^{192}Ir, and other industrial γ flaw detection sources and matching flaw detectors are simple and convenient tools for use in non-destructive testing of

pressure vessels and pipelines of all thicknesses used in the petrochemical, metallurgical, machinery, and other industries. There are also broad application and development prospects for various types of liquid position and materials position sources (counters) used in industry, isotope thickness meters and density meters, fire alarm sources, ^{55}Fe, ^{109}Cd, and other fluorescent analysis sources, ^{14}C and its labeled compounds, tracer isotopes used in petroleum well logging, water conservancy projects, and so on. The HFETR has obvious advantages and large batch supply capabilities in these isotope and irradiation production areas. We also should try to focus on source machine matching and applications service work, continually improve performance, and achieve automation and microcomputerization. We should establish an isotope and nuclear technology applied research center.

Moreover, using high-flux reactors for irradiation and production of transplutonium elements is an important project developed in foreign countries. The transplutonium elements ^{238}Pu, ^{241}Am, ^{242}Cm, ^{242}Cm...^{251}Cf, and so on have important uses in nuclear medicine, the military, and high scientific and technical realms (such as heart pacemakers, space energy sources, and seabottom cable amplifiers).

B. Irradiation processing research and applications

The HFETR and its 5MW low-power reactor have various types of neutron irradiation spaces and the largest irradiation processing capacity in China. The two reactors can irradiate 20 to 30 tons of monocrystalline silicon annually. As China's electronics industry develops, demand for neutron transmutation doped monocrystalline silicon will gradually increase. While stabilizing and improving the quality of irradiation, we should develop irradiation research on large-diameter silicon, vertically-pulled silicon, semiconductor component performance control, and so on and actively seek foreign users and enter international markets. There are excellent development prospects for gem coloring, nuclear pore filter membranes, and so on.

Success has already been achieved in using the γ irradiation field of fuel elements removed from the HFETR and in the production of industrial cobalt sources in the area of radiation cross linking for heat shrinking to make polyethylene products, and irradiation processing will develop from plants that produce raw materials to producing products. γ irradiation modifies polymer materials and has a broad range of uses in the plastics and rubber industries and in the chemical, textile, precision petroleum refining, and other industries, and γ irradiation can be used for sterilization of medical machinery, drugs, cosmetics, etc., and for food preservation, breeding improved varieties, and so on. We should strengthen research, development, and cooperation, actively strive for and create the proper conditions, and establish a large irradiation station and associated plants at Chengdu with a design capacity of 1 million curies to make the Southwest China Irradiation Processing Applied Research Center and strive for even greater economic benefits and better social benefits.

IV. Reinforce Domestic and International Exchanges and Cooperation

The state spent an enormous amount of money to build the HFETR. To fully utilize it and make the appropriate contributions to the development of China's nuclear industry and S&T, we must make major efforts to develop domestic and international exchanges and cooperative applications.

The neutrons and γ field of the HFETR can provide research services for the development of the materials and nuclear fuels sciences, solid physics, neutron physics, radiation chemistry and irradiation chemistry, isotopes and their applications, and other areas. The relevant experts can come to the HFETR on fixed or non-fixed schedules for cooperative research as well as bring their own project topics. It can be used to train personnel for nuclear power plants.

Research organs, universities, and experts from Japan, the United States, Brazil, Chile, and the International Atomic Energy Agency have expressed interest in using the HFETR for research on materials irradiation, plate fuel element inspection, nuclear measurements, low concentration of fuels used in research reactors, and other areas. We should try to create the conditions to make the HFETR China's window to the outside world, undertake wide-ranging substantive international cooperation and exchange, improve academic and technical levels in China, and promote the development of the nuclear sciences in China.

V. Perfect the Facility, Make It a National Laboratory

The HFETR is a large comprehensive experimental, engineering applications, and research facility and has also become known as a "tool reactor". It was not constructed mainly for its own unit or to serve the nuclear industry system, but instead should be an important link in the state's overall scientific development plans. Most research and experimental reactors of this type in foreign countries are national laboratories. Undertaking comprehensive utilization of the research reactor for China and foreign countries can provide definite economic benefits, compensate for part of the cost of its operation, and reduce the state's financial outlays. If we depend mainly on the reactor itself to continue operation, we will inevitably create many artificial obstacles that will greatly restrict utilization of the HFETR, which will lose the goals and importance of reactor construction to a substantial degree. This would have extremely negative long-term consequences for the nuclear industry and state S&T development.

To truly achieve opening up of the HFETR to the outside world and utilization, we must gradually perfect and improve the HFETR and its experimental facilities. Examples include updating of reactor equipment and instruments, perfection of safety facilities and processing

of the three wastes (waste water, waste gas, and industrial residues), construction of irradiation loops, improvement of irradiation devices and technology, perfection of post- irradiation inspection and testing measures, and so on.

For this reason, the HFETR should become a national laboratory and receive key state support to confirm the status and role it should have. Make it one of the world's most advanced high-flux engineering test reactors, fully foster its advantages and functions for irradiation inspection of nuclear fuel and materials, promote a shift to domestic production in China's nuclear power industry and the development of power reactors and new types of energy source reactors, promote domestic and international cooperation and exchange and personnel training, promote wide-ranging applications of nuclear power and nuclear technology in all realms of China's national economy, accelerate improvements in the levels of nuclear S&T in China, and contribute to a takeoff in the cause of science during the 21st Century.

Nation's First Pulsed Reactor Goes Critical

91FE0300A Beijing GUANGMING RIBAO in Chinese 12 Jan 91 p 1

[Article by Zhang Zuhuang [1728 4371 3874] and Ye Hui [0673 6540]: "Nation's First Pulsed Reactor Goes Critical"]

[Text] A piece of good news came from the southwest on New Year's Eve. China's first pulsed reactor has been completed and its power level was increased after reaching hot critical state. This marked that China has become the second nation in the world capable of constructing such a nuclear reactor behind the U.S.

China Research and Design Institute for Nuclear Power (originally the First Research and Design Institute of the Ministry of Nuclear Industry) located in the Ermei Mountains in Sichuan is the largest nuclear power base in China. In the past 25 years, it has built China's first nuclear powered submarine, the first high flux reactor, and now the first pulsed reactor. it has made significant contribution to the development of nuclear power in China.

The pulsed reactor was seen by reporters in the Second Research Institute. It was installed in a 2 m diameter 7 m deep pool. The fuel elements were clearly in sight through the crystal clear water. According to Associate Director Li Dazhong [2621 6671 1813], the pulsed reactor was completed in July 1990. Fuel was loaded on July 18 after it was certified by the Nuclear Safety Bureau. On July 22, it reached cold critical state. After reaching hot critical state and raising power, it can be pulsed to begin normal operation.

According to senior engineer Li Yingfa [2621 2503 4099], this is an idiot-proof reactor. It is just like a fool-proof camera, anyone can operate it without any incidents. This is the safest reactor in operation today.

After the construction of numerous nuclear power plants all over the world, scientists began to consider a new problem. How can reactors be operated safely with less dependence upon electrical and mechanical control? How can reactors be safely constructed in large urban areas so that atomic power can be better utilized? The technical staff at China Research and Design Institute for Nuclear Power began working on this subject in the late 1970's. They dedicated their efforts and voluntarily put in extra hours on weekends and holidays without any bonuses and overtime just like how people worked in the 1950's and 1960's. Senior engineer Xu Linxiang [1776 2651 4382] was suffering from an infection in his mouth during zero power testing. he could not open his mouth to talk and eat. Nevertheless, he still remained at his post. Project leader Wang Zisheng [3769 2737 3932] could not go home to attend his mother's funeral. Technical leader Xia Xianggui [1115 4382 6311] travelled all over the place carrying medicine on him despite his heart condition. The technical staff overcame a large number technical hurdles including physical computation and measurement of pulsed reactor parameters within a short period of time.

The pulsed reactor was constructed under extreme tight budget. They tried a variety of ways to save money. The main facility was located inside a modified old building. When they were making fuel elements in an arc furnace, they learned that a new technique was just developed. Immediately, they began to study this approach. Under the guidance of nuclear fuel expert Dai Shouhui [2071 0649 1920], senior engineer Jiang Bingyu [5592 0014 3768] spent years and finally overcame all the difficulties. This effort not only ended up in world class results but also saved the government over 1 million yuans in equipment alone.

Based on the experts on hand, this nuclear reactor is the most advanced kind in the world. it uses a special uranium-hydrogen-zirconium moderating fuel. when the reactor power increases abruptly, this moderating agent can instantaneously produce a negative temperature coefficient to automatically regulate its power. Therefore, it is inherently safe and can be constructed in urban areas or even in universities and large corporations. Because of its compact core design and simple structure, the safety and protection requirements are less stringent. Hence, its construction cost and operating expenses are lower. If it is used to generate electricity, its cost can be drastically reduced. Therefore, it has a bright prospect of becoming a commercial product.

Notes Concerning Pulsed Nuclear Reactor

A pulsed nuclear reactor is a multi-purpose small pool type reactor operating on a unique uranium-hydrogen-zirconium fuel. Compared to other types of reactor, the most distinct difference is that it not only can be run in a more stable fashion but also can reach critical instantaneously and safely begin pulsed operation. Within a short period of time, reactor power and neutron flux can be increased by several thousand times.

Its primary applications include: (1) isotope production, (2) neutron activation analysis, (3) neutron photography, (4) radiation experiment, (5) scientific research, and (6) training of teaching and other relevant personnel.

Due to its intrinsic safety features, not only the reactor is simple but also many safety devices are omitted. Therefore, the entire system is simple in design, less costly to construct and operate. It is especially suitable for use in China. It will raise the level of nuclear technology for civilian use in China.

Beijing Positron-Electron Collider Update

3.5 Million J Particle Events

91FE0300B Hefei ANHUI RIBAO in Chinese
7 Dec 90 p 3

[Article by correspondent Chen Jinwu [7115 6855 2976]: "3.5 Million J Particle Events Obtained by Beijing Positron-Electron Collider"]

[Text] Beijing Positron-Electron Collider has collected more than 3.5 million J particle events over two years of high energy physics experiments. Some interesting results were obtained. This study has attracted a great deal of attention in the international high energy physics community.

Since the first successful collision on 16 Oct 88, Beijing Positron-Electron Collider has been in stable operation for over 10,000 hours. This outstanding record provides technical assurance for high energy physics experiment and synchrotron radiation research.

According to Associate Director Zheng Zhipeng [6774 1807 7720] of the Institute of High Energy Physics of the Chinese Academy of Sciences, some of the high energy physics experiments conducted on the Beijing Positron-Electron Collider have provided evidence for the analysis of J particle decay paths which enables us to further understand the decay characteristics of J particles.

He pointed out that J particle is the first type of a class of large mass, long life mesons. It was discovered by Chinese American physicist Samuel Chao Chung Ting and American physicist Burton Richter in 1974 from independent studies. The discovery of the J particle demonstrated the presence of charmed mesons, a fourth straton, and thus created the field of charmed physics.

Just as the same as the discovery of other fundamental particles such as molecule, atom, nucleus, proton and neutron, the discovery of J particle provided a more profound understanding of the microscopic structure of matters. Nevertheless, scientists still do not understand some of its characteristics. There are contradictions which cannot be explained. Three positron-electron colliders were used primarily in charmed physics research. Some important results have been obtained. however, the work was stopped because these colliders are not bright enough.

The detector for the Beijing Positron-Electron Collider, the Beijing Spectrometer, has located potential gluon events. Theoretically, gluon is an elementary particle that is predicted to exist. However, there is no experimental proof to date. The Beijing Spectrometer may contribute in this area of research.

In addition to high energy physics experiments, the Beijing Positron-Electron Collider has been used in synchrotron radiation lithography experiments resulting in a resolution of better than 1 micron. This is an ideal soft X-ray source for VLSI. Some encouraging results were also obtained with the synchrotron radiation device in areas such as extended X-ray absorption fine structure, gas phase absorption spectroscopy, X-ray topography and X-ray photo-acoustic effect.

The Beijing Positron-Electron Collider is operating at a collision frequency of 1,250,000 Hz. It not only maintains stable operation over a long period of time but also yields so much results so quickly. This is rare in the high energy physics community in the world. Nobel laureate Richter commented that the Beijing Positron-Electron Collider is the only accelerator operating in that energy region in the world and its brightness is also higher than any other device operating in that region ever.

Collider Said To Be at Advanced World Levels

91FE0400A Beijing RENMIN RIBAO in Chinese
28 Jan 91 p 3

[Article by Wang Dianchen [3769 3013 5256]: "Beijing Positron-Electron Collider Said To Be at Advanced World Levels"]

[Text] The first high energy accelerator independently designed, developed and constructed in China has received very positive response from the international high energy physics community owing to the high quality of construction and high speed. Among existing accelerators in the J particle energy range, Beijing Electron-Positron Collider (BEPC) is the leader in terms of brightness (4-5 times higher than that of similar facilities in the U.S.), low energy dispersion, stability and reliability. In the 25th International High Energy Physics Conference in Singapore, Nobel prize laureate Burton Richter pointed out that BEPC is the brightest collider in this energy region.

BEPC was designed and constructed for two areas of applications. In high energy physics research, it is used for the discovery of gluons, hybrid states and other new particles and for the study of J physics and D mesons. In applied research of synchrotron radiation, because the synchrotron radiation emitted by circling electrons and positrons has a wide spectral range and is continuously tunable and very bright, and has high flux, low divergence, excellent polarization characteristics and specific time structure, it is superior to conventional light sources such as lasers and X-ray machines. It can be widely used in solid state physics, surface physics, atomic and molecular physics, material science, biochemistry, biophysics,

semiconductors, chemistry, microelectronics technology, lithography, geology, mineralogy and medicine. After two years of operation, BEPC has demonstrated that it is fully capable of meeting all the requirements in these two areas. It is at advanced levels in the 1980's. presently, the collider is in stable operation. High energy physics experiments and synchrotron radiation studies are in progress. Some preliminary results have been obtained. In high energy physics experiments, over 6 million J particle events have been observed. Programs and data bases for analysis have been established to some scale. Some off-line results were presented at the 25th International High Energy Physics Conference in Singapore and were praised by high energy physicists from different countries. In synchrotron radiation research, new phenomena were discovered in the gas phase absorption spectra of alkyl iodide molecules and in the X-ray photoacoustic effect of superconductors. The newly constructed photolithography station yielded 1 micron wide lines in the preliminary test stage. Minute elements in hair were determined by fluorescence analysis. The relation between athelete's health and the iron content in the hair has been discovered.

The development and construction of BEPC not only trained a large number of high-tech talents for China but also allowed us to acquire valuable experience in the organization and management of large scale engineering projects. Because a large number of advanced high technologies were imported during its development stage in the 1980's, this effectively pushes China's industrial technology forward as a result of digestion, absorption and diffusion. For instance, breakthroughs of original technical limitations have been made in the precision machining and welding of disc waveguide accelerator tubes and development of high power electrical vacuum devices. This improved the overall industrial level and put us among the leaders in the world.

BEPC also won worldwide reputation for high-tech products made in China and created new products for export. Chinese made high energy accelerator components such as accelerator tubes, waveguide elements and magnets are being exported to Europe and the U.S. Bids were solicited by BNL for the construction of a 200 MeV linear injector.

The excellent performance of BEPC is attracting scientists from all over the world. Many nations have proposed to conduct joint studies in high energy physics and synchrotron radiation research. BEPC's national laboratory is under construction. In the near future, it will be available to scientists from other countries.

END OF FICHE DATE FILMED

June 4, 1991